Chapter 2

Thermodynamics of Separation Operations

§2.0 INSTRUCTIONAL OBJECTIVES

After completing this chapter, you should be able to:

- Make energy, entropy, and availability balances around a separation process.
- Explain phase equilibria in terms of Gibbs free energy, chemical potential, fugacity, fugacity coefficient, activity, and activity coefficient.
- Understand the usefulness of equilibrium ratios (K-values and partition coefficients) for liquid and vapor phases.
- Derive K-value expressions in terms of fugacity coefficients and activity coefficients.
- Explain how computer programs use equations of state (e.g., Soave–Redlich–Kwong or Peng–Robinson) to compute thermodynamic properties of vapor and liquid mixtures, including K-values.
- Explain how computer programs use liquid-phase activity-coefficient correlations (e.g., Wilson, NRTL, UNIQUAC, or UNIFAC) to compute thermodynamic properties, including K-values.
- For a given weak acid or base (including amino acids), calculate pH, pK_a, degree of ionization, pI, and net charge.
- Identify a buffer suited to maintain activity of a biological species at a target pH and evaluate effects of temperature, ionic strength, solvent and static charge on pH, and effects of pH on solubility.
- Determine effects of electrolyte composition on electrostatic double-layer dimensions, energies of attraction, critical flocculation concentration, and structural stability of biocolloids.
- Characterize forces that govern ligand–receptor–binding interactions and evaluate dissociation constants from free energy changes or from batch solution or continuous sorption data.

Thermodynamic properties play a major role in separation operations with respect to energy requirements, phase equilibria, biological activity, and equipment sizing. This chapter develops equations for energy balances, for entropy and availability balances, and for determining densities and compositions for phases at equilibrium. The equations contain thermodynamic properties, including specific volume, enthalpy, entropy, availability, fugacities, and activities, all as functions of temperature, pressure, and composition. Both ideal and nonideal mixtures are discussed. Equations to determine ionization state, solubility, and interaction forces of biomolecular species are introduced. However, this chapter is not a substitute for any of the excellent textbooks on thermodynamics.

Experimental thermodynamic property data should be used, when available, to design and analyze the operation of separation equipment. When not available, properties can often be estimated with reasonable accuracy. Many of these estimation methods are discussed in this chapter. The most comprehensive source of thermodynamic properties for pure compounds and nonelectrolyte and electrolyte mixtures—including excess volume, excess enthalpy, activity coefficients at infinite dilution, azeotropes, and vapor–liquid, liquid–liquid, and solid–liquid equilibrium—is the computerized Dortmund Data Bank (DDB) (www.ddbst.com), initiated by Gmehling and Onken in 1973. It is updated annually and is widely used by industry and academic institutions. In 2009, the DDB contained more than 3.9 million data points for 32,000 components from more than 64,000 references. Besides openly available data from journals, DDB contains a large percentage of data from non-English sources, chemical industry, and MS and PhD theses.

§2.1 ENERGY, ENTROPY, AND AVAILABILITY BALANCES

Industrial separation operations utilize large quantities of energy in the form of heat and/or shaft work. Distillation separations account for about 3% of the total U.S. energy consumption (Mix et al. [1]). The distillation of crude oil into its fractions is very energy-intensive, requiring about 40% of the total energy used in crude-oil refining. Thus, it is important to know the energy consumption in a separation process, and to what degree energy requirements can be reduced.

Consider the continuous, steady-state, flow system for the separation process in Figure 2.1. One or more feed streams flowing into the system are separated into two or more

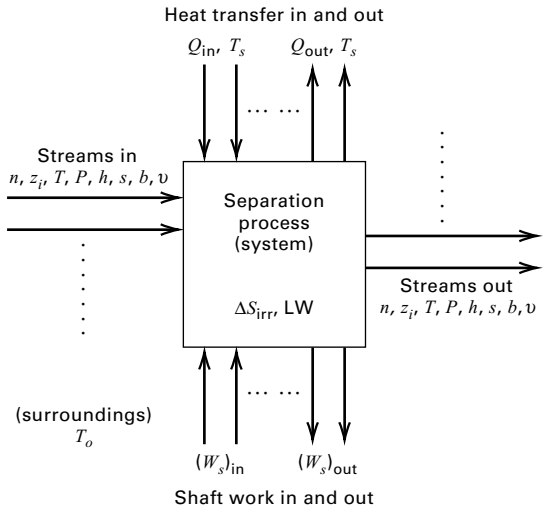

Figure 2.1 General separation system.

product streams. For each stream molar flow rates are denoted by n, the component mole fractions by z_i, the temperature by T, the pressure by P, the molar enthalpies and entropies by h and s, respectively, and the molar availabilities by b. If chemical reactions occur in the process, enthalpies and entropies are referred to the elements, as discussed by Felder and Rousseau [2]; otherwise they can be referred to the compounds. Flows of heat in or out are denoted by Q, and shaft work crossing the boundary of the system by W_s. At steady state, if kinetic, potential, and surface energy changes are neglected, the first law of thermodynamics states that the sum of energy flows into the system equals the sum of the energy flows leaving the system.

In terms of symbols, the energy balance is given by Eq. (1) in Table 2.1, where all flow-rate, heat-transfer, and shaft-work terms are positive. Molar enthalpies may be positive or negative, depending on the reference state.

The first law of thermodynamics provides no information on energy efficiency, but the second law of thermodynamics, given by Eq. (2) in Table 2.1, does.

In the entropy balance, the heat sources and sinks in Figure 2.1 are at absolute temperatures, T_s. For example, if condensing steam at 150°C supplies heat, Q, to the reboiler of a distillation column, $T_s = 150 + 273 = 423$ K. Unlike the energy balance, which states that energy is conserved, the entropy balance predicts the production of entropy, ΔS_{irr}, which is the irreversible increase in the entropy of the universe. This term, which must be positive, is a measure of the thermodynamic inefficiency. In the limit, as a reversible process is approached, ΔS_{irr} tends to zero. Unfortunately, ΔS_{irr} is difficult to apply because it does not have the units of energy/unit time (power).

A more useful measure of process inefficiency is lost work, LW. It is derived by combining Eqs. (1) and (2) to obtain a combined statement of the first and second laws, which is given as Eq. (3) in Table 2.1. To perform this derivation, it is first necessary to define an infinite source or sink available for heat transfer at the absolute temperature, $T_s = T_0$, of the surroundings. This temperature, typically 300 K, represents the largest source of coolant (heat sink) available. This might

Table 2.1 Universal Thermodynamic Laws for a Continuous, Steady-State, Flow System

Energy balance:

$$(1)\ \sum_{\substack{\text{out of}\\ \text{system}}} (nh + Q + W_s) - \sum_{\substack{\text{in to}\\ \text{system}}} (nh + Q + W_s) = 0$$

Entropy balance:

$$(2)\ \sum_{\substack{\text{out of}\\ \text{system}}} \left(ns + \frac{Q}{T_s}\right) - \sum_{\substack{\text{in to}\\ \text{system}}} \left(ns + \frac{Q}{T_s}\right) = \Delta S_{\text{irr}}$$

Availability balance:

$$(3)\ \sum_{\substack{\text{in to}\\ \text{system}}} \left[nb + Q\left(1 - \frac{T_0}{T_s}\right) + W_s\right] - \sum_{\substack{\text{out of}\\ \text{system}}} \left[nb + Q\left(1 - \frac{T_0}{T_s}\right) + W_s\right] = \text{LW}$$

Minimum work of separation:

$$(4)\ W_{\min} = \sum_{\substack{\text{out of}\\ \text{system}}} nb - \sum_{\substack{\text{in to}\\ \text{system}}} nb$$

Second-law efficiency:

$$(5)\ \eta = \frac{W_{\min}}{\text{LW} + W_{\min}}$$

where $b = h - T_0 s$ = availability function
$\text{LW} = T_0 - \Delta S_{\text{irr}}$ = lost work

be the average temperature of cooling water, air, or a nearby river, lake, or ocean. Heat transfer associated with this coolant and transferred from (or to) the process is Q_0. Thus, in both (1) and (2) in Table 2.1, the Q and Q/T_s terms include contributions from Q_0 and Q_0/T_0.

The derivation of (3) in Table 2.1 is made, as shown by de Nevers and Seader [3], by combining (1) and (2) to eliminate Q_0. It is referred to as an *availability* (or *exergy*) balance, where availability means "available for complete conversion to shaft work." The availability function, b, a thermodynamic property like h and s, is defined by

$$b = h - T_0 s \qquad (2\text{-}1)$$

and is a measure of the maximum amount of energy converted into shaft work if the stream is taken to the reference state. It is similar to Gibbs free energy, $g = h - Ts$, but differs in that the temperature, T_0, appears in the definition instead of T. Terms in (3) in Table 2.1 containing Q are multiplied by $(1 - T_0/T_s)$, which, as shown in Figure 2.2, is the reversible Carnot heat-engine cycle efficiency, representing the maximum amount of shaft work producible from Q at T_s, where the residual amount of energy $(Q - W_s)$ is transferred as heat to a sink at T_0. Shaft work, W_s, remains at its full value in (3). Thus, although Q and W_s have the same thermodynamic worth in (1) of Table 2.1, heat transfer has less worth in (3). Shaft work can be converted completely to heat, but heat cannot be converted completely to shaft work.

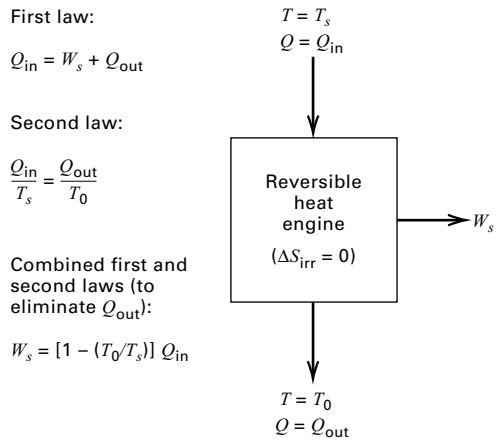

Figure 2.2 Carnot heat-engine cycle for converting heat to shaft work.

Availability, like entropy, is not conserved in a real, irreversible process. The total availability (i.e., ability to produce shaft work) into a system is always greater than the total availability leaving. Thus (3) in Table 2.1 is written with the ''in to system'' terms first. The difference is the *lost work*, LW, also called the loss of availability (or exergy), and is

$$\text{LW} = T_0 \Delta S_{\text{irr}} \tag{2-2}$$

Lost work is always positive. The greater its value, the greater the energy inefficiency. In the lower limit, for a reversible process, it is zero. The lost work has the units of energy, thus making it easy to attach significance to its numerical value.

Lost work can be computed from Eq. (3) in Table 2.1. Its magnitude depends on process irreversibilities, which include fluid friction, heat transfer due to finite temperature-driving forces, mass transfer due to finite concentration- or activity-driving forces, chemical reactions proceeding at finite displacements from chemical equilibrium, mixing streams of differing temperature, pressure, and/or composition, etc. To reduce lost work, driving forces for momentum, heat, and mass transfer; and chemical reaction must be reduced. Practical limits to reduction exist because, as driving forces decrease, equipment sizes increase, tending to infinity as driving forces approach zero.

For a separation without chemical reaction, the summation of the stream availability functions leaving the process is usually greater than that for streams entering the process. In the limit for a reversible process (LW = 0), (3) of Table 2.1 reduces to (4), where $W_{\min}$ is the minimum shaft work for the separation and is equivalent to the difference in the heat-transfer and shaft-work terms in (3). This minimum work is a property independent of the nature (or path) of the separation. The work of separation for an irreversible process is greater than the minimum value from (4).

Equation (3) of Table 2.1 shows that as a process becomes more irreversible, and thus more energy-inefficient, the increasing LW causes the required work of separation to increase. Thus, the equivalent work of separation for an irreversible process is the sum of lost work and the minimum work of separation. The *second-law efficiency*, therefore, is defined by (5) in Table 2.1.

EXAMPLE 2.1 Use of Thermodynamic Laws.

For the propylene–propane separation of Figure 1.16, using the following thermodynamic properties and the relations given in Table 2.1, compute in SI units: **(a)** the condenser duty, Q_C; **(b)** the reboiler duty, Q_R; **(c)** the irreversible entropy production, assuming 303 K for the condenser cooling-water sink and 378 K for the reboiler steam source; **(d)** the lost work, assuming $T_0 = 303$ K; **(e)** the minimum work of separation; and **(f)** the second-law efficiency.

Stream	Phase Condition	Enthalpy (h), kJ/kmol	Entropy (s), kJ/kmol-K
Feed (F)	Liquid	13,338	−4.1683
Overhead vapor (OV)	Vapor	24,400	24.2609
Distillate (D) and reflux (R)	Liquid	12,243	−13.8068
Bottoms (B)	Liquid	14,687	−2.3886

Solution

Let Q_C and Q_R cross the boundary of the system. The following calculations are made using the stream flow rates in Figure 1.16 and the properties above.

(a) From (1), Table 2.1, noting that the overhead-vapor molar flow rate is given by $n_{OV} = n_R + n_D$ and $h_R = h_D$, the condenser duty is

$$\begin{aligned} Q_C &= n_{OV}(h_{OV} - h_R) \\ &= (2{,}293 + 159.2)(24{,}400 - 12{,}243) \\ &= 29{,}811{,}000\ \text{kJ/h} \end{aligned}$$

(b) An energy balance around the reboiler cannot be made because data are not given for the boilup rate. From (1), Table 2.1, an energy balance around the column is used instead:

$$\begin{aligned} Q_R &= n_D h_D + n_B h_B + Q_C - n_F h_F \\ &= 159.2(12{,}243) + 113(14{,}687) \\ &\quad + 29{,}811{,}000 - 272.2(13{,}338) \\ &= 29{,}789{,}000\ \text{kJ/h} \end{aligned}$$

(c) Compute the production of entropy from an entropy balance around the entire distillation system. From Eq. (2), Table 2.1,

$$\begin{aligned} \Delta S_{\text{irr}} &= n_D s_D + n_B s_B + Q_C/T_C - n_F s_F - Q_R/T_R \\ &= 159.2(-13.8068) + 113(-2.3886) \\ &\quad + 29{,}811{,}000/303 - 272.2(-4.1683) \\ &\quad - 29{,}789{,}000/378 \\ &= 18{,}246\ \text{kJ/h-K} \end{aligned}$$

(d) Compute lost work from its definition at the bottom of Table 2.1:

$$\begin{aligned} \text{LW} &= T_0 \Delta S_{irr} \\ &= 303(18{,}246) = 5{,}529{,}000\ \text{kJ/h} \end{aligned}$$

Alternatively, compute lost work from an availability balance around the system. From (3), Table 2.1, where the availability function, b, is defined near the bottom of Table 2.1,

$$\begin{aligned}\text{LW} &= n_F b_F + Q_R(1 - T_0/T_R) \\ &\quad - n_D b_D - n_B b_B - Q_C(1 - T_0/T_C) \\ &= 272.2[13{,}338 - (303)(-4.1683)] \\ &\quad + 29{,}789{,}000(1 - 303/378) \\ &\quad - 159.2[12{,}243 - (303)(-13.8068)] \\ &\quad - 113[14{,}687 - (303)(-2.3886)] \\ &\quad - 29{,}811{,}000(1 - 303/303) \\ &= 5{,}529{,}000 \text{ kJ/h (same result)}\end{aligned}$$

(e) Compute the minimum work of separation for the entire distillation system. From (4), Table 2.1,

$$\begin{aligned}W_{\min} &= n_D b_D + n_B b_B - n_F b_F \\ &= 159.2[12{,}243 - (303)(-13.8068)] \\ &\quad + 113[14{,}687 - (303)(-2.3886)] \\ &\quad - 272.2[13{,}338 - (303)(-4.1683)] \\ &= 382{,}100 \text{ kJ/h}\end{aligned}$$

(f) Compute the second-law efficiency for the entire distillation system. From (5), Table 2.1,

$$\begin{aligned}\eta &= \frac{W_{\min}}{\text{LW} + W_{\min}} \\ &= \frac{382{,}100}{5{,}529{,}000 + 382{,}100} \\ &= 0.0646 \quad \text{or} \quad 6.46\%\end{aligned}$$

This low second-law efficiency is typical of a difficult distillation separation, which in this case requires 150 theoretical stages with a reflux ratio of almost 15 times the distillate rate.

§2.2 PHASE EQUILIBRIA

Many separations are determined by the extent to which the species are distributed among two or more phases at equilibrium at a specified T and P. The distribution is determined by application of the Gibbs free energy. For each phase in a multiphase, multicomponent system, the total Gibbs free energy is

$$G = G(T, P, N_1, N_2, \ldots, N_C)$$

where N_i = moles of species i. At equilibrium, the total G for all phases is a minimum, and methods for determining this are referred to as *free-energy minimization techniques*. Gibbs free energy is also the starting point for the derivation of commonly used equations for phase equilibria. From classical thermodynamics, the total differential of G is

$$dG = -S\,dT + V\,dP + \sum_{i=1}^{C} \mu_i dN_i \tag{2-3}$$

where μ_i is the chemical potential or partial molar Gibbs free energy of species i. For a closed system consisting of two or more phases in equilibrium, where each phase is an open system capable of mass transfer with another phase,

$$dG_{\text{system}} = \sum_{p=1}^{N} \left[\sum_{i=1}^{C} \mu_i^{(p)} dN_i^{(p)} \right]_{P,T} \tag{2-4}$$

where superscript (p) refers to each of N phases. Conservation of moles of species, in the absence of chemical reaction, requires that

$$dN_i^{(1)} = -\sum_{p=2}^{N} dN_i^{(p)} \tag{2-5}$$

which, upon substitution into (2-4), gives

$$\sum_{p=2}^{N} \left[\sum_{i=1}^{C} \left(\mu_i^{(p)} - \mu_i^{(1)} \right) dN_i^{(p)} \right] = 0 \tag{2-6}$$

With $dN_i^{(1)}$ eliminated in (2-6), each $dN_i^{(p)}$ term can be varied independently of any other $dN_i^{(p)}$ term. But this requires that each coefficient of $dN_i^{(p)}$ in (2-6) be zero. Therefore,

$$\mu_i^{(1)} = \mu_i^{(2)} = \mu_i^{(3)} = \cdots = \mu_i^{(N)} \tag{2-7}$$

Thus, the chemical potential of a species in a multicomponent system is identical in all phases at physical equilibrium.

§2.2.1 Fugacities and Activity Coefficients

Chemical potential is not an absolute quantity, and the numerical values are difficult to relate to more easily understood physical quantities. Furthermore, the chemical potential approaches an infinite negative value as pressure approaches zero. Thus, the chemical potential is not favored for phase-equilibria calculations. Instead, *fugacity*, invented by G. N. Lewis in 1901, is employed as a surrogate.

The partial fugacity of species i in a mixture is like a pseudo-pressure, defined in terms of the chemical potential by

$$\bar{f}_i = C \exp\left(\frac{\mu_i}{RT}\right) \tag{2-8}$$

where C is a temperature-dependent constant. Regardless of the value of C, it is shown by Prausnitz, Lichtenthaler, and de Azevedo [4] that (2-7) can be replaced with

$$\bar{f}_i^{(1)} = \bar{f}_i^{(2)} = \bar{f}_i^{(3)} = \cdots = \bar{f}_i^{(N)} \tag{2-9}$$

Thus, at equilibrium, a given species has the same partial fugacity in each phase. This equality, together with equality of phase temperatures and pressures,

$$T^{(1)} = T^{(2)} = T^{(3)} = \cdots = T^{(N)} \tag{2-10}$$

and

$$P^{(1)} = P^{(2)} = P^{(3)} = \cdots = P^{(N)} \tag{2-11}$$

constitutes the conditions for phase equilibria. For a pure component, the partial fugacity, $\bar{f}_i$, becomes the pure-component fugacity, f_i. For a pure, ideal gas, fugacity equals the total pressure, and for a component in an ideal-gas mixture, the partial fugacity equals its partial pressure, $p_i = y_i P$. Because of the close relationship between fugacity and pressure, it is convenient to define their ratio for a pure substance as

$$\phi_i = \frac{f_i}{P} \tag{2-12}$$

Table 2.2 Thermodynamic Quantities for Phase Equilibria

Thermodynamic Quantity	Definition	Physical Significance	Limiting Value for Ideal Gas and Ideal Solution
Chemical potential	$\mu_i \equiv \left(\frac{\partial G}{\partial N_i}\right)_{P,T,N_j}$	Partial molar free energy, $\bar{g}_i$	$\mu_i = \bar{g}_i$
Partial fugacity	$\bar{f}_i \equiv C \exp\left(\frac{\mu_i}{RT}\right)$	Thermodynamic pressure	$\bar{f}_{iV} = y_i P$ $\bar{f}_{iL} = x_i P_i^s$
Fugacity coefficient of a pure species	$\phi_i \equiv \frac{f_i}{P}$	Deviation to fugacity due to pressure	$\phi_{iV} = 1.0$ $\phi_{iL} = \frac{P_i^s}{P}$
Partial fugacity coefficient of a species in a mixture	$\bar{\phi}_{iV} \equiv \frac{\bar{f}_{iV}}{y_i P}$ $\bar{\phi}_{iL} \equiv \frac{\bar{f}_{iL}}{x_i P}$	Deviations to fugacity due to pressure and composition	$\bar{\phi}_{iV} = 1.0$ $\bar{\phi}_{iL} = \frac{P_i^s}{P}$
Activity	$a_i \equiv \frac{\bar{f}_i}{f_i^o}$	Relative thermodynamic pressure	$a_{iV} = y_i$ $a_{iL} = x_i$
Activity coefficient	$\gamma_{iV} \equiv \frac{a_{iV}}{y_i}$ $\gamma_{iL} \equiv \frac{a_{iL}}{x_i}$	Deviation to fugacity due to composition	$\gamma_{iV} = 1.0$ $\gamma_{iL} = 1.0$

where ϕ_i is the pure-species fugacity coefficient, which is 1.0 for an ideal gas. For a mixture, partial fugacity coefficients are

$$\bar{\phi}_{iV} \equiv \frac{\bar{f}_{iV}}{y_i P} \tag{2-13}$$

$$\bar{\phi}_{iL} \equiv \frac{\bar{f}_{iL}}{x_i P} \tag{2-14}$$

such that as ideal-gas behavior is approached, $\bar{\phi}_{iV} \to 1.0$ and $\bar{\phi}_{iL} \to P_i^s/P$, where $P_i^s =$ vapor pressure.

At a given temperature, the ratio of the partial fugacity of a component to its fugacity in a standard state is termed the *activity*. If the standard state is selected as the pure species at the same pressure and phase as the mixture, then

$$a_i \equiv \frac{\bar{f}_i}{f_i^o} \tag{2-15}$$

Since at phase equilibrium, the value of f_i^o is the same for each phase, substitution of (2-15) into (2-9) gives another alternative condition for phase equilibria,

$$a_i^{(1)} = a_i^{(2)} = a_i^{(3)} = \cdots = a_i^{(N)} \tag{2-16}$$

For an ideal solution, $a_{iV} = y_i$ and $a_{iL} = x_i$.

To represent departure of activities from mole fractions when solutions are nonideal, *activity coefficients* based on concentrations in mole fractions are defined by

$$\gamma_{iV} \equiv \frac{a_{iV}}{y_i} \tag{2-17}$$

$$\gamma_{iL} \equiv \frac{a_{iL}}{x_i} \tag{2-18}$$

For ideal solutions, $\gamma_{iV} = 1.0$ and $\gamma_{iL} = 1.0$.

For convenient reference, thermodynamic quantities useful in phase equilibria are summarized in Table 2.2.

§2.2.2 *K*-Values

A *phase-equilibrium ratio* is the ratio of mole fractions of a species in two phases at equilibrium. For vapor–liquid systems, the constant is referred to as the *K-value* or *vapor–liquid equilibrium ratio*:

$$\boxed{K_i \equiv \frac{y_i}{x_i}} \tag{2-19}$$

For the liquid–liquid case, the ratio is a *distribution* or *partition coefficient,* or *liquid–liquid equilibrium ratio:*

$$\boxed{K_{D_i} \equiv \frac{x_i^{(1)}}{x_i^{(2)}}} \tag{2-20}$$

For equilibrium-stage calculations, separation factors, like (1-4), are defined by forming ratios of equilibrium ratios. For the vapor–liquid case, *relative volatility* $\alpha_{i,j}$ between components i and j is given by

$$\boxed{\alpha_{ij} \equiv \frac{K_i}{K_j}} \tag{2-21}$$

Separations are easy for very large values of $\alpha_{i,j}$, but become impractical for values close to 1.00.

Similarly for the liquid–liquid case, the *relative selectivity* $\beta_{i,j}$ is

$$\beta_{ij} \equiv \frac{K_{D_i}}{K_{D_j}} \tag{2-22}$$

Equilibrium ratios can contain the quantities in Table 2.2 in a variety of formulations. The ones of practical interest are formulated next.

For vapor–liquid equilibrium, (2-9) becomes, for each component,

$$\bar{f}_{iV} = \bar{f}_{iL}$$

To form an equilibrium ratio, partial fugacities are commonly replaced by expressions involving mole fractions. From the definitions in Table 2.2:

$$\bar{f}_{iL} = \gamma_{iL} x_i f^o_{iL} \tag{2-23}$$

or

$$\bar{f}_{iL} = \bar{\phi}_{iL} x_i P \tag{2-24}$$

and

$$\bar{f}_{iV} = \bar{\phi}_{iV} y_i P \tag{2-25}$$

If (2-24) and (2-25) are used with (2-19), a so-called *equation-of-state form* of the K-value follows:

$$K_i = \frac{\bar{\phi}_{iL}}{\bar{\phi}_{iV}} \tag{2-26}$$

Applications of (2-26) include the Starling modification of the Benedict, Webb, and Rubin (B–W–R–S) equation of state [5], the Soave modification of the Redlich–Kwong (S–R–K or R–K–S) equation of state [6], the Peng–Robinson (P–R) equation of state [7], and the Plöcker et al. modification of the Lee–Kesler (L–K–P) equation of state [8].

If (2-23) and (2-25) are used, a so-called *activity coefficient form* of the K-value is obtained:

$$K_i = \frac{\gamma_{iL} f^o_{iL}}{\bar{\phi}_{iV} P} = \frac{\gamma_{iL} \bar{\phi}_{iL}}{\bar{\phi}_{iV}} \tag{2-27}$$

Since 1960, (2-27) has received some attention, with applications to industrial systems presented by Chao and Seader (C–S) [9], with a modification by Grayson and Streed [10].

Table 2.3 is a summary of formulations for vapor–liquid equilibrium K-values. Included are the two rigorous expressions (2-26) and (2-27) from which the other approximate formulations are derived. The Raoult's law or ideal K-value is obtained from (2-27) by substituting, from Table 2.2, for an ideal gas and for ideal gas and liquid solutions, $\gamma_{iL} = 1.0$, $\phi_{iL} = P_i^s/P$ and $\bar{\phi}_{iV} = 1.0$. The modified Raoult's law relaxes the assumption of an ideal liquid by including the liquid-phase activity coefficient. The Poynting-correction form for moderate pressures is obtained by approximating the pure-component liquid fugacity coefficient in (2-27) by

$$\phi_{iL} = \phi^s_{iV} \frac{P_i^s}{P} \exp\left(\frac{1}{RT}\int_{P_i^s}^{P} \upsilon_{iL} dP\right) \tag{2-28}$$

where the exponential term is the Poynting correction. If the liquid molar volume is reasonably constant over the pressure range, the integral in (2-28) becomes $\upsilon_{iL}\left(P - P_i^s\right)$.

For a light gas species, whose critical temperature is less than the system temperature, the Henry's law form for the K-value is convenient, provided H_i, the Henry's law coefficient, is available. This constant depends on composition, temperature, and pressure. Included in Table 2.3 are recommendations for the application of each of the vapor–liquid K-value expressions.

Table 2.3 Useful Expressions for Estimating K-Values for Vapor–Liquid Equilibria ($K_i = y_i/x_i$)

	Equation	Recommended Application
Rigorous forms:		
(1) Equation-of-state	$K_i = \dfrac{\bar{\phi}_{iL}}{\bar{\phi}_{iV}}$	Hydrocarbon and light gas mixtures from cryogenic temperatures to the critical region
(2) Activity coefficient	$K_i = \dfrac{\gamma_{iL}\bar{\phi}_{iL}}{\bar{\phi}_{iV}}$	All mixtures from ambient to near-critical temperature
Approximate forms:		
(3) Raoult's law (ideal)	$K_i = \dfrac{P_i^s}{P}$	Ideal solutions at near-ambient pressure
(4) Modified Raoult's law	$K_i = \dfrac{\gamma_{iL}P_i^s}{P}$	Nonideal liquid solutions at near-ambient pressure
(5) Poynting correction	$K_i = \gamma_{iL}\phi^s_{iV}\left(\dfrac{P_i^s}{P}\right)\exp\left(\dfrac{1}{RT}\displaystyle\int_{p_i^s}^{P}\upsilon_{iL}dP\right)$	Nonideal liquid solutions at moderate pressure and below the critical temperature
(6) Henry's law	$K_i = \dfrac{H_i}{P}$	Low-to-moderate pressures for species at supercritical temperature

Regardless of which thermodynamic formulation is used for estimating *K*-values, their accuracy depends on the correlations used for the thermodynamic properties (vapor pressure, activity coefficient, and fugacity coefficients). For practical applications, the choice of *K*-value formulation is a compromise among accuracy, complexity, convenience, and past experience.

For liquid–liquid equilibria, (2-9) becomes

$$\bar{f}_{iL}^{(1)} = \bar{f}_{iL}^{(2)} \tag{2-29}$$

where superscripts (1) and (2) refer to the immiscible liquids. A rigorous formulation for the distribution coefficient is obtained by combining (2-23) with (2-20) to obtain an expression involving only activity coefficients:

$$K_{D_i} = \frac{x_i^{(1)}}{x_i^{(2)}} = \frac{\gamma_{iL}^{(2)} f_{iL}^{o(2)}}{\gamma_{iL}^{(1)} f_{iL}^{o(1)}} = \frac{\gamma_{iL}^{(2)}}{\gamma_{iL}^{(1)}} \tag{2-30}$$

For vapor–solid equilibria, if the solid phase consists of just one of the components of the vapor phase, combination of (2-9) and (2-25) gives

$$f_{iS} = \bar{\phi}_{iV} y_i P \tag{2-31}$$

At low pressure, $\bar{\phi}_{iV} = 1.0$ and the fugacity of the solid is approximated by its vapor pressure. Thus for the vapor-phase mole fraction of the component forming the solid phase:

$$y_i = \frac{\left(P_i^s\right)_{\text{solid}}}{P} \tag{2-32}$$

For liquid–solid equilibria, if the solid phase is a pure component, the combination of (2-9) and (2-23) gives

$$f_{iS} = \gamma_{iL} x_i f_{iL}^o \tag{2-33}$$

At low pressure, fugacity of a solid is approximated by vapor pressure to give, for a component in the solid phase,

$$x_i = \frac{\left(P_i^s\right)_{\text{solid}}}{\gamma_{iL}\left(P_i^s\right)_{\text{liquid}}} \tag{2-34}$$

EXAMPLE 2.2 *K*-Values from Raoult's and Henry's Laws.

Estimate the *K*-values and α of a vapor–liquid mixture of water (W) and methane (M) at $P = 2$ atm, $T = 20$ and 80°C. What is the effect of *T* on the component distribution?

Solution

At these conditions, water exists mainly in the liquid phase and will follow Raoult's law, as given in Table 2.3. Because methane has a critical temperature of −82.5°C, well below the temperatures of interest, it will exist mainly in the vapor phase and follow Henry's law, in the form given in Table 2.3. From *Perry's Chemical Engineers' Handbook*, 6th ed., pp. 3-237 and 3-103, the vapor pressure data for water and Henry's law coefficients for CH_4 are:

T, °C	P^s for H_2O, atm	*H* for CH_4, atm
20	0.02307	3.76×10^4
80	0.4673	6.82×10^4

K-values for water and methane are estimated from (3) and (6), respectively, in Table 2.3, using P = 2 atm, with the following results:

T, °C	K_{H_2O}	K_{CH_4}	$\alpha_{M,W}$
20	0.01154	18,800	1,629,000
80	0.2337	34,100	146,000

These *K*-values confirm the assumptions of the phase distribution of the two species. The *K*-values for H_2O are low, but increase with temperature. The *K*-values for methane are extremely high and do not change rapidly with temperature.

§2.3 IDEAL-GAS, IDEAL-LIQUID-SOLUTION MODEL

Classical thermodynamics provides a means for obtaining fluid properties in a consistent manner from *P*–υ–*T* relationships, which are *equation-of-state* models. The simplest model applies when both liquid and vapor phases are ideal solutions (all activity coefficients equal 1.0) and the vapor is an ideal gas. Then the thermodynamic properties can be computed from unary constants for each species using the equations given in Table 2.4. These ideal equations apply only at pressures up to about 50 psia (345 kPa), for components of similar molecular structure.

For the vapor, the molar volume, υ, and mass density, ρ, are computed from (1), the ideal-gas law in Table 2.4, which requires the mixture molecular weight, *M*, and the gas constant, *R*. It assumes that Dalton's law of additive partial pressures and Amagat's law of additive volumes apply.

The vapor enthalpy, h_V, is computed from (2) by integrating an equation in temperature for the zero-pressure heat capacity at constant pressure, $C_{P_V}^o$, starting from a reference (datum) temperature, T_0, to the temperature of interest, and then summing the resulting species vapor enthalpies on a mole-fraction basis. Typically, T_0 is taken as 0 K or 25°C. Pressure has no effect on the enthalpy of an ideal gas. A common empirical representation of the effect of temperature on the zero-pressure vapor heat capacity of a component is the fourth-degree polynomial:

$$C_{P_V}^o = \left[a_0 + a_1 T + a_2 T^2 + a_3 T^3 + a_4 T^4\right] R \tag{2-35}$$

where the constants depend on the species. Values of the constants for hundreds of compounds, with *T* in *K*, are tabulated by Poling, Prausnitz, and O'Connell [11]. Because $C_P = dh/dT$, (2-35) can be integrated for each species to give the

Table 2.4 Thermodynamic Properties for Ideal Mixtures

Ideal gas and ideal-gas solution:

$$(1)\ \upsilon_V = \frac{V}{\sum_{i=1}^{C} N_i} = \frac{M}{\rho_V} = \frac{RT}{P}, \quad M = \sum_{i=1}^{C} y_i M_i$$

$$(2)\ h_V = \sum_{i=1}^{C} y_i \int_{T_0}^{T} \left(C_P^o\right)_{iV} dT = \sum_{i=1}^{C} y_i h_{iv}^o$$

$$(3)\ s_V = \sum_{i=1}^{C} y_i \int_{T_0}^{T} \frac{\left(C_P^o\right)_{iV}}{T} dT - R \ln\left(\frac{P}{P_0}\right) - R \sum_{i=1}^{C} y_i \ln y_i$$

where the first term is s_V^o

Ideal-liquid solution:

$$(4)\ \upsilon_L = \frac{V}{\sum_{i=1}^{C} N_i} = \frac{M}{\rho_L} = \sum_{i=1}^{C} x_i \upsilon_{iL}, \quad M = \sum_{i=1}^{C} x_i M_i$$

$$(5)\ h_L = \sum_{i=1}^{C} x_i \left(h_{iV}^o - \Delta H_i^{\text{vap}}\right)$$

$$(6)\ s_L = \sum_{i=1}^{C} x_i \left[\int_{T_0}^{T} \frac{\left(C_P^o\right)_{iV}}{T} dT - \frac{\Delta H_i^{\text{vap}}}{T}\right] - R \ln\left(\frac{P}{P_0}\right) - R \sum_{i=1}^{C} x_i \ln x_i$$

Vapor–liquid equilibria:

$$(7)\ K_i = \frac{P_i^s}{P}$$

Reference conditions (datum): h, ideal gas at T_0 and zero pressure; s, ideal gas at T_0 and 1 atm pressure.
Refer to elements if chemical reactions occur; otherwise refer to components.

ideal-gas species molar enthalpy:

$$h_V^o = \int_{T_0}^{T} C_{P_V}^o dT = \sum_{k=1}^{5} \frac{a_{k-1}\left(T^k - T_0^k\right)R}{k} \tag{2-36}$$

The vapor entropy is computed from (3) in Table 2.4 by integrating $C_{P_V}^o/T$ from T_0 to T for each species; summing on a mole-fraction basis; adding a term for the effect of pressure referenced to a datum pressure, P_0, which is generally taken to be 1 atm (101.3 kPa); and adding a term for the entropy change of mixing. Unlike the ideal vapor enthalpy, the ideal vapor entropy includes terms for the effects of pressure and mixing. The reference pressure is not zero, because the entropy is infinity at zero pressure. If (2-35) is used for the heat capacity,

$$\int_{T_0}^{T} \left(\frac{C_{P_V}^o}{T}\right) dT = \left[a_0 \ln\left(\frac{T}{T_0}\right) + \sum_{k=1}^{4} \frac{a_k\left(T^k - T_0^k\right)}{k}\right] R \tag{2-37}$$

The liquid molar volume and mass density are computed from the pure species using (4) in Table 2.4 and assuming additive volumes (not densities). The effect of temperature on pure-component liquid density from the freezing point to the critical region at saturation pressure is correlated well by the two-constant equation of Rackett [12]:

$$\rho_L = AB^{-(1-T/T_c)^{2/7}} \tag{2-38}$$

where values of the empirical constants A and B, and the critical temperature, T_c, are tabulated for approximately 700 organic compounds by Yaws et al. [13].

The vapor pressure of a liquid species is well represented over temperatures from below the normal boiling point to the critical region by an extended Antoine equation:

$$\ln P^s = k_1 + k_2/(k_3 + T) + k_4 T + k_5 \ln T + k_6 T^{k_7} \tag{2-39}$$

where the constants k_k depend on the species. Values of these constants for hundreds of compounds are built into the physical-property libraries of all process simulation programs. Constants for other vapor-pressure equations are tabulated by Poling et al. [11]. At low pressures, the enthalpy of vaporization is given in terms of vapor pressure by classical thermodynamics:

$$\Delta H^{\text{vap}} = RT^2 \left(\frac{d \ln P^s}{dT}\right) \tag{2-40}$$

If (2-39) is used for the vapor pressure, (2-40) becomes

$$\Delta H^{\text{vap}} = RT^2 \left[-\frac{k_2}{(k_3 + T)^2} + k_4 + \frac{k_5}{T} + k_7 k_6 T^{k_7 - 1}\right] \tag{2-41}$$

The enthalpy of an ideal-liquid mixture is obtained by subtracting the enthalpy of vaporization from the ideal vapor enthalpy for each species, as given by (2-36), and summing, as shown by (5) in Table 2.4. The entropy of the ideal-liquid mixture, given by (6), is obtained in a similar manner from the ideal-gas entropy by subtracting the molar entropy of vaporization, given by $\Delta H^{\text{vap}}/T$.

The final equation in Table 2.4 gives the expression for the ideal K-value, previously included in Table 2.3. It is the K-value based on Raoult's law, given as

$$p_i = x_i P_i^s \tag{2-42}$$

where the assumption of Dalton's law is also required:

$$p_i = y_i P \tag{2-43}$$

Combination of (2-42) and (2-43) gives the Raoult's law K-value:

$$\boxed{K_i \equiv \frac{y_i}{x_i} = \frac{P_i^s}{P}} \tag{2-44}$$

The extended Antoine equation, (2-39), can be used to estimate vapor pressure. The ideal K-value is independent of compositions, but exponentially dependent on temperature because of the vapor pressure, and inversely proportional to

pressure. From (2-21), the relative volatility using (2-44) is pressure independent.

EXAMPLE 2.3 Thermodynamic Properties of an Ideal-Gas Mixture.

Styrene is manufactured by catalytic dehydrogenation of ethylbenzene, followed by vacuum distillation to separate styrene from unreacted ethylbenzene [14]. Typical conditions for the feed are 77.5°C (350.6 K) and 100 torr (13.33 kPa), with the following vapor and liquid flows at equilibrium:

	n, kmol/h	
Component	Vapor	Liquid
Ethylbenzene (EB)	76.51	27.31
Styrene (S)	61.12	29.03

Based on the property constants given, and assuming that the ideal-gas, ideal-liquid-solution model of Table 2.4 is suitable at this low pressure, estimate values of υ_V, ρ_V, h_V, s_V, υ_L, ρ_L, h_L, and s_L in SI units, and the K-values and relative volatility, α.

Property Constants for (2-35), (2-38), (2-39) (In all cases, T is in K)

	Ethylbenzene	Styrene
M, kg/kmol	106.168	104.152
$C^o_{P_V}$, J/kmol-K:		
a_0R	−43,098.9	−28,248.3
a_1R	707.151	615.878
a_2R	−0.481063	−0.40231
a_3R	1.30084×10^{-4}	9.93528×10^{-5}
a_4R	0	0
P^s, Pa:		
k_1	86.5008	130.542
k_2	−7,440.61	−9,141.07
k_3	0	0
k_4	0.00623121	0.0143369
k_5	−9.87052	−17.0918
k_6	4.13065×10^{-18}	1.8375×10^{-18}
k_7	6	6
ρ_L, kg/m^3:		
A	289.8	299.2
B	0.268	0.264
T_c, K	617.9	617.1

$R = 8.314$ kJ/kmol-K or kPa-m^3/kmol-K = 8,314 J/kmol-K

Solution

Phase mole-fraction compositions and average molecular weights:

From $y_i = (n_{iV})/n_V, x_i = (n_{iL})/n_L$,

	Ethylbenzene	Styrene
y	0.5559	0.4441
x	0.4848	0.5152

From (1), Table 2.4,

$$M_V = (0.5559)(106.168) + (0.4441)(104.152) = 105.27$$
$$M_L = (0.4848)(106.168) + (0.5152)(104.152) = 105.13$$

Vapor molar volume and density: From (1), Table 2.4,

$$\upsilon_V = \frac{RT}{P} = \frac{(8.314)(350.65)}{(13.332)} = 219.2 \text{ m}^3/\text{kmol}$$
$$\rho_V = \frac{M_V}{\upsilon_V} = \frac{105.27}{219.2} = 0.4802 \text{ kg/m}^3$$

Vapor molar enthalpy (datum = ideal gas at 298.15 K and 0 kPa):

From (2-36) for ethylbenzene,

$$h^o_{\text{EB}_V} = -43098.9(350.65 - 298.15) + \left(\frac{707.151}{2}\right)(350.65^2 - 298.15^2) - \left(\frac{0.481063}{3}\right)(350.65^3 - 298.15^3) + \left(\frac{1.30084 \times 10^{-4}}{4}\right)(350.65^4 - 298.15^4)$$
$$= 7{,}351{,}900 \text{ J/kmol}$$

Similarly, $h^o_{\text{S}_V} = 6{,}957{,}700 \text{ J/kmol}$

From (2), Table 2.4, for the mixture,

$$h_V = \sum y_i h^o_{iV} = (0.5559)(7{,}351{,}900) + (0.4441)(6{,}957{,}100) = 7{,}176{,}800 \text{ J/kmol}$$

Vapor molar entropy (datum = pure components as vapor at 298.15 K, 101.3 kPa):

From (2-37), for each component,

$$\int_{T_0}^{T} \left(\frac{C^o_{P_V}}{T}\right) dT = 22{,}662 \text{ J/kmol-K for ethylbenzene and } 21{,}450 \text{ J/kmol-K for styrene}$$

From (3), Table 2.4, for the mixture,

$$s_V = [(0.5559)(22{,}662.4) + (0.4441)(21{,}450.3) - 8{,}314 \ln\left(\frac{13.332}{101.3}\right) - 8{,}314[(0.5559)\ln(0.5559) + (0.4441)\ln(0.4441)] = 44{,}695 \text{ J/kmol-K}$$

Note that the pressure effect and the mixing effect are significant.

Liquid molar volume and density:

From (2-38), for ethylbenzene,

$$\rho_{\text{EB}_L} = (289.8)(0.268)^{-(1-350.65/617.9)^{2/7}} = 816.9 \text{ kg/m}^3$$
$$\upsilon_{\text{EB}_L} = \frac{M_{\text{EB}}}{\rho_{\text{EB}_L}} = 0.1300 \text{ m}^3/\text{kmol}$$

Similarly, $\rho_{\text{S}_L} = 853.0 \text{ kg/m}^3$, $\upsilon_{\text{S}_L} = 0.1221 \text{ m}^3/\text{kmol}$

From (4), Table 2.4, for the mixture,

$$\upsilon_L = (0.4848)(0.1300) + (0.5152)(0.1221) = 0.1259 \text{ m}^3/\text{kmol}$$
$$\rho_L = \frac{M_L}{\upsilon_L} = \frac{105.13}{0.1259} = 835.0 \text{ kg/m}^3$$

Liquid molar enthalpy (datum = ideal gas at 298.15 K):

Use (5) in Table 2.4 for the mixture. For the enthalpy of vaporization of ethylbenzene, from (2-41),

$$\Delta H_{\text{EB}}^{\text{vap}} = 8{,}314(350.65)^2\left[\frac{-(-7{,}440.61)}{(0+350.65)^2} + 0.00623121 + \frac{-(9.87052)}{(350.65)} + 6\left(4.13065\times10^{-18}\right)(350.65)^5\right]$$

$$= 39{,}589{,}800\ \text{J/kmol}$$

Similarly, $\Delta H_{\text{S}}^{\text{vap}} = 40{,}886{,}700\ \text{J/kmol}$

Then, applying (5), Table 2.4, using $h^o_{\text{EB}_V}$ and $h^o_{\text{S}_V}$ from above,

$$h_L = [(0.4848)(7{,}351{,}900 - 39{,}589{,}800) + (0.5152)(6{,}957{,}700 - 40{,}886{,}700)] = -33{,}109{,}000\ \text{J/kmol}$$

Liquid molar entropy (datum = pure components as vapor at 298.15 K and 101.3 kPa):

From (6), Table 2.4 for the mixture, using values for $\int_{T_0}^{T}\left(C^o_{P_V}/T\right)dT$ and ΔH^{vap} of EB and S from above,

$$s_L = (0.4848)\left(22{,}662 - \frac{39{,}589{,}800}{350.65}\right) + (0.5152)\left(21{,}450 - \frac{40{,}886{,}700}{350.65}\right) - 8{,}314\ln\left(\frac{13.332}{101.3}\right) - 8{,}314[0.4848\ln(0.4848) + 0.5152\ln(0.5152)]$$

$$= -70{,}150\ \text{J/kmol-K}$$

***K*-values:** Because (7), Table 2.4, will be used to compute the *K*-values, first estimate the vapor pressures using (2-39). For ethylbenzene,

$$\ln P^s_{\text{EB}} = 86.5008 + \left(\frac{-7{,}440.61}{0+350.65}\right) + 0.00623121(350.65) + (-9.87052)\ln(350.65) + 4.13065\times10^{-18}(350.65)^6$$

$$= 9.63481$$

$$P^s_{\text{EB}} = \exp(9.63481) = 15{,}288\ \text{Pa} = 15.288\ \text{kPa}$$

Similarly, $P^s_{\text{S}} = 11.492\ \text{kPa}$

From (7), Table 2.4,

$$K_{\text{EB}} = \frac{15.288}{13.332} = 1.147$$

$$K_{\text{S}} = \frac{11.492}{13.332} = 0.862$$

Relative volatility: From (2-21),

$$\alpha_{\text{EB,S}} = \frac{K_{\text{EB}}}{K_{\text{S}}} = \frac{1.147}{0.862} = 1.331$$

§2.4 GRAPHICAL CORRELATIONS OF THERMODYNAMIC PROPERTIES

Plots of thermodynamic properties are useful not only for the data they contain, but also for the pictoral representation, which permits the user to make general observations, establish correlations, and make extrapolations. All process simulators that contain modules that calculate thermodynamic properties also contain programs that allow the user to make plots of the computed variables. Handbooks and all thermodynamic textbooks contain generalized plots of thermodynamic properties as a function of temperature and pressure. A typical plot is Figure 2.3, which shows vapor pressures of common chemicals for temperatures from below the normal boiling point to the critical temperature where the vapor pressure curves terminate. These curves fit the extended Antoine equation (2-39) reasonably well and are useful in establishing the phase of a pure species and for estimating Raoult's law *K*-values.

Nomographs for determining effects of temperature and pressure on *K*-values of hydrocarbons and light gases are presented in Figures 2.4 and 2.5, which are taken from Hadden and Grayson [15]. In both charts, all *K*-values collapse to 1.0 at a pressure of 5,000 psia (34.5 MPa). This *convergence pressure* depends on the boiling range of the components in the mixture. In Figure 2.6 the components (N_2 to nC_{10}) cover a wide boiling-point range, resulting in a convergence pressure of close to 2,500 psia. For narrow-boiling mixtures such as ethane and propane, the convergence pressure is generally less than 1,000 psia. The *K*-value charts of Figures 2.4 and 2.5 apply to a convergence pressure of 5,000 psia. A procedure for correcting for the convergence pressure is given by Hadden and Grayson [15]. Use of the nomographs is illustrated in Exercise 2.4.

No simple charts are available for estimating liquid–liquid distribution coefficients because of the pronounced effect of composition. However, for ternary systems that are dilute in the solute and contain almost immiscible solvents, a tabulation of distribution (partition) coefficients for the solute is given by Robbins [16].

EXAMPLE 2.4 *K*-Values from a Nomograph.

Petroleum refining begins with distillation of crude oil into different boiling-range fractions. The fraction boiling from 0 to 100°C is light naphtha, a blending stock for gasoline. The fraction boiling from 100 to 200°C, the heavy naphtha, undergoes subsequent processing. One such process is steam cracking, which produces a gas containing ethylene, propylene, and other compounds including benzene and toluene. This gas is sent to a distillation train to separate the mixture into a dozen or more products. In the first column, hydrogen and methane are removed by distillation at 3.2 MPa (464 psia). At a tray in the column where the temperature is 40°F, use Figure 2.4 to estimate *K*-values for H_2, CH_4, C_2H_4, and C_3H_6.

Solution

The *K*-value of hydrogen depends on the other compounds in the mixture. Because benzene and toluene are present, locate a point A

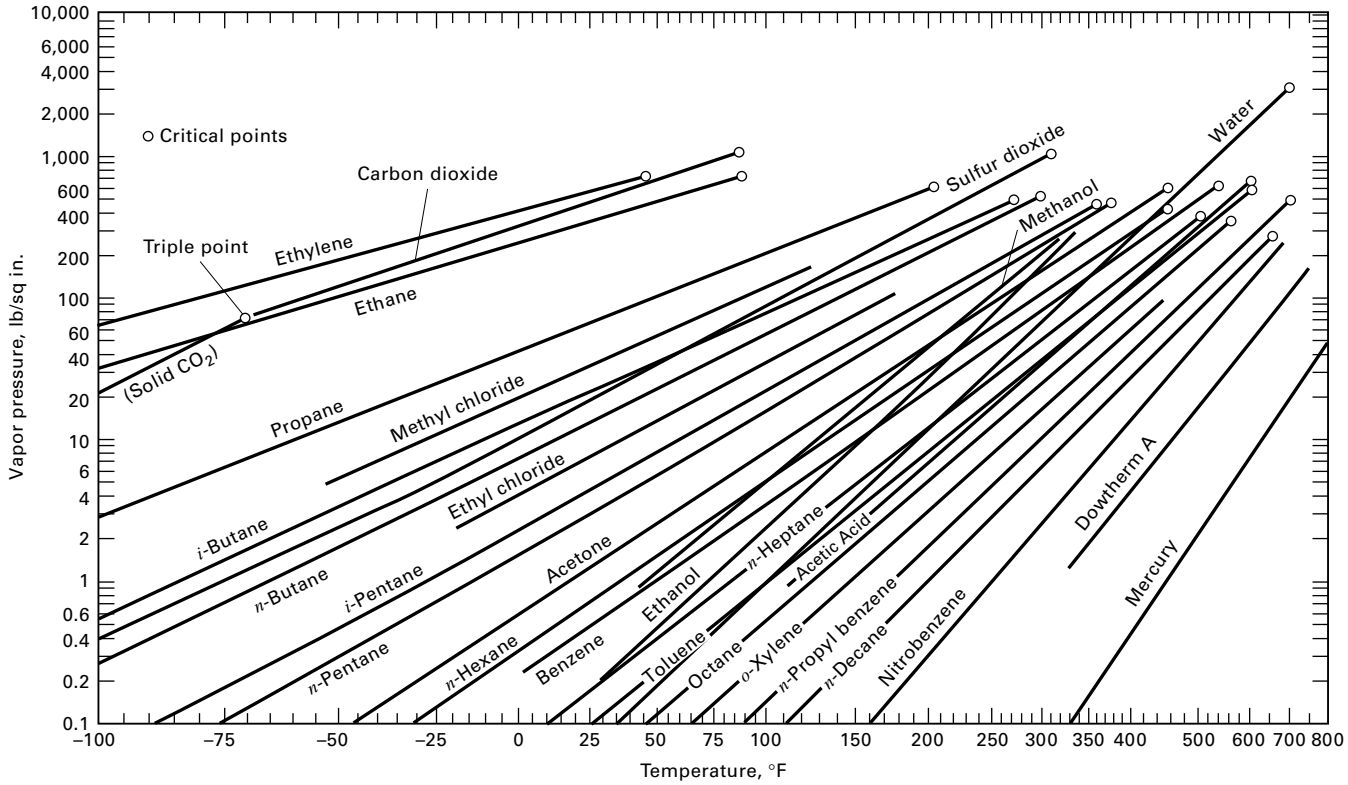

Figure 2.3 Vapor pressure as a function of temperature.

[Adapted from A.S. Faust, L.A. Wenzel, C.W. Clump, L. Maus, and L.B. Andersen, *Principles of Unit Operations*, John Wiley & Sons, New York (1960).]

midway between the points for "H_2 in benzene" and "H_2 in toluene." Next, locate a point B at 40°F and 464 psia on the *T*-*P* grid. Connect points A and B with a straight line and read $K = 100$ where the line intersects the *K* scale. With the same location for point B, read $K = 11$ for methane. For ethylene (ethene) and propylene (propene), the point A is located on the normal boiling-point scale; the same point is used for B. Resulting *K*-values are 1.5 and 0.32, respectively.

§2.5 NONIDEAL THERMODYNAMIC PROPERTY MODELS

Two types of models are used: (1) P–υ–T equation-of-state models and (2) activity coefficient or free-energy models. Their applicability depends on the nature of the components in the mixture and the reliability of the equation constants.

§2.5.1 P–υ–T Equation-of-State Models

A relationship between molar volume, temperature, and pressure is a P–υ–T equation of state. Numerous such equations have been proposed. The simplest is the ideal-gas law, which applies only at low pressures or high temperatures because it neglects the volume occupied by the molecules and the intermolecular forces. All other equations of state attempt to correct for these two deficiencies. The most widely used equations of state are listed in Table 2.5. These and other such equations are discussed by Poling et al. [11].

Not included in Table 2.5 is the van der Waals equation, $P = RT/(\upsilon - b) - a/\upsilon^2$, where a and b are species-dependent constants. The van der Waals equation was the first successful formulation of an equation of state for a nonideal gas. It is rarely used anymore because of its narrow range of application. However, its development suggested that all species have equal reduced molar volumes, $\upsilon_r = \upsilon/\upsilon_c$, at the same reduced temperature, $T_r = T/T_c$, and reduced pressure, $P_r = P/P_c$. This finding, referred to as the *law of corresponding states*, was utilized to develop (2) in Table 2.5 and defines the *compressibility factor*, Z, which is a function of P_r, T_r, and the critical compressibility factor, Z_c, or the *acentric factor*, ω. This was introduced by Pitzer et al. [17] to account for differences in molecular shape and is determined from the vapor pressure curve by:

$$\omega = \left[-\log\left(\frac{P^s}{P_c}\right)_{T_r=0.7}\right] - 1.000 \qquad (2\text{-}45)$$

The value for ω is zero for symmetric molecules. Some typical values of ω are 0.264, 0.490, and 0.649 for toluene, *n*-decane, and ethyl alcohol, respectively, as taken from the extensive tabulation of Poling et al. [11].

In 1949, Redlich and Kwong [18] published an equation of state that, like the van der Waals equation, contains only two constants, both of which can be determined from T_c and P_c, by applying the critical conditions

$$\left(\frac{\partial P}{\partial \upsilon}\right)_{T_c} = 0 \quad \text{and} \quad \left(\frac{\partial^2 P}{\partial \upsilon^2}\right)_{T_c} = 0$$

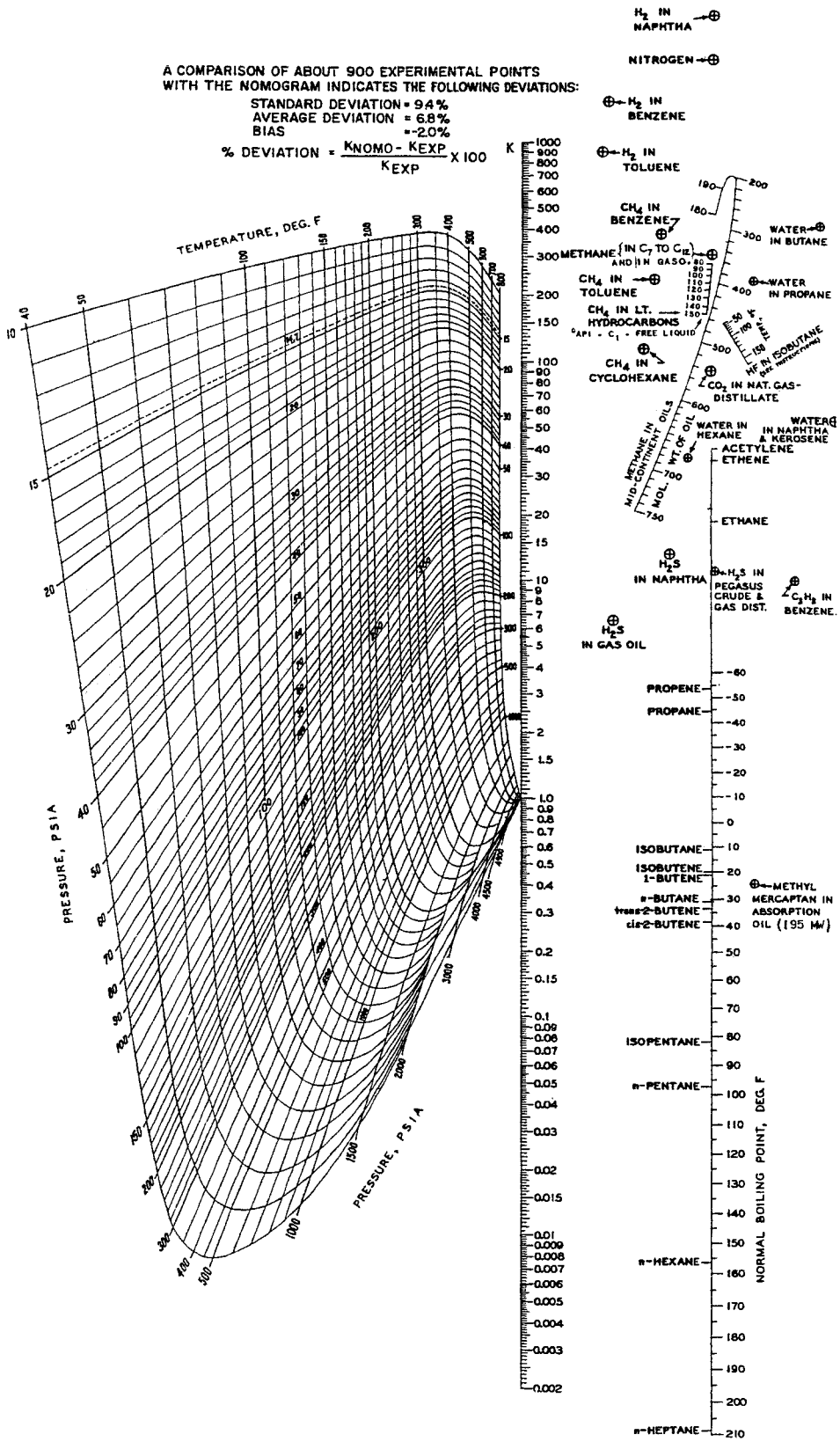

Figure 2.4 Vapor–liquid equilibria, 40 to 800°F.

[From S.T. Hadden and H.G. Grayson, *Hydrocarbon Proc. and Petrol. Refiner*, **40**, 207 (Sept. 1961), with permission.]

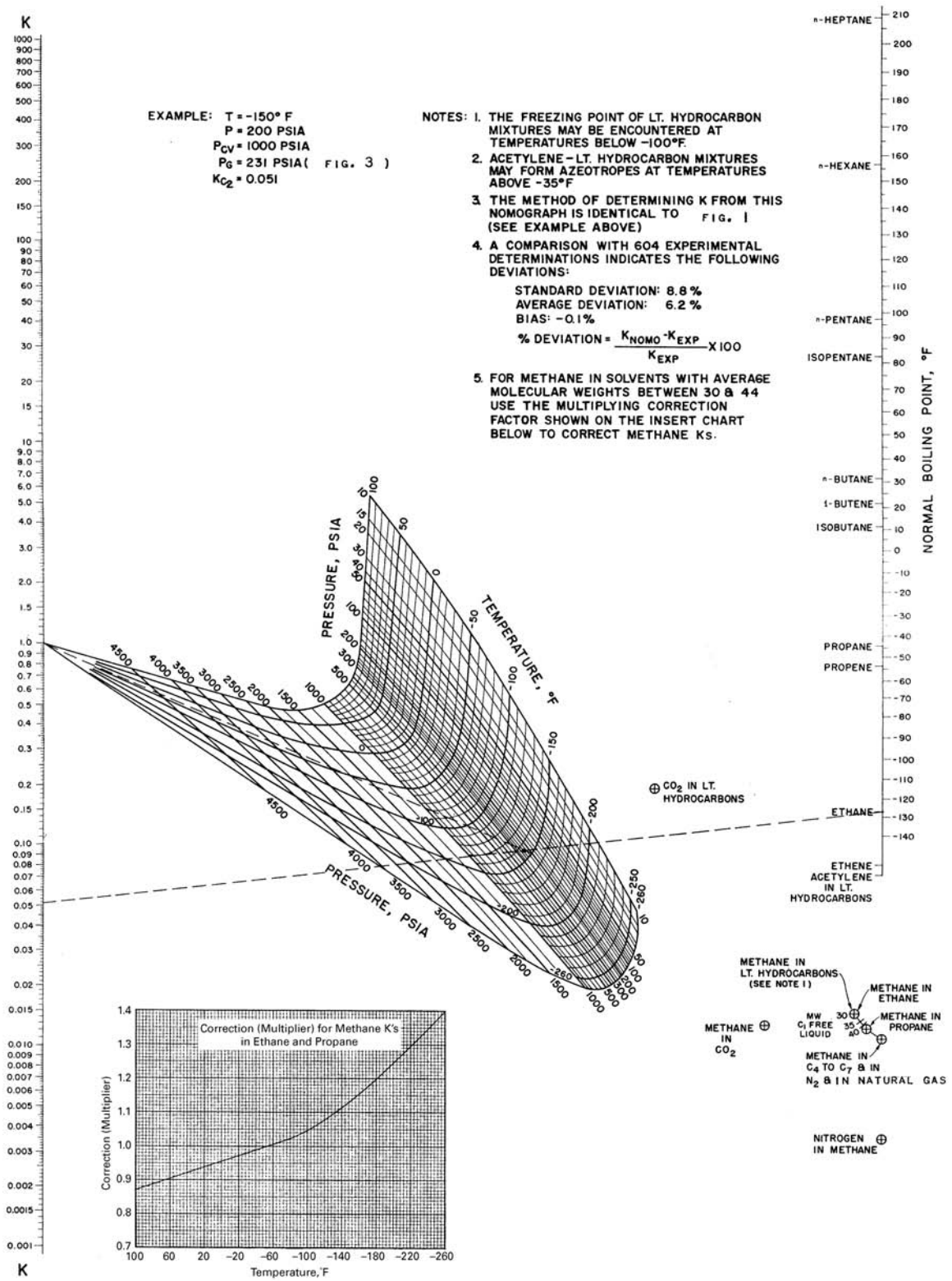

Figure 2.5 Vapor–liquid equilibria, −260 to 100°F.

[From S.T. Hadden and H.G. Grayson, *Hydrocarbon Proc. and Petrol. Refiner*, **40**, 207 (Sept. 1961), with permission.]

The R–K equation, given as (3) in Table 2.5, is an improvement over the van der Waals equation. Shah and Thodos [19] showed that the R–K equation, when applied to nonpolar compounds, has accuracy comparable with that of equations containing many more constants. Furthermore, the R–K equation can approximate the liquid-phase region.

If the R–K equation is expanded to obtain a common denominator, a cubic equation in v results. Alternatively, (2)

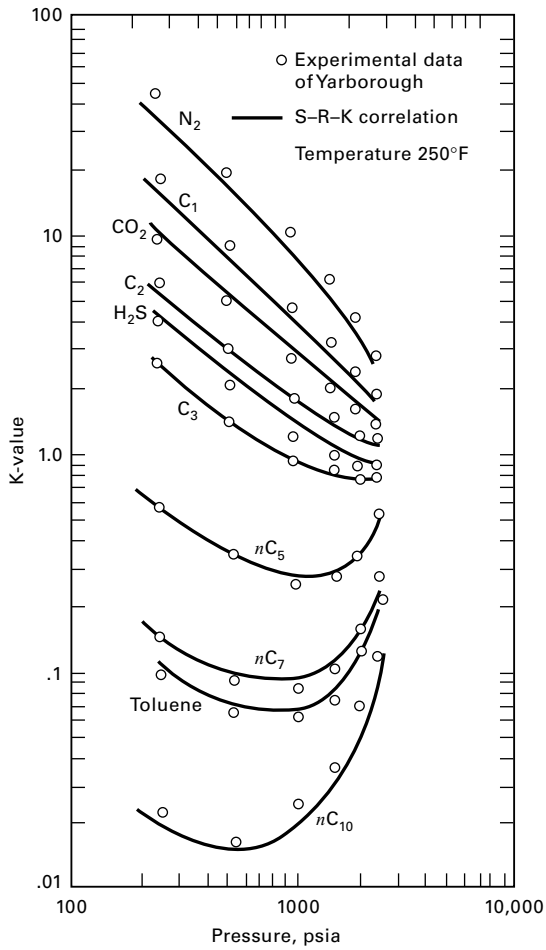

Figure 2.6 Comparison of experimental *K*-value data and S–R–K correlation.

and (3) in Table 2.5 can be combined to eliminate υ to give the compressibility factor, Z, form of the equation:

$$Z^3 - Z^2 + \left(A - B - B^2\right)Z - AB = 0 \qquad (2\text{-}46)$$

where

$$A = \frac{aP}{R^2T^2} \qquad (2\text{-}47)$$

$$B = \frac{bP}{RT} \qquad (2\text{-}48)$$

Equation (2-46), a cubic in Z, can be solved analytically for three roots (e.g., see *Perry's Handbook*, 8th ed., p. 3-10). At supercritical temperatures, where only one phase exists, one real root and a complex conjugate pair of roots are obtained. Below the critical temperature, where vapor and/or liquid phases can exist, three real roots are obtained, with the largest value of Z applying to the vapor and the smallest root corresponding to the liquid (Z_V and Z_L).

The intermediate value of Z is discarded.

To apply the R–K equation to mixtures, *mixing rules* are used to average the constants a and b for each component. The recommended rules for vapor mixtures of C components are

$$a = \sum_{i=1}^{C}\left[\sum_{j=1}^{C} y_i y_j \left(a_i a_j\right)^{0.5}\right] \qquad (2\text{-}49)$$

$$b = \sum_{i=1}^{C} y_i b_i \qquad (2\text{-}50)$$

EXAMPLE 2.5 Specific Volume of a Mixture from the R–K Equation.

Use the R–K equation to estimate the specific volume of a vapor mixture containing 26.92 wt% propane at 400°F (477.6 K) and a saturation pressure of 410.3 psia (2,829 kPa). Compare the results with the experimental data of Glanville et al. [20].

Table 2.5 Useful Equations of State

Name	Equation	Equation Constants and Functions
(1) Ideal-gas law	$P = \dfrac{RT}{\upsilon}$	None
(2) Generalized	$P = \dfrac{ZRT}{\upsilon}$	$Z = Z\{P_r, T_r, Z_c \text{ or } \omega\}$ as derived from data
(3) Redlich–Kwong (R–K)	$P = \dfrac{RT}{\upsilon - b} - \dfrac{a}{\upsilon^2 + b\upsilon}$	$b = 0.08664RT_c/P_c$ $a = 0.42748R^2T_c^{2.5}/P_cT^{0.5}$
(4) Soave–Redlich–Kwong (S–R–K or R–K–S)	$P = \dfrac{RT}{\upsilon - b} - \dfrac{a}{\upsilon^2 + b\upsilon}$	$b = 0.08664RT_c/P_c$ $a = 0.42748R^2T_c^2\left[1 + f_\omega\left(1 - T_r^{0.5}\right)\right]^2/P_c$ $f_\omega = 0.48 + 1.574\omega - 0.176\omega^2$
(5) Peng–Robinson (P–R)	$P = \dfrac{RT}{\upsilon - b} - \dfrac{a}{\upsilon^2 + 2b\upsilon - b^2}$	$b = 0.07780RT_c/P_c$ $a = 0.45724R^2T_c^2\left[1 + f_\omega\left(1 - T_r^{0.5}\right)\right]^2/P_c$ $f_\omega = 0.37464 + 1.54226\omega - 0.26992\omega^2$

Solution

Let propane be denoted by P and benzene by B. The mole fractions are

$$y_P = \frac{0.2692/44.097}{(0.2692/44.097) + (0.7308/78.114)} = 0.3949$$

$$y_B = 1 - 0.3949 = 0.6051$$

The critical constants are given by Poling et al. [11]:

	Propane	Benzene
T_c, K	369.8	562.2
P_c, kPa	4,250	4,890

From Table 2.5, b and a for propane in the R–K equation, in SI units, are:

$$b_P = \frac{0.08664(8.3144)(369.8)}{4{,}250} = 0.06268 \text{ m}^3/\text{kmol}$$

$$a_P = \frac{0.42748(8.3144)^2(369.8)^{2.5}}{(4{,}250)(477.59)^{0.5}}$$

$$= 836.7 \text{ kPa-m}^6/\text{kmol}^2$$

Similarly, for benzene, $b_B = 0.08263$ m^3/kmol and $a_B = 2{,}072$ kPa-m^6/kmol^2.

From (2-50),

$$b = (0.3949)(0.06268) + (0.6051)(0.08263) = 0.07475 \text{ m}^3/\text{kmol}$$

From (2-49),

$$a = y_P^2 a_P + 2y_P y_B (a_P a_B)^{0.5} + y_B^2 a_B$$

$$= (0.3949)^2(836.7) + 2(0.3949)(0.6051)[(836.7)(2{,}072)]^{0.5} + (0.6051)^2(2{,}072) = 1{,}518 \text{ kPa-m}^6/\text{kmol}^2$$

From (2-47) and (2-48) using SI units,

$$A = \frac{(1{,}518)(2{,}829)}{(8.314)^2(477.59)^2} = 0.2724$$

$$B = \frac{(0.07475)(2{,}829)}{(8.314)(477.59)^2} = 0.05326$$

From (2-46), the cubic Z form of the R–K equation is obtained:

$$Z^3 - Z^2 + 0.2163Z - 0.01451 = 0$$

This equation gives one real root and a pair of complex roots:

$$Z = 0.7314, \quad 0.1314 + 0.04243i, \quad 0.1314 - 0.04243i$$

The one real root is assumed to be that for the vapor phase.
From (2) of Table 2.5, the molar volume is

$$\upsilon = \frac{ZRT}{P} = \frac{(0.7314)(8.314)(477.59)}{2{,}829} = 1.027 \text{ m}^3/\text{kmol}$$

The average molecular weight of the mixture is 64.68 kg/kmol. The specific volume is

$$\frac{\upsilon}{M} = \frac{1.027}{64.68} = 0.01588 \text{ m}^3/\text{kg} = 0.2543 \text{ ft}^3/\text{lb}$$

Glanville et al. report experimental values of $Z = 0.7128$ and $\upsilon/M = 0.2478$ ft^3/lb, which are within 3% of the estimated values.

Following the work of Wilson [21], Soave [6] added a third parameter, the acentric factor, ω, to the R–K equation. The resulting Soave–Redlich–Kwong (S–R–K) or Redlich–Kwong–Soave (R–K–S) equation, given as (4) in Table 2.5, was accepted for application to mixtures of hydrocarbons because of its simplicity and accuracy. It makes the parameter a a function of ω and T, thus achieving a good fit to vapor pressure data and thereby improving the ability of the equation to predict liquid-phase properties.

Four years after the introduction of the S–R–K equation, Peng and Robinson [7] presented a modification of the R–K and S–R–K equations to achieve improved agreement in the critical region and for liquid molar volume. The Peng–Robinson (P–R) equation of state is (5) in Table 2.5. The S–R–K and P–R equations of state are widely applied in calculations for saturated vapors and liquids. For mixtures of hydrocarbons and/or light gases, the mixing rules are given by (2-49) and (2-50), except that (2-49) is often modified to include a binary interaction coefficient, k_{ij}:

$$a = \sum_{i=1}^{C} \left[\sum_{j=1}^{C} y_i y_j (a_i a_j)^{0.5} (1 - k_{ij}) \right] \tag{2-51}$$

Values of k_{ij} from experimental data have been published for both the S–R–K and P–R equations, e.g., Knapp et al. [22]. Generally k_{ij} is zero for hydrocarbons paired with hydrogen or other hydrocarbons.

Although the S–R–K and P–R equations were not intended to be used for mixtures containing polar organic compounds, they are applied by employing large values of k_{ij} in the vicinity of 0.5, as back-calculated from data. However, a preferred procedure for polar organics is to use a mixing rule such as that of Wong and Sandler, which is discussed in Chapter 11 and which bridges the gap between a cubic equation of state and an activity-coefficient equation.

Another model for polar and nonpolar substances is the virial equation of state due to Thiesen [23] and Onnes [24]. A common representation is a power series in $1/\upsilon$ for Z:

$$Z = 1 + \frac{B}{\upsilon} + \frac{C}{\upsilon^2} + \cdots \tag{2-52}$$

A modification of the virial equation is the Starling form [5] of the Benedict–Webb–Rubin (B–W–R) equation for hydrocarbons and light gases. Walas [25] presents a discussion of B–W–R-type equations, which—because of the large number of terms and species constants (at least 8)—is not widely used except for pure substances at cryogenic temperatures. A more useful modification of the B–W–R equation is a generalized corresponding-states form developed by Lee and Kesler [26] with an extension to mixtures by Plöcker et al. [8]. All of the constants in the L–K–P equation are given in terms of the acentric factor and reduced temperature and pressure, as developed from P–υ–T data for three simple fluids (ω = 0), methane, argon, and krypton, and a reference fluid (ω = 0.398), *n*-octane. The equations, constants, and mixing rules are given by Walas [25]. The L–K–P equation describes vapor and liquid mixtures of hydrocarbons and/or light gases over wide ranges of T and P.

§2.5.2 Derived Thermodynamic Properties from *P–υ–T* Models

If a temperature-dependent, ideal-gas heat capacity or enthalpy equation such as (2-35) or (2-36) is available, along with an equation of state, all other vapor- and liquid-phase properties can be derived from the integral equations in Table 2.6. These equations, in the form of departure from the ideal-gas equations of Table 2.4, apply to vapor or liquid.

When the ideal-gas law, $P = RT/\upsilon$, is substituted into Eqs. (1) to (4) of Table 2.6, the results for the vapor are

$$(h - h_V^o) = 0, \ \phi = 1$$
$$(s - s_V^o) = 0, \ \phi = 1$$

When the R–K equation is substituted into the equations of Table 2.6, the results for the vapor phase are:

$$h_V = \sum_{i=1}^{C} \left(y_i h_{iV}^o\right) + RT\left[Z_V - 1 - \frac{3A}{2B}\ln\left(1 + \frac{B}{Z_V}\right)\right] \quad (2\text{-}53)$$

$$s_V = \sum_{i=1}^{C} \left(y_i s_{iV}^o\right) - R\ln\left(\frac{P}{P^o}\right) - R\sum_{i=1}^{C}(y_i \ln y_i) + R\ln(Z_V - B) \quad (2\text{-}54)$$

$$\phi_V = \exp\left[Z_V - 1 - \ln(Z_V - B) - \frac{A}{B}\ln\left(1 + \frac{B}{Z_V}\right)\right] \quad (2\text{-}55)$$

Table 2.6 Integral Departure Equations of Thermodynamics

At a given temperature and composition, the following equations give the effect of pressure above that for an ideal gas.

Mixture enthalpy:

(1) $$\left(h - h_V^o\right) = P\upsilon - RT - \int_\infty^\upsilon \left[P - T\left(\frac{\partial P}{\partial T}\right)_\upsilon\right] d\upsilon$$

Mixture entropy:

(2) $$\left(s - s_V^o\right) = \int_\infty^\upsilon \left(\frac{\partial P}{\partial T}\right)_\upsilon d\upsilon - \int_\infty^\upsilon \frac{R}{\upsilon} d\upsilon$$

Pure-component fugacity coefficient:

(3) $$\phi_{iV} = \exp\left[\frac{1}{RT}\int_0^P \left(\upsilon - \frac{RT}{P}\right) dP\right] = \exp\left[\frac{1}{RT}\int_\upsilon^\infty \left(P - \frac{RT}{\upsilon}\right) d\upsilon - \ln Z + (Z - 1)\right]$$

Partial fugacity coefficient:

(4) $$\bar{\phi}_{iV} = \exp\left\{\frac{1}{RT}\int_V^\infty \left[\left(\frac{\partial P}{\partial N_i}\right)_{T,V,N_j} - \frac{RT}{V}\right] dV - \ln Z\right\}$$

where $V = \upsilon\sum_{i=1}^{C} N_i$

$$\bar{\phi}_{iV} = \exp\left[(Z_V - 1)\frac{B_i}{B} - \ln(Z_V - B) - \frac{A}{B}\left(2\sqrt{\frac{A_i}{A}} - \frac{B_i}{B}\right)\ln\left(1 + \frac{B}{Z_V}\right)\right] \quad (2\text{-}56)$$

The results for the liquid phase are identical if y_i and Z_V (but not h_{iV}^o) are replaced by x_i and Z_L, respectively. The liquid-phase forms of (2-53) and (2-54) account for the enthalpy and entropy of vaporization. This is because the R–K equation of state, as well as the S–R–K and P–R equations, are continuous functions through the vapor and liquid regions, as shown for enthalpy in Figure 2.7. Thus, the liquid enthalpy is determined by accounting for four effects, at a temperature below the critical. From (1), Table 2.6, and Figure 2.7:

$$h_L = h_V^o + P\upsilon - RT - \int_\infty^\upsilon \left[P - T\left(\frac{\partial P}{\partial T}\right)_\upsilon\right] d\upsilon$$
$$= \underbrace{h_V^o}_{\text{(1) Vapor at zero pressure}}$$
$$+ \underbrace{(P\upsilon)_{V_s} - RT - \int_\infty^{\upsilon_{V_s}} \left[P - T\left(\frac{\partial P}{\partial T}\right)_\upsilon\right] d\upsilon}_{\text{(2) Pressure correction for vapor to saturation pressure}}$$
$$- \underbrace{T\left(\frac{\partial P}{\partial T}\right)_s (\upsilon_{V_s} - \upsilon_{L_s})}_{\text{(3) Latent heat of vaporization}}$$
$$+ \underbrace{\left[(P\upsilon)_L - (P\upsilon)_{L_s}\right] - \int_{\upsilon_{L_s}}^{\upsilon_L} \left[P - T\left(\frac{\partial P}{\partial T}\right)_\upsilon\right] d\upsilon}_{\text{(4) Correction to liquid for pressure in excess of saturation pressure}} \quad (2\text{-}57)$$

where the subscript s refers to the saturation pressure.

The fugacity coefficient, ϕ, of a pure species from the R–K equation, as given by (2-55), applies to the vapor for $P < P_i^s$. For $P > P_i^s$, ϕ is the liquid fugacity coefficient. Saturation pressure corresponds to the condition of $\phi_V = \phi_L$. Thus, at a temperature $T < T_c$, the vapor pressure, P^s, can be

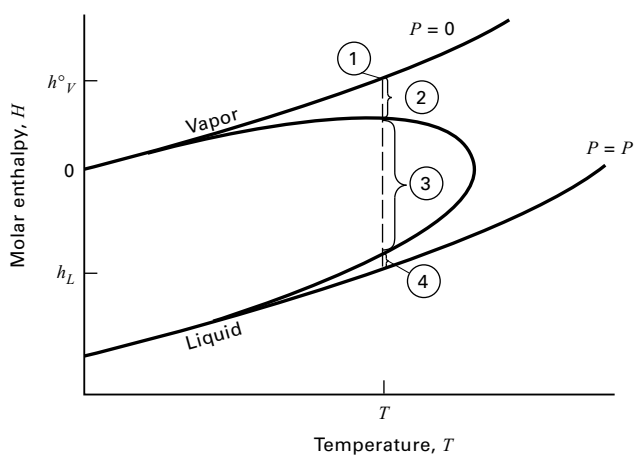

Figure 2.7 Contributions to enthalpy.

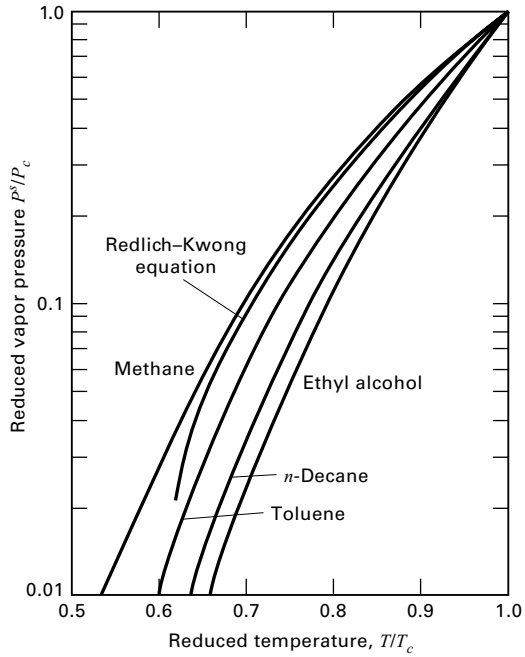

Figure 2.8 Reduced vapor pressure.

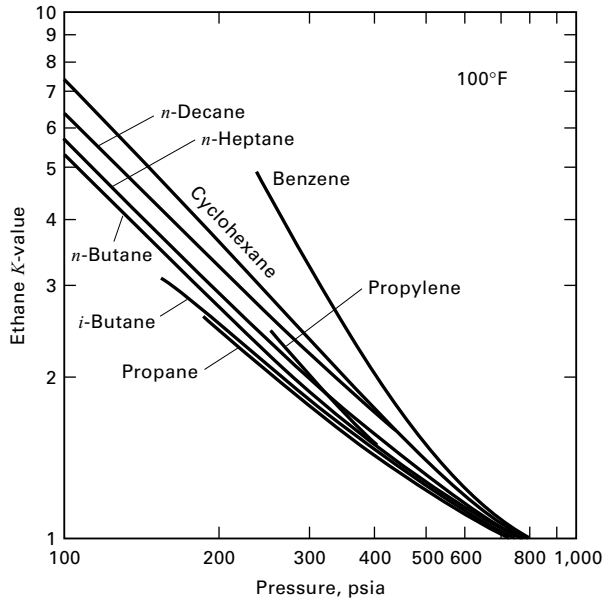

Curves represent experimental data of:
Kay et al. (Ohio State Univ.) Robinson et al. (Univ. Alberta)
Sage et al. (Calif. Inst. Tech.) Thodos (Northwestern)

Figure 2.9 *K*-values of ethane in binary hydrocarbon mixtures at 100°F.

estimated from the R–K equation of state by setting (2-55) for the vapor equal to (2-55) for the liquid and solving for P, which equals P^s.

The results of Edmister [27] are plotted in Figure 2.8. The R–K vapor-pressure curve does not satisfactorily represent data for a wide range of molecular shapes, as witnessed by the data for methane, toluene, *n*-decane, and ethyl alcohol. This failure represents a shortcoming of the R–K equation and is why Soave [6] modified the R–K equation by introducing the acentric factor, ω. Thus, while the critical constants T_c and P_c are insufficient to generalize thermodynamic behavior, a substantial improvement results by incorporating a third parameter that represents the generic differences in the reduced-vapor-pressure curves.

As seen in (2-56), partial fugacity coefficients depend on pure-species properties, A_i and B_i, and mixture properties, A and B. Once $\bar{\phi}_{iV}$ and $\bar{\phi}_{iL}$ are computed from (2-56), a *K*-value can be estimated from (2-26).

The most widely used P–υ–T equations of state are the S–R–K, P–R, and L–K–P. These are combined with the integral departure equations of Table 2.6 to obtain equations for estimating enthalpy, entropy, fugacity coefficients, partial fugacity coefficients, and *K*-values. The results of the integrations are complex and unsuitable for manual calculations. However, the calculations are readily made by computer programs incorporated into all process simulation programs.

Ideal *K*-values as determined from Eq. (7) in Table 2.4 depend only on temperature and pressure. Most frequently, they are suitable for mixtures of nonpolar compounds such as paraffins and olefins. Figure 2.9 shows experimental *K*-value curves for ethane in binary mixtures with other, less volatile hydrocarbons at 100°F (310.93 K), which is close to ethane's critical temperature of 305.6 K, for pressures from 100 psia (689.5 kPa) to *convergence pressures* between 720 and 780 psia (4.964 MPa to 5.378 MPa). At the convergence pressure, separation by distillation is impossible because *K*-values become 1.0. Figure 2.9 shows that at 100°F, ethane does not form ideal solutions with all the other components because the *K*-values depend on the other component, even for paraffin homologs. For example, at 300 psia, the *K*-value of ethane in benzene is 80% higher than the *K*-value of ethane in propane.

The ability of equations of state, such as S–R–K, P–R, and L–K–P equations, to predict the effects of composition, temperature, and pressure on *K*-values of mixtures of hydrocarbons and light gases is shown in Figure 2.6. The mixture contains 10 species ranging in volatility from nitrogen to *n*-decane. The experimental data points, covering almost a 10-fold range of pressure at 250°F, are those of Yarborough [28]. Agreement with the S–R–K equation is very good.

EXAMPLE 2.6 Effect of EOS on Calculations.

In the thermal hydrodealkylation of toluene to benzene ($C_7H_8 + H_2 \rightarrow C_6H_6 + CH_4$), excess hydrogen minimizes cracking of aromatics to light gases. In practice, conversion of toluene per pass through the reactor is only 70%. To separate and recycle hydrogen, hot reactor-effluent vapor of 5,597 kmol/h at 500 psia (3,448 kPa) and 275°F (408.2 K) is partially condensed to 120°F (322 K), with phases separated in a flash drum. If the composition of the reactor effluent is as given below and the flash pressure is 485 psia (3,344 kPa), calculate equilibrium compositions and flow rates of vapor and liquid leaving the drum and the amount of heat transferred, using a process simulation program for each of the equation-of-state models discussed above. Compare the results, including *K*-values and enthalpy and entropy changes.

Component	Mole Fraction
Hydrogen (H)	0.3177
Methane (M)	0.5894
Benzene (B)	0.0715
Toluene (T)	0.0214
	1.0000

Solution

The computations were made using the S–R–K, P–R, and L–K–P equations of state. The results at 120°F and 485 psia are:

	Equation of State		
	S–R–K	P–R	L–K–P
Vapor flows, kmol/h:			
Hydrogen	1,777.1	1,774.9	1,777.8
Methane	3,271.0	3,278.5	3,281.4
Benzene	55.1	61.9	56.0
Toluene	6.4	7.4	7.0
Total	5,109.6	5,122.7	5,122.2
Liquid flows, kmol/h:			
Hydrogen	1.0	3.3	0.4
Methane	27.9	20.4	17.5
Benzene	345.1	338.2	344.1
Toluene	113.4	112.4	112.8
Total	487.4	474.3	474.8
***K*-values:**			
Hydrogen	164.95	50.50	466.45
Methane	11.19	14.88	17.40
Benzene	0.01524	0.01695	0.01507
Toluene	0.00537	0.00610	0.00575
Enthalpy change, GJ/h	35.267	34.592	35.173
Entropy change, MJ/h-K	−95.2559	−93.4262	−95.0287
Percent of benzene and toluene condensed	88.2	86.7	87.9

Because the reactor effluent is mostly hydrogen and methane, the effluent at 275°F and 500 psia, and the equilibrium vapor at 120°F and 485 psia, are nearly ideal gases ($0.98 < Z < 1.00$), despite the moderately high pressures. Thus, the enthalpy and entropy changes are dominated by vapor heat capacity and latent heat effects, which are independent of which equation of state is used. Consequently, the enthalpy and entropy changes differ by less than 2%.

Significant differences exist for the *K*-values of H_2 and CH_4. However, because the values are large, the effect on the amount of equilibrium vapor is small. Reasonable *K*-values for H_2 and CH_4, based on experimental data, are 100 and 13, respectively. *K*-values for benzene and toluene differ among the three equations of state by as much as 11% and 14%, respectively, which, however, causes less than a 2% difference in the percentage of benzene and toluene condensed. Raoult's law *K*-values for benzene and toluene are 0.01032 and 0.00350, which are considerably lower than the values computed from the three equations of state because deviations to fugacities due to pressure are important.

Note that the material balances are always precisely satisfied. Users of simulation programs should never take this as an indication that the results are correct but instead should always verify results in all possible ways.

§2.6 LIQUID ACTIVITY-COEFFICIENT MODELS

Predictions of liquid properties based on *Gibbs free-energy models* for predicting liquid-phase activity coefficients, and other excess functions such as volume and enthalpy of mixing, are developed in this section. Regular-solution theory, which describes mixtures of nonpolar compounds using only constants for the pure components, is presented first, followed by models useful for mixtures containing polar compounds, which require experimentally determined *binary interaction parameters*. If these are not available, group-contribution methods can be used to make estimates. All models can predict vapor–liquid equilibria; and some can estimate liquid–liquid and even solid–liquid and polymer–liquid equilibria.

For polar compounds, dependency of *K*-values on composition is due to nonideal behavior in the liquid phase. For hydrocarbons, Prausnitz, Edmister, and Chao [29] showed that the relatively simple *regular-solution theory* of Scatchard and Hildebrand [30] can be used to estimate deviations due to nonideal behavior. They expressed *K*-values in terms of (2-27), $K_i = \gamma_{iL}\phi_{iL}/\bar{\phi}_{iV}$. Chao and Seader [9] simplified and extended application of this equation to hydrocarbons and light gases in the form of a compact set of equations. These were widely used before the availability of the S–R–K and P–R equations.

For hydrocarbon mixtures, regular-solution theory is based on the premise that nonideality is due to differences in van der Waals forces of attraction among the molecules present. Regular solutions have an endothermic heat of mixing, and activity coefficients are greater than 1. These solutions are regular in that molecules are assumed to be randomly dispersed. Unequal attractive forces between like and unlike molecule pairs cause segregation of molecules. However, for regular solutions the species concentrations on a molecular level are identical to overall solution concentrations. Therefore, excess entropy due to segregation is zero and entropy of regular solutions is identical to that of ideal solutions, where the molecules are randomly dispersed.

§2.6.1 Activity Coefficients from Gibbs Free Energy

Activity-coefficient equations are often based on Gibbs free-energy models. The molar Gibbs free energy, g, is the sum of the molar free energy of an ideal solution and an excess molar free energy g^E for nonideal effects. For a liquid

$$\begin{aligned} g &= \sum_{i=1}^{C} x_i g_i + RT \sum_{i=1}^{C} x_i \ln x_i + g^E \\ &= \sum_{i=1}^{C} x_i \left(g_i + RT \ln x_i + \bar{g}_i^E\right) \end{aligned} \tag{2-58}$$

where $g = h - Ts$ and excess molar free energy is the sum of the partial excess molar free energies, which are related to the liquid-phase activity coefficients by

$$\frac{\bar{g}_i^E}{RT} = \ln \gamma_i = \left[\frac{\partial(N_t g^E/RT)}{\partial N_i}\right]_{P,T,N_j} = \frac{g^E}{RT} - \sum_k x_k \left[\frac{\partial(g^E/RT)}{\partial x_k}\right]_{P,T,x_r} \tag{2-59}$$

where $j \neq i, r \neq k, k \neq i$, and $r \neq i$.

The relationship between excess molar free energy and excess molar enthalpy and entropy is

$$g^E = h^E - Ts^E = \sum_{i=1}^{C} x_i\left(\bar{h}_i^E - T\bar{s}_i^E\right) \tag{2-60}$$

§2.6.2 Regular-Solution Model

For a regular liquid solution, the excess molar free energy is based on nonideality due to differences in molecular size and intermolecular forces. The former are expressed in terms of liquid molar volume, and the latter in terms of the enthalpy of vaporization. The resulting model is

$$g^E = \sum_{i=1}^{C} (x_i \upsilon_{iL}) \left[\frac{1}{2}\sum_{i=1}^{C}\sum_{j=1}^{C} \Phi_i \Phi_j \left(\delta_i - \delta_j\right)^2\right] \tag{2-61}$$

where Φ is the volume fraction assuming additive molar volumes, given by

$$\Phi_i = \frac{x_i \upsilon_{iL}}{\sum_{j=1}^{C} x_j \upsilon_{jL}} = \frac{x_i \upsilon_{iL}}{\upsilon_L} \tag{2-62}$$

and δ is the solubility parameter, which is defined in terms of the volumetric internal energy of vaporization as

$$\delta_i = \left(\frac{\Delta E_i^{\text{vap}}}{\upsilon_{iL}}\right)^{1/2} \tag{2-63}$$

Combining (2-59) with (2-61) yields an expression for the activity coefficient in a regular solution:

$$\ln \gamma_{iL} = \frac{\upsilon_{iL}\left(\delta_i - \sum_{j=1}^{C} \Phi_j \delta_j\right)^2}{RT} \tag{2-64}$$

Because $\ln \gamma_{iL}$ varies almost inversely with absolute temperature, υ_{iL} and δ_j are taken as constants at a reference temperature, such as 25°C. Thus, the estimation of γ_L by regular-solution theory requires only the pure-species constants υ_L and δ. The latter parameter is often treated as an empirical constant determined by back-calculation from experimental data. For species with a critical temperature below 25°C, υ_L and δ at 25°C are hypothetical. However, they can be evaluated by back-calculation from data.

When molecular-size differences—as reflected by liquid molar volumes—are appreciable, the Flory–Huggins size correction given below can be added to the regular-solution free-energy contribution:

$$g^E = RT \sum_{i=1}^{C} x_i \ln\left(\frac{\Phi_i}{x_i}\right) \tag{2-65}$$

Substitution of (2-65) into (2-59) gives

$$\ln \gamma_{iL} = \ln\left(\frac{\upsilon_{iL}}{\upsilon_L}\right) + 1 - \left(\frac{\upsilon_{iL}}{\upsilon_L}\right) \tag{2-66}$$

Thus, the activity coefficient of a species in a regular solution, including the Flory–Huggins correction, is

$$\gamma_{iL} = \exp\left[\frac{\upsilon_{iL}\left(\delta_i - \sum_{j=1}^{C} \Phi_j \delta_j\right)^2}{RT} + \ln\left(\frac{\upsilon_{iL}}{\upsilon_L}\right) + 1 - \frac{\upsilon_{iL}}{\upsilon_L}\right] \tag{2-67}$$

EXAMPLE 2.7 Activity Coefficients from Regular-Solution Theory.

Yerazunis et al. [31] measured liquid-phase activity coefficients for the *n*-heptane/toluene system at 1 atm (101.3 kPa). Estimate activity coefficients using regular-solution theory both with and without the Flory–Huggins correction. Compare estimated values with experimental data.

Solution

Experimental liquid-phase compositions and temperatures for 7 of 19 points are as follows, where H denotes heptane and T denotes toluene:

T, °C	x_H	x_T
98.41	1.0000	0.0000
98.70	0.9154	0.0846
99.58	0.7479	0.2521
101.47	0.5096	0.4904
104.52	0.2681	0.7319
107.57	0.1087	0.8913
110.60	0.0000	1.0000

At 25°C, liquid molar volumes are $\upsilon_{H_L} = 147.5\ \text{cm}^3/\text{mol}$ and $\upsilon_{T_L} = 106.8\ \text{cm}^3/\text{mol}$. Solubility parameters are 7.43 and 8.914 $(\text{cal/cm}^3)^{1/2}$, respectively, for H and T. As an example, consider 104.52°C. From (2-62), volume fractions are

$$\Phi_H = \frac{0.2681(147.5)}{0.2681(147.5) + 0.7319(106.8)} = 0.3359$$

$$\Phi_T = 1 - \Phi_H = 1 - 0.3359 = 0.6641$$

Substitution of these values, together with the solubility parameters, into (2-64) gives

$$\gamma_H = \exp\left\{\frac{147.5[7.430 - 0.3359(7.430) - 0.6641(8.914)]^2}{1.987(377.67)}\right\} = 1.212$$

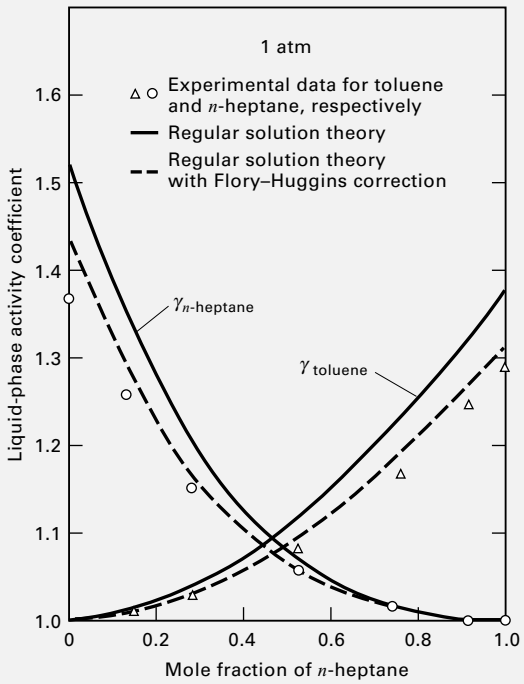

Figure 2.10 Liquid-phase activity coefficients for *n*-heptane/toluene system at 1 atm.

Values of γ_H and γ_T computed in this manner for all seven liquid-phase conditions are plotted in Figure 2.10.

Applying (2-67) at 104.52°C with the Flory–Huggins correction gives

$$\gamma_H = \exp\left[0.1923 + \ln\left(\frac{147.5}{117.73}\right) + 1 - \left(\frac{147.5}{117.73}\right)\right] = 1.179$$

Values of the computed γ_H and γ_T are included in Figure 2.10.

Deviations from experimental data are not greater than 12% for regular-solution theory and not greater than 6% with the Flory–Huggins correction. Unfortunately, good agreement is not always obtained for nonpolar hydrocarbon solutions, as shown, for example, by Hermsen and Prausnitz [32], who studied the cyclopentane/benzene system.

§2.6.3 Nonideal Liquid Solutions

With dissimilar polar species that can form or break hydrogen bonds, the ideal-liquid-solution assumption is invalid and regular-solution theory is also not applicable. Ewell, Harrison, and Berg [33] provide a classification based on the potential for association or solvation due to hydrogen-bond formation. If a molecule contains a hydrogen atom attached to a donor atom (O, N, F, and in certain cases C), the active hydrogen atom can form a bond with another molecule containing a donor atom. The classification in Table 2.7 permits qualitative estimates of deviations from Raoult's law for binary pairs when used in conjunction with Table 2.8. Positive deviations correspond to values of $\gamma_{iL} > 1$. Nonideality results in variations of γ_{iL} with composition, as shown in Figure 2.11 for several binary systems, where the Roman numerals refer to classification in Tables 2.7 and 2.8. Starting with Figure 2.11a, the following explanations for the nonidealities are offered: *n*-heptane (V) breaks ethanol (II) hydrogen bonds, causing strong positive deviations. In Figure 2.11b, similar, but less positive, deviations occur when acetone (III) is added to formamide (I). Hydrogen bonds are broken and formed with chloroform (IV) and methanol (II) in Figure 2.11c, resulting in an unusual deviation curve for chloroform that passes through a maximum. In Figure 2.11d, chloroform (IV) provides active hydrogen atoms that form hydrogen bonds with oxygen atoms of acetone (III), thus causing negative deviations. For water (I) and *n*-butanol (II) in Figure 2.11e, hydrogen bonds of both molecules are broken, and nonideality is sufficiently strong to cause formation of two immiscible liquid phases.

Nonideal-solution effects can be incorporated into *K*-value formulations by the use of the partial fugacity coefficient, $\bar{\Phi}_i$, in conjunction with an equation of state and adequate mixing rules. This method is most frequently used for handling nonidealities in the vapor phase. However, $\bar{\Phi}_{iV}$ reflects the combined effects of a nonideal gas and a nonideal gas solution. At low pressures, both effects are negligible. At moderate pressures, a vapor solution may still be ideal even

Table 2.7 Classification of Molecules Based on Potential for Forming Hydrogen Bonds

Class	Description	Example
I	Molecules capable of forming three-dimensional networks of strong H-bonds	Water, glycols, glycerol, amino alcohols, hydroxylamines, hydroxyacids, polyphenols, and amides
II	Other molecules containing both active hydrogen atoms and donor atoms (O, N, and F)	Alcohols, acids, phenols, primary and secondary amines, oximes, nitro and nitrile compounds with α-hydrogen atoms, ammonia, hydrazine, hydrogen fluoride, and hydrogen cyanide
III	Molecules containing donor atoms but no active hydrogen atoms	Ethers, ketones, aldehydes, esters, tertiary amines (including pyridine type), and nitro and nitrile compounds without α-hydrogen atoms
IV	Molecules containing active hydrogen atoms but no donor atoms that have two or three chlorine atoms on the same carbon as a hydrogen or one chlorine on the carbon atom and one or more chlorine atoms on adjacent carbon atoms	$CHCl_3$, CH_2Cl_2, CH_3CHCl_2, CH_2ClCH_2Cl, $CH_2ClCHClCH_2Cl$, and $CH_2ClCHCl_2$
V	All other molecules having neither active hydrogen atoms nor donor atoms	Hydrocarbons, carbon disulfide, sulfides, mercaptans, and halohydrocarbons not in class IV

Table 2.8 Molecule Interactions Causing Deviations from Raoult's Law

Type of Deviation	Classes	Effect on Hydrogen Bonding
Always negative	III + IV	H-bonds formed only
Quasi-ideal; always positive or ideal	III + III III + V IV + IV IV + V V + V	No H-bonds involved
Usually positive, but some negative	I + I I + II I + III II + II II + III	H-bonds broken and formed
Always positive	I + IV (frequently limited solubility) II + IV	H-bonds broken and formed, but dissociation of Class I or II is more important effect
Always positive	I + V II + V	H-bonds broken only

though the gas mixture does not follow the ideal-gas law. Nonidealities in the liquid phase, however, can be severe even at low pressures. When polar species are present, mixing rules can be modified to include binary interaction parameters, k_{ij}, as in (2-51). The other technique for handling solution nonidealities is to retain $\bar{\phi}_{iV}$ in the K-value formulation but replace $\bar{\phi}_{iL}$ by the product of γ_{iL} and ϕ_{iL}, where the former accounts for deviations from nonideal solutions. Equation (2-26) then becomes

$$K_i = \frac{\gamma_{iL}\phi_{iL}}{\bar{\phi}_{iV}} \tag{2-68}$$

which was derived previously as (2-27). At low pressures, from Table 2.2, $\phi_{iL} = P_i^s/P$ and $\bar{\phi}_{iV} = 1.0$, so (2-68) reduces to a modified Raoult's law K-value, which differs from (2-44) in the added γ_{iL} term:

$$K_i = \frac{\gamma_{iL}P_i^s}{P} \tag{2-69}$$

At moderate pressures, (5) of Table 2.3 is preferred.

Regular-solution theory is useful only for estimating values of γ_{iL} for mixtures of nonpolar species. Many semitheoretical equations exist for estimating activity coefficients of binary mixtures containing polar species. These contain binary interaction parameters back-calculated from experimental data. Six of the more useful equations are listed in Table 2.9 in binary-pair form. For a given activity-coefficient correlation, the equations of Table 2.10 can be used to determine excess volume, excess enthalpy, and excess entropy. However, unless the dependency on pressure is known, excess liquid volumes cannot be determined directly from (1) of Table 2.10. Fortunately, the contribution of excess volume to total volume is small for solutions of nonelectrolytes. For example, a 50 mol% solution of ethanol in *n*-heptane at 25°C is shown in Figure 2.11a to be a nonideal but miscible liquid mixture. From the data of Van Ness, Soczek, and Kochar [34], excess volume is only 0.465 cm^3/mol, compared to an estimated ideal-solution molar volume of 106.3 cm^3/mol. By contrast, excess liquid enthalpy and excess liquid entropy may not be small. Once the partial molar excess functions for enthalpy and entropy are estimated for each species, the excess functions for the mixture are computed from the mole fraction sums.

§2.6.4 Margules Equations

Equations (1) and (2) in Table 2.9 date back to 1895, yet the two-constant form is still in use because of its simplicity. These equations result from power-series expansions for $\bar{g}_i^E$ and conversion to activity coefficients by (2-59). The one-constant form is equivalent to symmetrical activity-coefficient curves, which are rarely observed.

§2.6.5 van Laar Equation

Because of its flexibility, simplicity, and ability to fit many systems well, the van Laar equation is widely used. It was derived from the van der Waals equation of state, but the constants, shown as A_{12} and A_{21} in (3) of Table 2.9, are, in theory, constant only for a particular binary pair at a given temperature. In practice, the constants are best back-calculated from isobaric data covering a range of temperatures. The van Laar theory expresses the temperature dependence of A_{ij} as

$$A_{ij} = \frac{A'_{ij}}{RT} \tag{2-70}$$

Regular-solution theory and the van Laar equation are equivalent for a binary solution if

$$A_{ij} = \frac{v_{iL}}{RT}\left(\delta_i - \delta_j\right)^2 \tag{2-71}$$

The van Laar equation can fit activity coefficient–composition curves corresponding to both positive and negative deviations from Raoult's law, but cannot fit curves that exhibit minima or maxima such as those in Figure 2.11c.

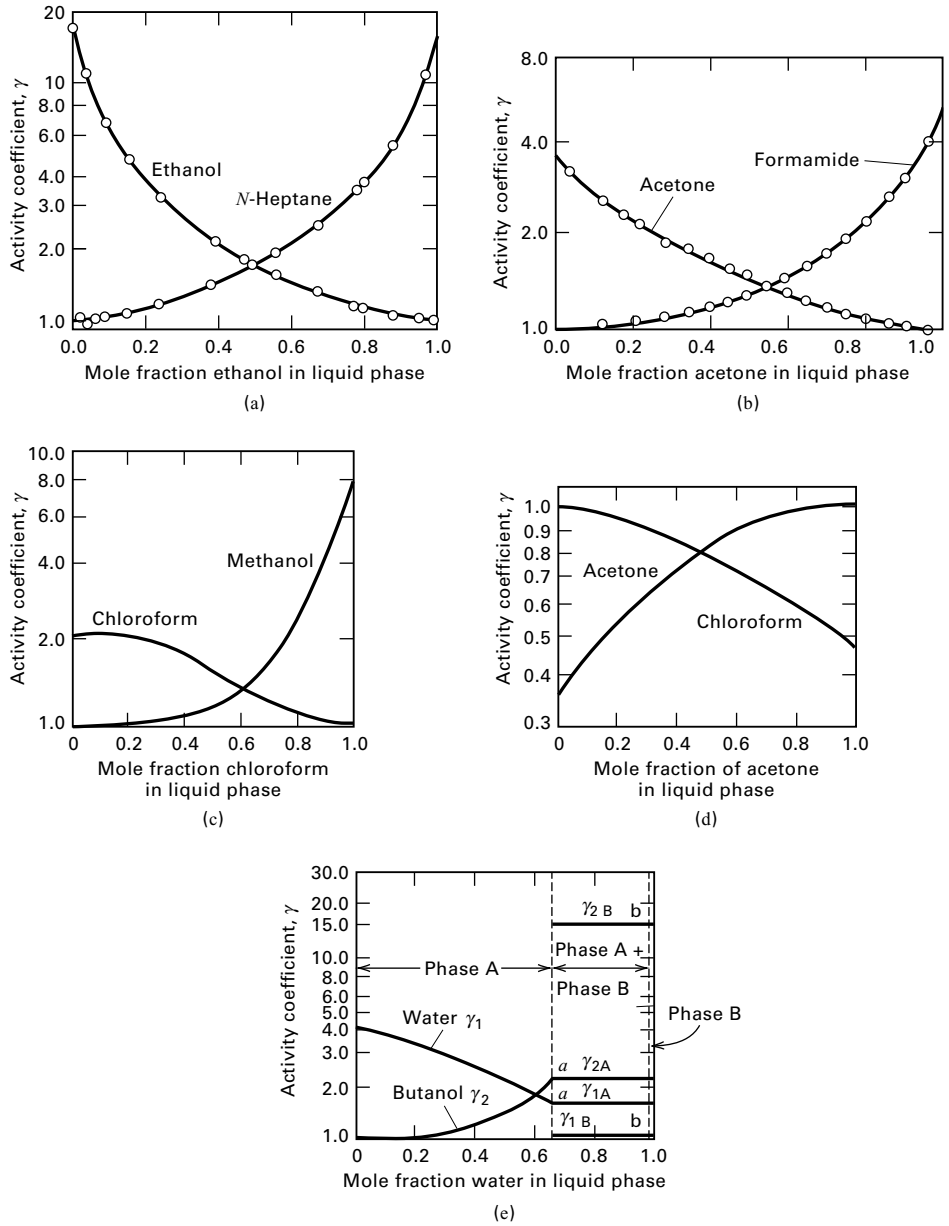

Figure 2.11 Typical variations of activity coefficients with composition in binary liquid systems: (a) ethanol(II)/*n*-heptane(V); (b) acetone (III)/formamide(I); (c) chloroform(IV)/methanol(II); (d) acetone(III)/chloroform(IV); (e) water(I)/*n*-butanol(II).

When data are isothermal or isobaric over only a narrow range of temperature, determination of van Laar constants is conducted in a straightforward manner. The most accurate procedure is a nonlinear regression to obtain the best fit to the data over the entire range of binary composition, subject to minimization of some objective function. A less accurate, but extremely rapid, manual-calculation procedure can be used when experimental data can be extrapolated to infinite-dilution conditions. Modern experimental techniques are available for accurately and rapidly determining activity coefficients at infinite dilution. Applying (3) of Table 2.9 to the conditions $x_i = 0$ and then $x_j = 0$,

$$A_{ij} = \ln \gamma_i^{\infty}, \quad x_i = 0$$

and

$$A_{ji} = \ln \gamma_j^{\infty}, \quad x_j = 0 \tag{2-72}$$

It is important that the van Laar equation predict azeotrope formation, where $x_i = y_i$ and $K_i = 1.0$. If activity coefficients are known or can be computed at the azeotropic composition say, from (2-69) ($\gamma_{iL} = P/P_i^s$, since $K_i = 1.0$), these coefficients can be used to determine the van Laar constants by solving (2-73) and (2-74), which describe activity-coefficient data at any single composition:

$$A_{12} = \ln \gamma_1 \left(1 + \frac{x_2 \ln \gamma_2}{x_1 \ln \gamma_1}\right)^2 \tag{2-73}$$

$$A_{21} = \ln \gamma_2 \left(1 + \frac{x_1 \ln \gamma_1}{x_2 \ln \gamma_2}\right)^2 \tag{2-74}$$

Table 2.9 Empirical and Semitheoretical Equations for Correlating Liquid-Phase Activity Coefficients of Binary Pairs

Name	Equation for Species 1	Equation for Species 2
(1) Margules	$\log\gamma_1 = Ax_2^2$	$\log\gamma_2 = Ax_1^2$
(2) Margules (two-constant)	$\log\gamma_1 = x_2^2[\bar{A}_{12} + 2x_1(\bar{A}_{21} - \bar{A}_{12})]$	$\log\gamma_2 = x_1^2[\bar{A}_{21} + 2x_2(\bar{A}_{12} - \bar{A}_{21})]$
(3) van Laar (two-constant)	$\ln\gamma_1 = \dfrac{A_{12}}{[1 + (x_1A_{12})/(x_2A_{21})]^2}$	$\ln\gamma_2 = \dfrac{A_{21}}{[1 + (x_2A_{21})/(x_1A_{12})]^2}$
(4) Wilson (two-constant)	$\ln\gamma_1 = -\ln(x_1 + \Lambda_{12}x_2) + x_2\left(\dfrac{\Lambda_{12}}{x_1 + \Lambda_{12}x_2} - \dfrac{\Lambda_{21}}{x_2 + \Lambda_{21}x_1}\right)$	$\ln\gamma_2 = -\ln(x_2 + \Lambda_{21}x_1) - x_1\left(\dfrac{\Lambda_{12}}{x_1 + \Lambda_{12}x_2} - \dfrac{\Lambda_{21}}{x_2 + \Lambda_{21}x_1}\right)$
(5) NRTL (three-constant)	$\ln\gamma_1 = \dfrac{x_2^2\tau_{21}G_{21}^2}{(x_1 + x_2G_{21})^2} + \dfrac{x_1^2\tau_{12}G_{12}}{(x_2 + x_1G_{12})^2}$ $G_{ij} = \exp(-\alpha_{ij}\tau_{ij})$	$\ln\gamma_2 = \dfrac{x_1^2\tau_{12}G_{12}^2}{(x_2 + x_1G_{12})^2} + \dfrac{x_2^2\tau_{21}G_{21}}{(x_1 + x_2G_{21})^2}$ $G_{ij} = \exp(-\alpha_{ij}\tau_{ij})$
(6) UNIQUAC (two-constant)	$\ln\gamma_1 = \ln\dfrac{\Psi_1}{x_1} + \dfrac{\bar{Z}}{2}q_1\ln\dfrac{\theta_1}{\Psi_1} + \Psi_2\left(l_1 - \dfrac{r_1}{r_2}l_2\right) - q_1\ln(\theta_1 + \theta_2T_{21}) + \theta_2q_1\left(\dfrac{T_{21}}{\theta_1 + \theta_2T_{21}} - \dfrac{T_{12}}{\theta_2 + \theta_1T_{12}}\right)$	$\ln\gamma_2 = \ln\dfrac{\Psi_2}{x_2} + \dfrac{\bar{Z}}{2}q_2\ln\dfrac{\theta_2}{\Psi_2} + \Psi_1\left(l_2 - \dfrac{r_2}{r_1}l_1\right) - q_2\ln(\theta_2 + \theta_1T_{12}) + \theta_1q_2\left(\dfrac{T_{12}}{\theta_2 + \theta_1T_{12}} - \dfrac{T_{21}}{\theta_1 + \theta_2T_{21}}\right)$

Mixtures of self-associated polar molecules (class II in Table 2.7) with nonpolar molecules (class V) can exhibit strong nonideality of the positive-deviation type shown in Figure 2.11a. Figure 2.12 shows experimental data of Sinor and Weber [35] for ethanol (1)/*n*-hexane (2), a system of this type, at 101.3 kPa. These data were correlated with the van Laar equation by Orye and Prausnitz [36] to give $A_{12} = 2.409$ and $A_{21} = 1.970$. From $x_1 = 0.1$ to 0.9, the data fit to the van Laar equation is good; in the dilute regions, however, deviations are quite severe and the predicted activity coefficients for ethanol are low. An even more serious problem with highly nonideal mixtures is that the van Laar equation may erroneously predict phase splitting (formation of two liquid phases) when values of activity coefficients exceed approximately 7.

Table 2.10 Partial Molar Excess Functions

Excess volume:

$$(1)\quad \left(\bar{v}_{iL} - \bar{v}_{iL}^{\mathrm{ID}}\right) \equiv \bar{v}_{iL}^{\mathrm{E}} = RT\left(\frac{\partial \ln\gamma_{iL}}{\partial P}\right)_{T,x}$$

Excess enthalpy:

$$(2)\quad \left(\bar{h}_{iL} - \bar{h}_{iL}^{\mathrm{ID}}\right) \equiv \bar{h}_{iL}^{\mathrm{E}} = -RT^2\left(\frac{\partial \ln\gamma_{iL}}{\partial T}\right)_{P,x}$$

Excess entropy:

$$(3)\quad \left(\bar{s}_{iL} - \bar{s}_{iL}^{\mathrm{ID}}\right) \equiv \bar{s}_{iL}^{\mathrm{E}} = -R\left[T\left(\frac{\partial \ln\gamma_{iL}}{\partial T}\right)_{P,x} + \ln\gamma_{iL}\right]$$

ID = ideal mixture; E = excess because of nonideality.

§2.6.6 Local-Composition Concept and the Wilson Model

Following its publication in 1964, the Wilson equation [37], in Table 2.9 as (4), received wide attention because of its ability to fit strongly nonideal, but miscible systems. As shown in Figure 2.12, the Wilson equation, with binary

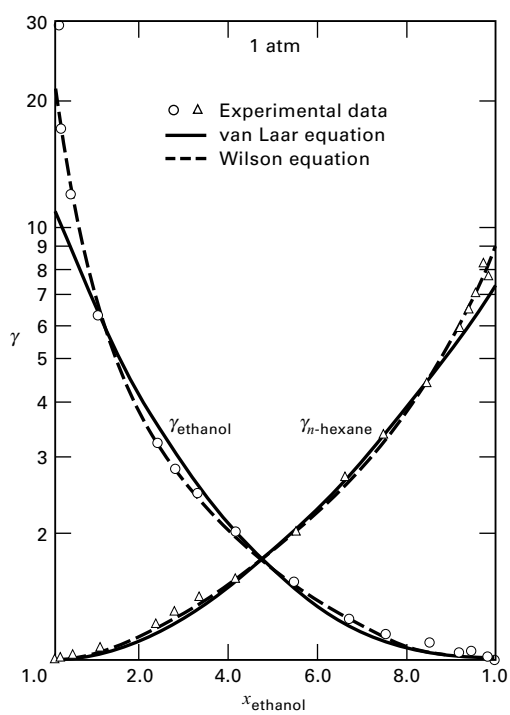

Figure 2.12 Activity coefficients for ethanol/*n*-hexane.

[Data from J.E. Sinor and J.H. Weber, *J. Chem. Eng. Data*, **5**, 243–247 (1960).]

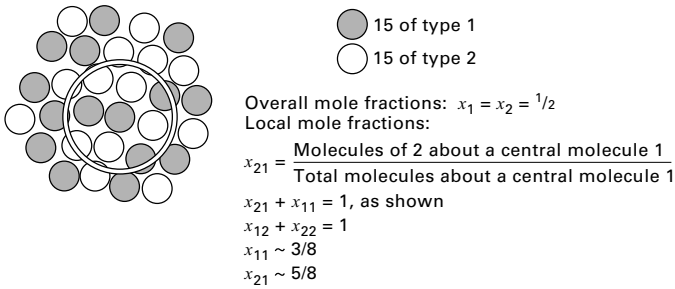

Figure 2.13 The concept of local compositions.
[From P.M. Cukor and J.M. Prausnitz, *Int. Chem. Eng. Symp. Ser. No. 32*, **3**, 88 (1969).]

interaction parameters $\Lambda_{12} = 0.0952$ and $\Lambda_{21} = 0.2713$ from Orye and Prausnitz [36], fits experimental data well even in dilute regions where the variation of γ_1 becomes exponential. Corresponding infinite-dilution activity coefficients computed from the Wilson equation are $\gamma_1^\infty = 21.72$ and $\gamma_2^\infty = 9.104$.

The Wilson equation accounts for differences in both molecular size and intermolecular forces, consistent with the Flory–Huggins relation (2-65). Overall solution volume fractions ($\Phi_i = x_i v_{iL}/v_L$) are replaced by local-volume fractions, $\bar{\Phi}_i$, related to local-molecule segregations caused by differing energies of interaction between pairs of molecules. The concept of local compositions that differ from overall compositions is illustrated for an overall, equimolar, binary solution in Figure 2.13, from Cukor and Prausnitz [38]. About a central molecule of type 1, the local mole fraction of type 2 molecules is shown to be 5/8, while the overall composition is 1/2.

For local-volume fraction, Wilson proposed

$$\bar{\Phi}_i = \frac{v_{iL} x_i \exp(-\lambda_{ii}/RT)}{\sum_{j=1}^{C} v_{jL} x_j \exp(-\lambda_{ij}/RT)} \tag{2-75}$$

where energies of interaction $\lambda_{ij} = \lambda_{ji}$, but $\lambda_{ii} \neq \lambda_{jj}$. Following Orye and Prausnitz [36], substitution of the binary form of (2-75) into (2-65) and defining the binary interaction parameters as

$$\Lambda_{12} = \frac{v_{2L}}{v_{1L}} \exp\left[-\frac{(\lambda_{12} - \lambda_{11})}{RT}\right] \tag{2-76}$$

$$\Lambda_{21} = \frac{v_{1L}}{v_{2L}} \exp\left[-\frac{(\lambda_{12} - \lambda_{22})}{RT}\right] \tag{2-77}$$

leads to an equation for a binary system:

$$\frac{g^E}{RT} = -x_1 \ln(x_1 + \Lambda_{12} x_2) - x_2 \ln(x_2 + \Lambda_{21} x_1) \tag{2-78}$$

The Wilson equation is effective for dilute compositions where entropy effects dominate over enthalpy effects. The Orye–Prausnitz form for activity coefficient, in Table 2.9, follows from combining (2-59) with (2-78). Values of $\Lambda_{ij} < 1$ correspond to positive deviations from Raoult's law, while values > 1 signify negative deviations. Ideal solutions result when $\Lambda_{ij} = 1$. Studies indicate that λ_{ii} and λ_{ij} are temperature-dependent. Values of v_{iL}/v_{jL} depend on temperature also, but the variation is small compared to the effect of temperature on the exponential terms in (2-76) and (2-77).

The Wilson equation is extended to multicomponent mixtures by neglecting ternary and higher interactions and assuming a pseudo-binary mixture. The following multicomponent Wilson equation involves only binary interaction constants:

$$\ln \gamma_k = 1 - \ln\left(\sum_{j=1}^{C} x_j \Lambda_{kj}\right) - \sum_{i=1}^{C}\left(\frac{x_i \Lambda_{ik}}{\sum_{j=1}^{C} x_j \Lambda_{ij}}\right) \tag{2-79}$$

where $\Lambda_{ii} = \Lambda_{jj} = \Lambda_{kk} = 1$.

For highly nonideal, but still miscible, mixtures, the Wilson equation is markedly superior to the Margules and van Laar equations. It is consistently superior for multicomponent solutions. The constants in the Wilson equation for many binary systems are tabulated in the DECHEMA collection of Gmehling and Onken [39] and the Dortmund Data Bank. Two limitations of the Wilson equation are its inability to predict immiscibility, as in Figure 2.11e, and maxima and minima in activity-coefficient–mole fraction relationships, as in Figure 2.11c.

When insufficient data are available to determine binary parameters from a best fit of activity coefficients, infinite-dilution or single-point values can be used. At infinite dilution, the Wilson equation in Table 2.9 becomes

$$\ln \gamma_1^\infty = 1 - \ln \Lambda_{12} - \Lambda_{21} \tag{2-80}$$

$$\ln \gamma_2^\infty = 1 - \ln \Lambda_{21} - \Lambda_{12} \tag{2-81}$$

If temperatures corresponding to γ_1^∞ and γ_2^∞ are not close or equal, (2-76) and (2-77) should be substituted into (2-80) and (2-81)—with values of $(\lambda_{12} - \lambda_{11})$ and $(\lambda_{12} - \lambda_{22})$ determined from estimates of pure-component liquid molar volumes—to estimate Λ_{12} and Λ_{21}.

When the data of Sinor and Weber [35] for *n*-hexane/ethanol, shown in Figure 2.12, are plotted as a *y*–*x* diagram in ethanol (Figure 2.14), the equilibrium curve crosses the 45° line at $x = 0.332$. The temperature corresponding to this composition is 58°C. Ethanol has a normal boiling point of 78.33°C, which is higher than the boiling point of 68.75°C

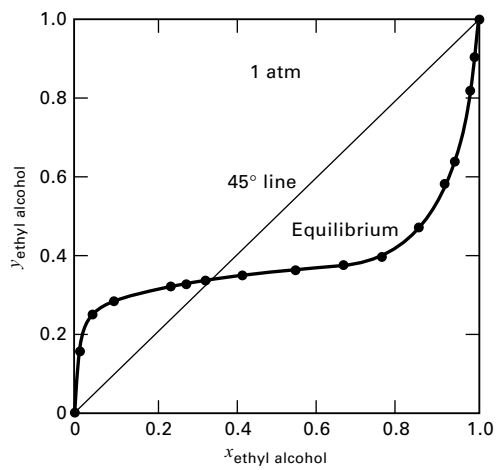

Figure 2.14 Equilibrium curve for *n*-hexane/ethanol.

for *n*-hexane. Nevertheless, ethanol is more volatile than *n*-hexane up to an ethanol mole fraction of $x = 0.322$, the minimum-boiling azeotrope. This occurs because of the close boiling points of the two species and the high activity coefficients for ethanol at low concentrations. At the azeotropic composition, $y_i = x_i$; therefore, $K_i = 1.0$. Applying (2-69) to both species,

$$\boxed{\gamma_1 P_1^s = \gamma_2 P_2^s} \tag{2-82}$$

If pure species 2 is more volatile $\left(P_2^s > P_1^s\right)$, the criteria for formation of a minimum-boiling azeotrope are

$$\gamma_1 \geq 1 \tag{2-83}$$

$$\gamma_2 \geq 1 \tag{2-84}$$

and

$$\frac{\gamma_1}{\gamma_2} < \frac{P_2^s}{P_1^s} \tag{2-85}$$

for x_1 less than the azeotropic composition. These criteria are most readily applied at $x_1 = 0$. For example, for the *n*-hexane (2)/ethanol (1) system at 1 atm when the liquid-phase mole fraction of ethanol approaches zero, the temperature approaches 68.75°C (155.75°F), the boiling point of pure *n*-hexane. At this temperature, $P_1^s = 10$ psia (68.9 kPa) and $P_2^s = 14.7$ psia (101.3 kPa). Also from Figure 2.12, $\gamma_1^\infty = 21.72$ when $\gamma_2 = 1.0$. Thus, $\gamma_1^\infty/\gamma_2 = 21.72$, but $P_2^s/P_1^s = 1.47$. Therefore, a minimum-boiling azeotrope will occur.

Maximum-boiling azeotropes are less common. They occur for close-boiling mixtures when negative deviations from Raoult's law arise, giving $\gamma_i < 1.0$. Criteria are derived in a manner similar to that for minimum-boiling azeotropes. At $x_1 = 1$, where species 2 is more volatile,

$$\gamma_1 = 1.0 \tag{2-86}$$

$$\gamma_2^\infty < 1.0 \tag{2-87}$$

and

$$\frac{\gamma_2^\infty}{\gamma_1} < \frac{P_1^s}{P_2^s} \tag{2-88}$$

For azeotropic binary systems, interaction parameters Λ_{12} and Λ_{21} can be determined by solving (4) of Table 2.9 at the azeotropic composition, as shown in the following example.

EXAMPLE 2.8 Wilson Constants from Azeotropic Data.

From measurements by Sinor and Weber [35] of the azeotropic condition for the ethanol (E)/*n*-hexane (H) system at 1 atm (101.3 kPa, 14.696 psia), calculate Λ_{12} and Λ_{21}.

Solution

The azeotrope occurs at $x_E = 0.332$, $x_H = 0.668$, and $T = 58°C$ (331.15 K). At 1 atm, (2-69) can be used to approximate *K*-values. Thus, at azeotropic conditions, $\gamma_i = P/P_i^s$. The vapor pressures at 58°C are $P_E^s = 6.26$ psia and $P_H^s = 10.28$ psia. Therefore,

$$\gamma_E = \frac{14.696}{6.26} = 2.348$$

$$\gamma_H = \frac{14.696}{10.28} = 1.430$$

Substituting these values together with the above corresponding values of x_i into the binary form of the Wilson equation in Table 2.9 gives

$$\ln 2.348 = -\ln(0.332 + 0.668\Lambda_{EH}) + 0.668\left(\frac{\Lambda_{EH}}{0.332 + 0.668\Lambda_{EH}} - \frac{\Lambda_{HE}}{0.332\Lambda_{HE} + 0.668}\right)$$

$$\ln 1.430 = -\ln(0.668 + 0.332\Lambda_{HE}) - 0.332\left(\frac{\Lambda_{EH}}{0.332 + 0.668\Lambda_{EH}} - \frac{\Lambda_{HE}}{0.332\Lambda_{HE} + 0.668}\right)$$

Solving these two nonlinear equations simultaneously, $\Lambda_{EH} = 0.041$ and $\Lambda_{HE} = 0.281$. From these constants, the activity-coefficient curves can be predicted if the temperature variations of Λ_{EH} and Λ_{HE} are ignored. The results are plotted in Figure 2.15. The fit of experimental data is good except, perhaps, for near-infinite-dilution conditions, where $\gamma_E^\infty = 49.82$ and $\gamma_H^\infty = 9.28$. The former is considerably greater than the value of 21.72 obtained by Orye and Prausnitz [36] from a fit of all data points. A comparison of Figures 2.12 and 2.15 shows that widely differing γ_E^∞ values have little effect on γ in the region $x_E = 0.15$ to 1.00, where the Wilson curves are almost identical. For accuracy over the entire composition range, data for at least three liquid compositions per binary are preferred.

The Wilson equation can be extended to liquid–liquid or vapor–liquid–liquid systems by multiplying the right-hand side of (2-78) by a third binary-pair constant evaluated from experimental data [37]. However, for multicomponent systems of three or more species, the third binary-pair constants must be the same for all binary pairs. Furthermore, as shown by Hiranuma [40], representation of ternary systems

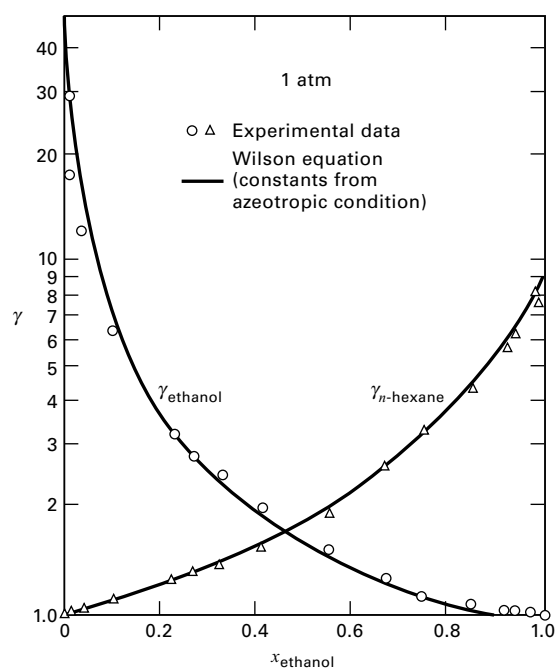

Figure 2.15 Liquid-phase activity coefficients for ethanol/*n*-hexane system.

involving only one partially miscible binary pair can be extremely sensitive to the third binary-pair Wilson constant. For these reasons, the Wilson equation is not favored for liquid–liquid systems.

§2.6.7 NRTL Model

The nonrandom, two-liquid (NRTL) equation developed by Renon and Prausnitz [41, 42], given in Table 2.9, represents an extension of Wilson's concept to multicomponent liquid–liquid, and vapor–liquid–liquid systems. It is widely used for liquid–liquid extraction. For multicomponent vapor–liquid systems, only binary-pair constants from binary-pair experimental data are required. For a multicomponent system, the NRTL expression is

$$\ln \gamma_i = \frac{\sum_{j=1}^{C} \tau_{ji} G_{ji} x_j}{\sum_{k=1}^{C} G_{ki} x_k} + \sum_{j=1}^{C} \left[\frac{x_j G_{ij}}{\sum_{k=1}^{C} G_{kj} x_k} \left(\tau_{ij} - \frac{\sum_{k=1}^{C} x_k \tau_{kj} G_{kj}}{\sum_{k=1}^{C} G_{kj} x_k} \right) \right] \tag{2-89}$$

where

$$G_{ji} = \exp\left(-\alpha_{ji} \tau_{ji}\right) \tag{2-90}$$

The coefficients τ are given by

$$\tau_{ij} = \frac{g_{ij} - g_{jj}}{RT} \tag{2-91}$$

$$\tau_{ji} = \frac{g_{ji} - g_{ii}}{RT} \tag{2-92}$$

where the double-subscripted g values are energies of interaction for molecule pairs. In the equations, $G_{ji} \neq G_{ij}$, $\tau_{ij} \neq \tau_{ji}$, $G_{ii} = G_{jj} = 1$, and $\tau_{ii} = \tau_{jj} = 0$. Often $(g_{ij} - g_{jj})$ and other constants are linear in temperature. For ideal solutions, $\tau_{ji} = 0$.

The parameter α_{ji} characterizes the tendency of species j and i to be distributed nonrandomly. When $\alpha_{ji} = 0$, local mole fractions equal overall solution mole fractions. Generally, α_{ji} is independent of temperature and depends on molecule properties similar to the classifications in Tables 2.7 and 2.8. Values of α_{ji} usually lie between 0.2 and 0.47. When $\alpha_{ji} > 0.426$, phase immiscibility is predicted. Although α_{ji} can be treated as an adjustable parameter determined from experimental binary-pair data, commonly α_{ji} is set according to the following rules, which are occasionally ambiguous:

1. $\alpha_{ji} = 0.20$ for hydrocarbons and polar, nonassociated species (e.g., *n*-heptane/acetone).
2. $\alpha_{ji} = 0.30$ for nonpolar compounds (e.g., benzene/*n*-heptane), except fluorocarbons and paraffins; nonpolar and polar, nonassociated species (e.g., benzene/acetone); polar species that exhibit negative deviations from Raoult's law (e.g., acetone/chloroform) and moderate positive deviations (e.g., ethanol/water); mixtures of water and polar nonassociated species (e.g., water/acetone).
3. $\alpha_{ji} = 0.40$ for saturated hydrocarbons and homolog perfluorocarbons (e.g., *n*-hexane/perfluoro-*n*-hexane).
4. $\alpha_{ji} = 0.47$ for alcohols or other strongly self-associated species with nonpolar species (e.g., ethanol/benzene); carbon tetrachloride with either acetonitrile or nitromethane; water with either butyl glycol or pyridine.

§2.6.8 UNIQUAC Model

In an attempt to place calculations of activity coefficients on a more theoretical basis, Abrams and Prausnitz [43] used statistical mechanics to derive an expression for excess free energy. Their model, UNIQUAC (universal quasichemical), generalizes an analysis by Guggenheim and extends it to molecules that differ in size and shape. As in the Wilson and NRTL equations, local concentrations are used. However, rather than local volume fractions or local mole fractions, UNIQUAC uses local area fraction θ_{ij} as the primary concentration variable.

The local area fraction is determined by representing a molecule by a set of bonded segments. Each molecule is characterized by two structural parameters determined relative to a standard segment, taken as an equivalent sphere of a unit of a linear, infinite-length, polymethylene molecule. The two structural parameters are the relative number of segments per molecule, r (volume parameter), and the relative surface area, q (surface parameter). These parameters, computed from bond angles and bond distances, are given for many species by Abrams and Prausnitz [43–45] and Gmehling and Onken [39]. Values can also be estimated by the group-contribution method of Fredenslund et al. [46].

For a multicomponent liquid mixture, the UNIQUAC model gives the excess free energy as

$$\frac{g^E}{RT} = \sum_{i=1}^{C} x_i \ln\left(\frac{\Psi_i}{x_i}\right) + \frac{\bar{Z}}{2} \sum_{i=1}^{C} q_i x_i \ln\left(\frac{\theta_i}{\Psi_i}\right) - \sum_{i=1}^{C} q_i x_i \ln\left(\sum_{j=1}^{C} \theta_i T_{ji}\right) \tag{2-93}$$

The first two terms on the right-hand side account for *combinatorial* effects due to differences in size and shape; the last term provides a *residual* contribution due to differences in intermolecular forces, where

$$\Psi_i = \frac{x_i r_i}{\sum_{i=1}^{C} x_i r_i} = \text{segment fraction} \tag{2-94}$$

$$\theta = \frac{x_i q_i}{\sum_{i=1}^{C} x_i q_i} = \text{area fraction} \tag{2-95}$$

where $\bar{Z}$ = lattice coordination number set equal to 10, and

$$T_{ji} = \exp\left(\frac{u_{ji} - u_{ii}}{RT}\right) \tag{2-96}$$

Equation (2-93) contains two adjustable parameters for each binary pair, $(u_{ji} - u_{ii})$ and $(u_{ij} - u_{jj})$. Abrams and Prausnitz show that $u_{ji} = u_{ij}$ and $T_{ii} = T_{jj} = 1$. In general, $(u_{ji} - u_{ii})$ and $(u_{ij} - u_{jj})$ are linear functions of absolute temperature.

If (2-59) is combined with (2-93), the activity coefficient for a species in a multicomponent mixture becomes:

$$\ln\gamma_i = \ln\gamma_i^C + \ln\gamma_i^R$$

$$= \underbrace{\ln\left(\Psi_i/x_i\right) + \left(\bar{Z}/2\right)q_i \ln\left(\theta_i/\Psi_i\right) + l_i - \left(\Psi_i/x_i\right)\sum_{j=1}^{C} x_j l_j}_{C,\ \text{combinatorial}}$$

$$+ \underbrace{q_i\left[1 - \ln\left(\sum_{j=1}^{C}\theta_j T_{ji}\right) - \sum_{j=1}^{C}\left(\frac{\theta_j T_{ij}}{\sum_{k=1}^{C}\theta_k T_{kj}}\right)\right]}_{R,\ \text{residual}} \tag{2-97}$$

where

$$l_j = \left(\frac{\bar{Z}}{2}\right)\left(r_j - a_j\right) - \left(r_j - 1\right) \tag{2-98}$$

For a mixture of species 1 and 2, (2-97) reduces to (6) in Table 2.9 for $\bar{Z} = 10$.

§2.6.9 UNIFAC Model

Liquid-phase activity coefficients are required for design purposes even when experimental equilibria data are not available and the assumption of regular solutions is not valid because polar compounds are present. For such situations, Wilson and Deal [47], and then Derr and Deal [48], in the 1960s presented estimation methods based on functional groups instead of molecules. In a solution of toluene and acetone, the contributions might be 5 aromatic CH groups, 1 aromatic C group, and 1 CH_3 group from toluene; and 2 CH_3 groups plus 1 CO carbonyl group from acetone. Alternatively, larger groups might be employed to give 5 aromatic CH groups and 1 CCH_3 group from toluene; and 1 CH_3 group and 1 CH_3CO group from acetone. As larger functional groups are used, the accuracy increases, but the advantage of the group-contribution method decreases because more groups are required. In practice, about 50 functional groups represent thousands of multicomponent liquid mixtures.

For partial molar excess free energies, $\bar{g}_i^E$, and activity coefficients, size parameters for each functional group and interaction parameters for each pair are required. Size parameters can be calculated from theory. Interaction parameters are back-calculated from existing phase-equilibria data and used with the size parameters to predict properties of mixtures for which data are unavailable.

The UNIFAC (UNIQUAC Functional-group Activity Coefficients) group-contribution method—first presented by Fredenslund, Jones, and Prausnitz [49] and further developed by Fredenslund, Gmehling, and Rasmussen [50], Gmehling, Rasmussen, and Fredenslund [51], and Larsen, Rasmussen, and Fredenslund [52]—has advantages over other methods in that: (1) it is theoretically based; (2) the parameters are essentially independent of temperature; (3) size and binary interaction parameters are available for a range of functional groups; (4) predictions can be made over a temperature range of 275–425 K and for pressures to a few atmospheres; and (5) extensive comparisons with experimental data are available. All components must be condensable at near-ambient conditions.

The UNIFAC method is based on the UNIQUAC equation (2-97), wherein the molecular volume and area parameters are replaced by

$$r_i = \sum_k v_k^{(i)} R_k \tag{2-99}$$

$$q_i = \sum_k v_k^{(i)} Q_k \tag{2-100}$$

where $v_k^{(i)}$ is the number of functional groups of type k in molecule i, and R_k and Q_k are the volume and area parameters, respectively, for the type-k functional group.

The residual term in (2-97), which is represented by $\ln\gamma_i^R$, is replaced by the expression

$$\ln\gamma_i^R = \underbrace{\sum_k v_k^{(i)}\left(\ln\Gamma_k - \ln\Gamma_k^{(i)}\right)}_{\text{all functional groups in mixture}} \tag{2-101}$$

where Γ_k is the residual activity coefficient of group k, and $\Gamma_k^{(i)}$ is the same quantity but in a reference mixture that contains only molecules of type i. The latter quantity is required so that $\gamma_i^R \to 1.0$ as $x_i \to 1.0$. Both Γ_k and $\Gamma_k^{(i)}$ have the same form as the residual term in (2-97). Thus,

$$\ln\Gamma_k = Q_k\left[1 - \ln\left(\sum_m \theta_m T_{mk}\right) - \sum_m \frac{\theta_m T_{mk}}{\sum_n \theta_n T_{nm}}\right] \tag{2-102}$$

where θ_m is the area fraction of group m, given by an equation similar to (2-95),

$$\theta_m = \frac{X_m Q_m}{\sum_n X_n Q_m} \tag{2-103}$$

where X_m is the mole fraction of group m in the solution,

$$X_m = \frac{\sum_j v_m^{(j)} x_j}{\sum_j \sum_n \left(v_n^{(j)} x_j\right)} \tag{2-104}$$

and T_{mk} is a group interaction parameter given by an equation similar to (2-96),

$$T_{mk} = \exp\left(-\frac{a_{mk}}{T}\right) \tag{2-105}$$

where $a_{mk} \neq a_{km}$. When $m = k$, then $a_{mk} = 0$ and $T_{mk} = 1.0$. For $\Gamma_k^{(i)}$, (2-102) also applies, where θ terms correspond to the pure component i. Although R_k and Q_k differ for each functional group, values of a_{mk} are equal for all subgroups within a main group. For example, main group CH_2 consists of subgroups CH_3, CH_2, CH, and C. Accordingly,

$$a_{CH_3,CHO} = a_{CH_2,CHO} = a_{CH,CHO} = a_{C,CHO}$$

Thus, the experimental data required to obtain values of a_{mk} and a_{km} and the size of the corresponding bank of data for these parameters are not as great as might be expected.

The group-contribution method was improved by the introduction of a modified UNIFAC method by Gmehling et al. [51], referred to as UNIFAC (Dortmund). For mixtures having a range of molecular sizes, they modified the combinatorial part of (2-97). For temperature dependence they replaced (2-105) with a three-coefficient equation. These changes permit reliable predictions of activity coefficients (including dilute solutions and multiple liquid phases), heats of mixing, and azeotropic compositions. Values of UNIFAC (Dortmund) parameters for 51 groups have been available in publications starting in 1993 with Gmehling, Li, and Schiller [53] and more recently with Wittig, Lohmann, and Gmehling [54], Gmehling et al. [92], and Jakob et al. [93].

§2.6.10 Liquid–Liquid Equilibria

When species are notably dissimilar and activity coefficients are large, two or more liquid phases may coexist. Consider the binary system methanol (1) and cyclohexane (2) at 25°C. From measurements of Takeuchi, Nitta, and Katayama [55], van Laar constants are $A_{12} = 2.61$ and $A_{21} = 2.34$, corresponding, respectively, to infinite-dilution activity coefficients of 13.6 and 10.4 from (2-72). Parameters A_{12} and A_{21} can be used to construct an equilibrium plot of y_1 against x_1 assuming 25°C. Combining (2-69), where $K_i = y_i/x_i$, with

$$P = \sum_{i=1}^{C} x_i \gamma_{iL} P_i^s \tag{2-106}$$

gives the following for computing y_i from x_i:

$$y_1 = \frac{x_1 \gamma_1 P_1^s}{x_1 \gamma_1 P_1^s + x_2 \gamma_2 P_2^s} \tag{2-107}$$

Vapor pressures at 25°C are $P_1^s = 2.452$ psia (16.9 kPa) and $P_2^s = 1.886$ psia (13.0 kPa). Activity coefficients can be computed from the van Laar equation in Table 2.9. The resulting equilibrium is shown in Figure 2.16, where over much of the liquid-phase region, three values of x_1 exist for a given y_1. This indicates phase instability with the formation of two liquid phases. Single liquid phases can exist only for cyclohexane-rich mixtures of $x_1 = 0.8248$ to 1.0 and for methanol-rich mixtures of $x_1 = 0.0$ to 0.1291. Because a coexisting vapor phase exhibits one composition, two coexisting liquid phases prevail at opposite ends of the dashed line in Figure 2.16. The liquid phases represent solubility limits of methanol in cyclohexane and cyclohexane in methanol.

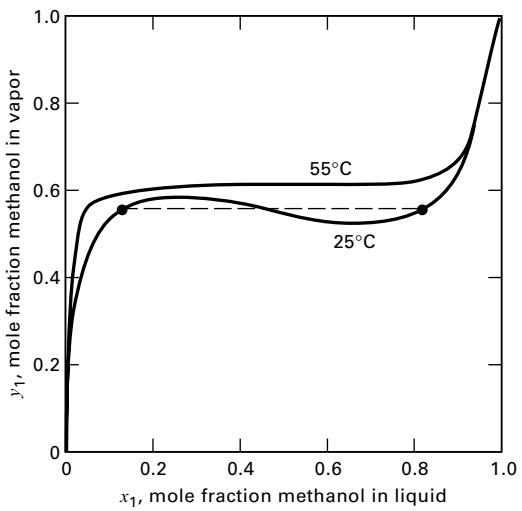

Figure 2.16 Equilibrium curves for methanol/cyclohexane.

[Data from K. Strubl, V. Svoboda, R. Holub, and J. Pick, *Collect. Czech. Chem. Commun.*, **35**, 3004–3019 (1970).]

For two coexisting liquid phases, $\gamma_{iL}^{(1)} x_i^{(1)} = \gamma_{iL}^{(2)} x_i^{(2)}$ must hold. This permits determination of the two-phase region in Figure 2.16 from the van Laar or other suitable activity-coefficient equation for which the constants are known. Also shown in Figure 2.16 is an equilibrium curve for the binary mixture at 55°C, based on data of Strubl et al. [56]. At this higher temperature, methanol and cyclohexane are miscible. The data of Kiser, Johnson, and Shetlar [57] show that phase instability ceases to exist at 45.75°C, the critical solution temperature. Rigorous methods for determining phase instability and, thus, existence of two liquid phases are based on free-energy calculations, as discussed by Prausnitz et al. [4]. Most of the semitheoretical equations for the liquid-phase activity coefficient listed in Table 2.9 apply to liquid–liquid systems. The Wilson equation is a notable exception. The NRTL equation is the most widely used.

§2.7 DIFFICULT MIXTURES

The equation-of-state and activity-coefficient models in §2.5 and §2.6 are inadequate for estimating *K*-values of mixtures containing: (1) polar and supercritical (light-gas) components, (2) electrolytes, (3) polymers and solvents, and (4) biomacromolecules. For these difficult mixtures, special models are briefly described in the following subsections. Detailed discussions are given by Prausnitz, Lichtenthaler, and de Azevedo [4].

§2.7.1 Predictive Soave–Redlich–Kwong (PSRK) Model

Equation-of-state models are useful for mixtures of nonpolar and slightly polar compounds. Gibbs free-energy activity-coefficient models are suitable for liquid subcritical nonpolar and polar compounds. When a mixture contains both polar compounds and supercritical gases, neither method applies. To describe vapor–liquid equilibria for such mixtures, more theoretically based mixing rules for use with the S–R–K and P–R equations of state have been developed. To broaden the range of applications of these models, Holderbaum and Gmehling [58] formulated a group-contribution equation of state called the predictive Soave–Redlich–Kwong (PSRK) model, which combines the S–R–K equation of state with UNIFAC. To improve the ability of the S–R–K equation to predict vapor pressure of polar compounds, they make the pure-component parameter, a, in Table 2.5 temperature dependent.To handle mixtures of nonpolar, polar, and supercritical components, they use a mixing rule for a that includes the UNIFAC model for nonideal effects. Pure-component and group-interaction parameters for use in the PSRK model are provided by Fischer and Gmehling [59]. In

particular, [58] and [59] provide parameters for nine light gases in addition to UNIFAC parameters for 50 groups.

§2.7.2 Electrolyte Solution Models

Solutions of electrolytes are common in the chemical and biochemical industries. For example, sour water, found in many petroleum plants, consists of water and five dissolved gases: CO, CO_2, CH_4, H_2S, and NH_3. Because of dissociation, the aqueous solution includes ionic as well as molecular species. For sour water, the ionic species include H^+, OH^-, HCO_3^-, $CO_3^=$, HS^-, $S^=$, NH_4^+, and NH_2COO^-, with the positive and negative ions subject to electroneutrality. For example, while the apparent concentration of NH_3 in the solution might be 2.46 moles per kg of water, the molality is 0.97 when dissociation is taken into account, with NH_4^+ having a molality of 1.49. All eight ionic species are nonvolatile, while all six molecular species are volatile to some extent. Calculations of vapor–liquid equilibrium for multicomponent electrolyte solutions must consider both chemical and physical equilibrium, both of which involve liquid-phase activity coefficients.

Models have been developed for predicting activity coefficients in multicomponent systems of electrolytes. Of particular note are those of Pitzer [60] and Chen and associates [61, 62, 63] , both of which are included in process simulation programs. Both models can handle dilute to concentrated solutions, but only the model of Chen and associates, which is a substantial modification of the NRTL model, can handle mixed-solvent systems.

§2.7.3 Polymer Solution Models

Polymer processing commonly involves solutions of solvent, monomer, and soluble polymer, thus requiring vapor–liquid and, sometimes, liquid–liquid phase-equilibria calculations, for which activity coefficients of all components are needed. In general, the polymer is nonvolatile, but the solvent and monomer are volatile. When the solution is dilute in the polymer, activity-coefficient methods of §2.6, such as the NRTL method, are suitable. Of more interest are mixtures with appreciable concentrations of polymer, for which the methods of §2.5 and §2.6 are inadequate, so, special-purpose models have been developed. One method, which is available in process simulation programs, is the modified NRTL model of Chen [64], which combines a modification of the Flory–Huggins equation (2-65) for widely differing molecular size with the NRTL concept of local composition. Because Chen represents the polymer with segments, solvent–solvent, solvent–segment, and segment–segment binary interaction parameters are required. These are available from the literature and may be assumed to be independent of temperature, polymer chain length, and polymer concentration.

Aqueous two-phase extraction (ATPE) is a nondenaturing and nondegrading method for recovering and separating large biomolecules such as cells, cell organelles, enzymes, lipids, proteins, and viruses from fermentation broths and solutions of lysed cells. An aqueous two-phase system (ATPS) consists of water and two polymers [e.g., polyethylene glycol (PEG) and dextran] or one polymer (e.g., PEG) and a salt (e.g., K_2SO_4, Na_2SO_4, and KCl). At equilibrium, the aqueous top phase is enriched in PEG and depleted in dextran or salt, while the aqueous bottom phase is depleted in PEG and enriched in dextran or a salt. When an ATPS is dilute in biochemical solutes, they partition between the two aqueous phases, leaving the phase equilibria for the ATPS essentially unaltered. Therefore, the design of an ATPE separation requires a phase diagram for the ATPS and partition coefficients for the biochemical solutes. As discussed in §8.6, ternary phase diagrams, similar to Figure 8.44, for over 100 ATPSs have been published. Also, partition coefficients have been measured for a number of biomolecules in several ATPSs, e.g., Madeira et al. [89]. When the ternary phase diagram and/or the partition coefficients are not available, they may be estimated by methods developed by King et al. [90] and Haynes et al. [91].

§2.8 SELECTING AN APPROPRIATE MODEL

Design or analysis of a separation process requires a suitable thermodynamic model. This section presents recommendations for making at least a preliminary selection.

The procedure includes a few models not covered in this chapter but for which a literature reference is given. The procedure begins by characterizing the mixture by chemical types: Light gases (LG), Hydrocarbons (HC), Polar organic compounds (PC), and Aqueous solutions (A), with or without Electrolytes (E) or biomacromolecules (B).

If the mixture is (A) with no (PC), and if electrolytes are present, select the modified NRTL equation. Otherwise, select a special model, such as one for sour water (containing NH_3, H_2S, CO_2, etc.) or aqueous amine solutions.

If the mixture contains (HC), with or without (LG), for a wide boiling range, choose the corresponding-states method of Lee–Kesler–Plöcker [8, 65]. If the HC boiling range is not wide, selection depends on the pressure and temperature. The Peng–Robinson equation is suitable for all temperatures and pressures. For all pressures and noncryogenic temperatures, the Soave–Redlich–Kwong equation is applicable. For all temperatures, but not pressures in the critical region, the Benedict–Webb–Rubin–Starling [5, 66, 67] method is viable.

If the mixture contains (PC), selection depends on whether (LG) are present. If they are, the PSRK method is recommended. If not, then a liquid-phase activity-coefficient method should be chosen. If the binary interaction coefficients are not available, select the UNIFAC method, which should be considered as only a first approximation. If the binary interaction coefficients are available and splitting into two liquid phases will not occur, select the Wilson or NRTL equation. Otherwise, if phase splitting is probable, select the NRTL or UNIQUAC equation.

All process simulators have expert systems that chose what the program designers believe to be the optimal thermodynamic package for the chemical species involved. However, since temperature, composition, and pressure in the

various processing units vary, care must be taken to use the expert system correctly.

§2.9 THERMODYNAMIC ACTIVITY OF BIOLOGICAL SPECIES

Effective bioseparations economically and reliably recover active biological product. Common petrochemical separations (e.g., distillation) occur by creating or adding a second phase, often a vapor. This is seldom possible with bioproduct separations, since most small molecules, polymers, and particulates of biological origin are unstable in the vapor phase. Thermodynamics of bioseparations thus focuses on molecular ionization states, interactions, and forces at physiologic conditions rather than the state of a continuous fluid phase. Biological activity is influenced by (1) *solution conditions* (e.g., pH buffering, ionization, solubility); (2) *biocolloid interactions* (e.g., van der Waals interactions, electrostatic forces, solvation forces, and hydrophobic effects); and (3) *biomolecule reactions* (e.g., actions of proteases, nucleases, lipases; effects of divalent cations, metals, chelating agents; rate/equilibrium of enzyme/substrate interactions and deactivation). Understanding these interrelated influences allows an engineer to (1) choose effectively between alternative bioseparation process options and (2) optimize operational parameters of a selected bioseparation operation to maintain activity of target biological species.

Solution conditions, biocolloid interactions, and biomolecule reactions affect separation of bioproducts by extraction (§8.6), membranes (§14.8), electrophoresis (§15.8), adsorption (§15.3), and crystallization (§17.11). In this section are important fundamental concepts upon which discussion in these later sections will be based. Biological suspensions contain a large number of complex biochemical species and are often incompletely specified. Therefore, the application of fundamental principles is balanced in practice with relevant experience from similar systems and careful attention to detail.

§2.9.1 Solution Conditions

Effects of temperature, ionic strength, solvent, and static charge on pH buffering impact biological stability as well as chromatographic adsorption and elution, membrane selectivity and fouling, and precipitation of biological molecules and entities.

pH buffers

Controlling pH by adding a well-suited buffer to absorb (or release) protons produced (or consumed) in biochemical reactions is important to maintain activity of biological products (e.g., to preserve catalytic activity). For example, reducing pH to <5.0 is sufficient to dissociate the rigid, 80-nm icosahedral protein coat of adenovirus, a nonenveloped, 165 MDalton double-stranded DNA (dsDNA) virus used as a viral vector for gene therapy [68]. Suitability is determined by several buffer attributes: (1) *acid-ionization* constant, which can vary with temperature and ionic strength; (2) charge(s)—positive or negative; (3) interactions with solution components such as metal ions or chelating agents; (4) solubility and expense; and (5) interference with analytical methods.

Simple monovalent ($n = 1$) buffers in aqueous solution yield an uncharged form of weak acid, HA, after proton addition [69,70]:

$$H_2O + HA \rightleftarrows H_3O^+ + A^- \tag{2-108}$$

or a charged form, HB^+, after proton addition to an uncharged weak base, B:

$$H_2O + HB^+ \rightleftarrows H_3O^+ + B \tag{2-109}$$

Acid-ionization constant

In practice, buffers and biological species are commonly employed in complex solutions at dilutions sufficient to evaluate activity coefficients at unity and to neglect deviation in water concentration away from 55.5 mol/L, M, in calculating pH. Apparent acid-ionization constants (i.e., apparent equilibrium constants) are rarely distinguished from true equilibrium constants by using the Debye–Hückel limiting law or its extensions to calculate activity coefficients. Use of dilute buffers allows rearranging the expression for the equilibrium constant, K_c, for proton dissociation in order to write the acid ionization constant, K_a, for an uncharged weak acid as

$$\boxed{K_a = K_c[H_2O] = \frac{[H^+][A^-]}{[HA]}} \tag{2-110}$$

Similarly, the K_a for an uncharged base is

$$\boxed{K_a = K_c[H_2O] = \frac{[H^+][B]}{[HB^+]}} \tag{2-111}$$

Adding a small volume of simple, dilute, weak acid (acetic acid, $\leq$1 M) or weak base (Tris, $\leq$1 M) to a well-stirred protein solution, for example, allows its pH to be adjusted between 5 and 8 in the presence of buffering salts with minimal risk of inactivation. Acetic acid, CH_3COOH, is an important weak biochemical acid responsible for vinegar's pungent odor. It is excreted from bacteria such as *Acetobacter* and *Clostridium* which oxidize vinegar from ethanol and sugar substrates during food spoilage. Acetic acid has a measured $K_c = 3.19 \times 10^{-7}$. By comparison, the ion product for the dissociation of water, K_w, at 25°C is

$$K_w = [H^+][OH^-] = 1.0 \times 10^{-14} \tag{2-112}$$

Determining pK_a, pH, *and ionization*

Small values of K_c are typical, and so K_a is conveniently expressed in logarithmic form as

$$\boxed{pK_a = -\log(K_a)} \tag{2-113}$$

Substituting (2-110) or (2-111) into (2-113) and using the definition of pH,

$$\boxed{\text{pH} = -\log(\text{H}^+)} \tag{2-114}$$

yields, upon rearrangement, the *Henderson–Hasselbalch equation*

$$\boxed{\text{pH} = \text{p}K_a + \log \frac{[basic\ form]}{[acid\ form]}} \tag{2-115}$$

which gives the pH of a solution containing both forms of a buffer. The pK of an acid or base is the pH at which it is half-dissociated, which corresponds to the *inflection point* in a *titration curve*.

Equation (2-115) allows the ratio of ionized basic form (A^-) to un-ionized acid form (HA) of a weak acid buffer to be determined using a measured pH and a known value of pK_a (and, similarly, for a weak base ionized acid —HB^+— and un-ionized basic—B—forms).

Determining pI *and net charge*

Amino acids each contain a primary –COOH that ionizes at pH ~2 to 3 and a primary $–NH_2$ group that ionizes at pH ~8 to 10. In some cases another ionizable group appears on a side chain. Amino acids exist mostly as *zwitterions*, which contain both acidic and basic groups (i.e., *amphoteric*) across a wide range of pH values that brackets a physiologic value of ~7.4. Zwitterions buffer solutions at high pH by releasing H^+, as well as at low pH by accepting H^+. Table 2.11 lists pK values for α-carboxylic acid, α-amino base, and the ionizable side chain (if present) on representative amino acids.

Using the base-to-acid ratio in (2-115) for α-carboxylic acid, α-amino base, and side-chain groups, the net charge at a given pH and *isolectric point*, pI (i.e., pH at which net charge is zero), for an amino acid can be determined. This is illustrated in Example 2.9 and Exercises 2.25 and 2.26.

Table 2.11 pK Values of Some Amino Acids, R-C(NH_2)(H)-COOH

	pK Values (25°C)		
Amino Acid	α-COOH group	α-NH_3^+ group	Side chain
Alanine	2.3	9.9	
Glycine	2.4	9.8	
Phenylalanine	1.8	9.1	
Serine	2.1	9.2	
Valine	2.3	9.6	
Aspartic acid	2.0	10.0	3.9
Glutamic acid	2.2	9.7	4.3
Histidine	1.8	9.2	6.0
Cysteine	1.8	10.8	8.3
Tyrosine	2.2	9.1	10.9
Lysine	2.2	9.2	10.8
Arginine	1.8	9.0	12.5

Source: Stryer [69].

EXAMPLE 2.9 Net Charge on an Amino Group.

The amino acid glycine has hydrogen as its side-chain (R) group. Values of $\text{p}K_a^c = 2.36$ and $\text{p}K_a^a = 9.56$ have been previously reported for glycine. Superscripts *c*, *a*, and *s* refer to α-carboxylic acid, α-amino base, and side chain, respectively. Using these values, determine the net charge on the α-amino group of glycine at a physiologic pH of 7.2 and a pH of 3 [70].

Solution

The ionization reactions for glycine are:

$$\underset{\text{glycinium cation}}{\overset{\text{low pH}}{\overset{+}{\text{H}_3\text{N}}\text{CH}_2\text{CO}_2\text{H}}} \xleftrightarrow[-\text{H}^+/+\text{H}^+]{K_a^c} \underset{\text{glycine zwitterion}}{\overset{\text{pH 7}}{\overset{+}{\text{H}_3\text{N}}\text{CH}_2\text{CO}_2^-}} \xleftrightarrow[-\text{H}^+/+\text{H}^+]{K_a^a} \underset{\text{glycinate cation}}{\overset{\text{high pH}}{\text{H}_2\text{N}\,\text{CH}_2\text{CO}_2^-}}$$

The fraction of α-carboxylic groups present as glycine zwitterions with net neutral charge is obtained by rearranging (2-115) to obtain the *deprotonation ratio*:

$$\frac{[\text{A}^-]}{[\text{HA}]} = 10^{(\text{pH}-\text{p}K_a^c)} \tag{2-116}$$

The corresponding fraction of the protonated α-carboxylic group present as glycinium cation is then:

$$\frac{[\text{HA}]}{[\text{HA}] + [\text{A}^-]} = \frac{1}{1 + 10^{(\text{pH}-\text{p}K_a^c)}} \tag{2-117}$$

This fraction is equivalent to the magnitude of the fractional charge of the amino group. To obtain the net charge, multiply the fraction by the unit charge of +1. At a physiologic pH of 7.2, this gives $+1.4 \times 10^{-5}$. In other words, there are ~14 glycinium cations with protonated α-amino groups and a net molecular charge of +1 for every 10^6 glycine zwitterions in solution. At a pH of 3, the net charge increases to 1.9×10^{-1}—nearly 2 glycinium cations with protonated α-amino groups and net positive charge per 10 amphoteric glycines. An analogous development for net charge on α-carboxylic acid shows that the *isoelectric point*, pI, of an amino acid with a nonionizing side group is (see Exercise 2.25):

$$\text{pH}_{\text{zero\_net\_charge}} = \text{pI} = \frac{\text{p}K_a^c + \text{p}K_a^a}{2} \tag{2-118}$$

Protein pI values are similar to those of the predominant constituent amino acid residue and are almost always <7.0 (anionic at physiologic pH). Exact calculation of protein pI using (2-118) is precluded by complex factors that influence ionizability. Ionization of one amino acid group in a polypeptide chain, for example, affects ionization of functional groups farther along the same chain. Tertiary structure, desolvation, and post-translational modifications also influence ionizability.

pK_a *criterion for buffer selection*

Equation (2-115) and corresponding acid/base titration curves show that the pH of solution changes less per proton absorbed (or released) as [basic form] approaches [acid form]. For this reason, it is preferable to (1) use a buffer whose pK_a is ±0.5 unit of desired pH—on the (−) side if

acidification is anticipated, or on the (+) side for expected basification; and (2) prepare the buffer with equal portions of acid and basic forms. A constant value of targeted pH is maintained by selecting from among buffers such as MES, 2-(N-morpholino) ethanesulfonic acid ($pK_a = 6.8$); inorganic orthophosphate ($pK_a = 7.2$); HEPES, N-hydroxyethylpiperazine-N'-2-ethanesulfonic acid ($pK_a = 6.8$); or Tris, tris (hydroxymethyl) amino-methane ($pK_a = 8.3$).

Ionic strength effects

Values of pK_a change more with buffer concentrations in solutions of multivalent buffers like phosphate or citrate than in simple monovalent buffers like acetate or Tris. The amount of change is indicated by the simplified *Debye–Hückel equation*

$$pK_a = pK_a^0 + \frac{0.5nI^{1/2}}{1 + 1.6I^{1/2}} \quad (\text{at } 25^\circ\text{C}) \tag{2-119}$$

where I represents *ionic strength*, given by

$$\boxed{I = \frac{1}{2}\sum_i c_i(z_i)^2} \tag{2-120}$$

where c_i = concentration of ionic species i, which has charge z_i; pK_a^0 represents a value of pK_a in (2-119) extrapolated to $I = 0$; and $n = 2z - 1$ for a given charge (valence) z on the acid buffer form. Examples of ionic strength effects on buffers with representative values of pK_a^0, n, and z are illustrated in Table 2.12.

Note that the value of n in (2-119) is always odd and increases pK_a as ionic strength is increased only when the acid form of the buffer has valence +1 or higher.

Temperature effects

Increasing temperature, T, decreases the pK_a value of a buffer. Tris buffer provides an extreme example: its pK_a in solution at 37°C physiologic conditions is 1 pH unit lower than at 4°C (on ice). Heating increases a buffer's standard-state free energy, ΔG^o, in proportion to the value of pK_a:

$$\Delta G^o = \Delta H^o - T\Delta S^o = -RT \ln K_a = 2.3RT(pK_a) \tag{2-121}$$

Equation (2-121) shows that the standard-state enthalpy of dissociation, ΔH^o, likewise increases with pK_a, particularly for small values of standard-state entropy of dissociation, ΔS^o. This decreases pK_a as T increases, viz.

$$\frac{-d \log K_a}{dT} = \frac{\Delta H^o}{2.3RT^2} \tag{2-122}$$

The value of ΔS^o depends mainly on the number of H_2O molecules that hydrate dissolved species, a process that produces order in a solution. Dissociation of amine buffers (e.g., Tris; $n = +1$), for example, yields no net formation of charged ions, so entropy increases slightly—$\Delta S^o = 5.7$ J/mol-K—and the free-energy change is absorbed by ΔH^o. Equation (2-122) thus shows that pK_a decreases substantially upon heating. On the other hand, physiologic buffers, acetic acid ($n = -1$) and sodium phosphate ($n = -3$), dissociate to form two new charged ions. This orders surrounding water molecules and significantly decreases entropy:

$\Delta S^o = -90.5$ J/mol-K for acetic acid and $\Delta S^o = -122$ J/mol-K for phosphoric acid at pK_2. Therefore, ΔH^o changes less for acetic and phosphoric acid buffers, which exhibit relatively constant pK_a values upon heating. This preserves cell and organism viability.

Freezing

Lowering the temperature of biological samples in order to slow microbial growth and preserve enzymatic activity can significantly change local pH and solute concentrations during phase changes [71]. Free water freezes first, growing ice crystals that destroy membrane layers and organelles and locally concentrating electrolytes and biocolloids, which precipitates insoluble salts, changes pH, increases osmolarity, and depresses local freezing point. Proteins are left largely intact, so freeze-thaw cycles are used to lyse mammalian cells to release intracellular proteins and propagated virus. Any dissolved salt crystallizes as temperature approaches its eutectic point. Freezer temperatures between −15° and −25°C allow protease and nuclease degradation at reduced rates. Consequently, flash freezing to −80°C and rapid thawing without local overheating preserves cell viability and enzymatic activity more effectively than freezing to about −20°C in a conventional freezer.

Table 2.12 Effect of Ionic Strength on pK_a of Some Characteristic Buffers

Common acid form	z	n	pK_a^0	pK_a $I = 0.01$	pK_a $I = 0.1$
Tris HCl, $Cl^-H^+NH_2C(CH_2OH)_3$	1	1	8.06	8.10	8.16
acetic acid, CH_3COOH	0	−1	4.76	4.72	4.66
monobasic sodium phosphate, NaH_2PO_4	−1	−3	7.2	7.08	6.89
disodium citrate 2-hydrate, $HOC(COOH)(CH_2COONa)_2{\cdot}2H_2O$	−2	−5	6.4	6.29	5.88

EXAMPLE 2.10 Preparation of Phosphate-Buffered Saline (PBS).

Phosphate-buffered saline (PBS) finds wide usage in biological processing, formulation, and research. Its pK_a and ionic strength mimic physiologic conditions and maintain pH across temperature changes expected in biological systems (4–37°C). PBS contains sodium chloride, sodium phosphate, and (in some formulations) potassium chloride and potassium phosphate at osmolarity (the concentration of osmotically active particles in solution) and ion concentrations that match those in the human body (isotonic). One common formulation is to prepare 10-liter stock of 10 × PBS by dissolving 800 g NaCl, 20 g KCl, 144 g $Na_2HPO_4{\cdot}2H_2O$, and 24 g KH_2PO_4 in 8 L of distilled water, and topping up to 10 L. Estimate the pH of this solution in its concentrated form when stored at 4°C, after being diluted to 1 × PBS at 4°C, and after being warmed to 37°C.

Solution

The ionic strength of the 10 × PBS solution is

$$I = \frac{1}{2}\sum_i c_i(z_i)^2 = \frac{1}{2}\begin{bmatrix} 2\cdot\left(\dfrac{800\text{g}}{58.44\text{g/mol}\cdot 10\text{L}}\right)\cdot(\pm 1)^2 \\ +2\cdot\left(\dfrac{20\text{g}}{74.55\text{g/mol}\cdot 10\text{L}}\right)\cdot(\pm 1)^2 \end{bmatrix} = 1.396$$

The effect of ionic strength on pK_a from Table 2.12 using the simplified Debye–Hückel equation (2-119) is

$$\text{p}K_a = 7.2 + \frac{0.5(-3)(1.396)^{1/2}}{1 + 1.6(1.396)^{1/2}} = 6.59$$

Using $\Delta H^o = 4.2$ kJ/mol for monobasic phosphate, decreasing temperature increases pK_a according to

$$\begin{aligned}\text{p}K_a^{277\text{K}} &= \text{p}K_a^{298\text{K}} - \frac{4200\,\text{Jmol}^{-1}}{(2.3)8.314\,\text{Jmol}^{-1}\text{K}^{-1}\cdot(287.5\,\text{K})^2} \\ &\quad\times(277-298) \\ &= 6.59 + 0.06 = 6.65\end{aligned}$$

Using MW for the mono- and dibasic phosphate salts of 178.0 g/mol and 136.1 g/mol, respectively, the pH of a solution with the given masses is, using (2-115),

$$\text{pH} = \text{p}K_a + \log\frac{\left[\dfrac{144}{178\cdot 10}\right]}{\left[\dfrac{24}{136.1\cdot 10}\right]} = 7.31$$

After 10× dilution, $I = 0.1396$, $\text{p}K_a^{298\text{ K}} = 6.85$, $\text{p}K_a^{277\text{ K}} = 6.91$, and pH = 7.57.

After increasing T to a physiologic value of 310 K, $\text{p}K_a^{310\text{ K}} = 6.82$, and pH = 7.48.

Upon dilution, the resultant 1× PBS at physiologic conditions has a final concentration of 137 mM NaCl, 10 mM phosphate, and 2.7 mM KCl, at a pH near that of arterial blood plasma, pH = 7.4.

pH affects solubility

Water solubility of ionized species is high. An uncharged or undissociated weak acid, HA, exhibits partial solubility, S_o. In a solution saturated with undissolved HA, the partial solubility is

$$S_o = M_{\text{HA}} \tag{2-123}$$

where M_i represents molality (moles of solute per kg solvent) of component i. Total solubility, S_T, the concentration of both undissociated and ionized acid is given by

$$S_T = M_{\text{HA}} + M_{\text{A}^-} = S_o + M_{\text{A}^-} \tag{2-124}$$

Substituting the relations for $M_{\text{A}}-$ and M_{HA} given by (2-123) and (2-124), respectively, into the corresponding terms in the Henderson–Hasselbalch equation (2-115) and solving for S_T provides total solubility in terms of pH:

$$S_T(\text{pH}) = S_o\left(1 + 10^{-[\text{p}K_{HA}-\text{pH}]}\right) = S_o\left(1 + \frac{K_{\text{HA}}}{M_{\text{H}^+}}\right) \tag{2-125}$$

Equation (2-125) shows that solubility of a weak acid increases above the partial solubility of its undissociated form to the extent that $K_{\text{HA}} > M_{\text{H}^+}$. Relative to a solubility value reported for pure water, $S_T^{\text{pH}=7}$, the pH effect on total solubility is given by

$$S_T(\text{pH}) = S_T^{\text{pH}=7}\frac{\left[1 + 10^{-(\text{p}K_{\text{HA}}-\text{pH})}\right]}{\left[1 + 10^{-(\text{p}K_{\text{HA}}-7)}\right]} \tag{2-126}$$

Similarly, the total solubility of a partially soluble weak base that ionizes according to

$$\text{BOH} \rightleftarrows \text{B}^+ + \text{OH}^- \tag{2-127}$$

with an ionization constant given by

$$K_{\text{BOH}} = \frac{[\text{B}^+][\text{OH}^-]}{[\text{BOH}]} \tag{2-128}$$

relative to solubility in water is

$$S_T(\text{pH}) = S_T^{\text{pH}=7}\frac{\left[1 + 10^{-(\text{p}K_{\text{BOH}}+\text{pH}-\text{p}K_{\text{W}})}\right]}{\left[1 + 10^{-(\text{p}K_{\text{BOH}}+7-\text{p}K_{\text{W}})}\right]} \tag{2-129}$$

It can be shown that the total solubility of a zwitterionic amino acid relative to water solubility is given by

$$S_T(\text{pH}) = S_T^{\text{pH}=7}\frac{\left[1 + 10^{-\left(\text{p}K_a^a-\text{pH}\right)} + 10^{-\left(\text{pH}-\text{p}K_a^c\right)}\right]}{\left[1 + 10^{-\left(\text{p}K_a^a-7\right)} + 10^{-\left(7-\text{p}K_a^c\right)}\right]} \tag{2-130}$$

EXAMPLE 2.11 Effect of pH on Solubility in Biological Systems.

As an example of solubility of weak organic acids, bases, and zwitterions in biological systems, prepare total solubility curves for the following species across a broad pH range (∼pH = 1 to pH = 11).

1. Caprylic acid ($C_8H_{16}O_2$) is an oily, naturally occurring liquid in coconuts that has anti-fungal and anti-bacterial properties. Its water solubility is 0.068 g/100 g at 20°C with a value of p$K_a = 4.89$.
2. Thymidine (T, $C_5H_6N_2O_2$, 5-methyluracil) is a pyrimidine base that forms two hydrogen bonds with adenine (A) to stabilize dsDNA. Its water solubility is 4.0 g/kg at 25°C and its pK_{BOH} is 9.9 (neglect further dissociation that occurs at higher pH).
3. The hydrophobic amino acid valine ($C_5H_{11}NO_2$), which substitutes for hydrophilic glutamic acid in hemoglobin, causes misfolding, which results in sickle-cell anemia. Its water solubility is 8.85 g/100 mL at 25°C. Its ionization constants are $\text{p}K_a^c = 2.3$ and $\text{p}K_a^c = 9.6$.

Calculate the solubility of each component in the following bodily fluids: cell cytosol, pH = 7.2; saliva, pH = 6.4; urine, pH = 5.8.

Solution

The solubilities are calculated from (2-126) for the acid, (2-129) for the base, and (2-130) for the zwitterion. In (2-130), the pK for water is computed to be 14 from (2-129). Table 2.13 shows solubility values in each bodily fluid. Figure 2.17 shows extended, calculated solubility curves for each component. Caprylic acid solubility

Table 2.13 Solubility of Organic Acid, Base, and Amino Acid in Bodily Fluids

	Solubilities (g/kg)		
Fluid: pH	Caprylic acid	Thymidine	Valine
Cell cytosol: 7.2	1.07	4.00	88.6
Saliva: 6.4	0.175	4.01	88.3
Urine: 5.8	0.0478	4.07	88.3

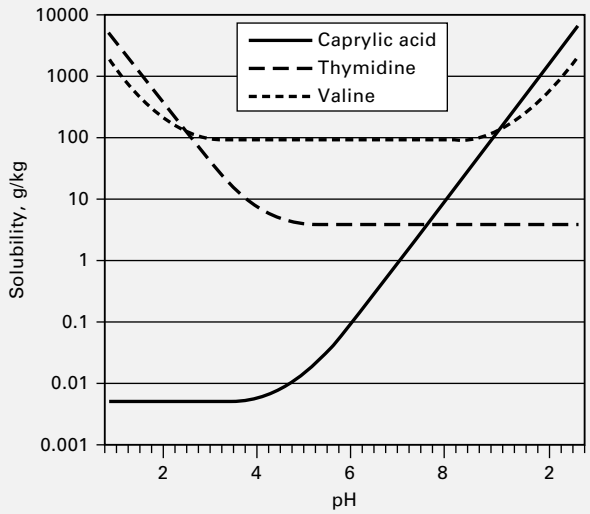

Figure 2.17 Solubility curves for caprylic (biological acid), thymidine (base), and valine (zwitterion) acids.

increases at pH $\geq$ pK_a. Thymidine solubility increases at pOH $= -\log[OH^-] = 14$ pH $\geq$ pK_{BOH}. Valine exhibits solubility increases at pH $\geq$ p$K_a{}^a$ and pOH $\geq$ p$K_a{}^c$. Reduced water solubility at the pI of a biomolecule may be used for selective precipitation or for extraction into a less-polar phase. Effect of pH on bioproduct solubility is further illustrated in Examples 8.13 and 8.14 of §8.6.1. Pharmaceutical formulation for drug delivery requires good understanding of solubility.

Solvent effects

Adding miscible organic solvents increases pK_a values of acetate, phosphate, and other buffers with negative n values by reducing activity of water, which causes resistance to proton dissociation. For example, the pK_a of phosphate increases 1 pH unit upon increasing the volumetric content of ethanol from 0 to 50%. On the other hand, values of pK_a for buffers like Tris, which have positive n values, are only slightly affected.

Static charges (Donnan effects)

Static negative (positive) charges attract (repel) protons, producing an adjacent micro-environment with lower (higher) pH—the *Donnan effect*. For example, porous cation exchange media used for adsorptive biochromatography (see §15.3.3) has a pH in the matrix about 1 unit lower than that in the eluting buffer—a difference that increases with decreasing buffer ionic strength. An enzyme that remains stable in eluent buffered at pH 5.5 may be denatured upon purification by cation exchange adsorption on media whose local pH is 4.5. On the other hand, since most enzymes are anionic (pI $<$ 7.0) and remain stable at mildly alkaline conditions (pH $=$ 8–10), fewer problems occur in anion exchange purification. Protein elution from ion-exchange media can produce sudden, large, local pH changes, particularly at low ionic strength, which decreases resolution of closely related species. On the other hand, some ion-exchange adsorbents like DEAE and some proteins may provide significant local buffering capacity. Donnan effects thus affect selection of operational pH ranges of ion-exchange adsorption separations.

Applications to Bioseparations

In *solvent selection* (§8.6.1, "Organic-Aqueous Extraction of Bioproducts"), it is shown how pH, I, T, and S_T affect the state of a bioproduct (e.g., pI) to influence its solvent partition coefficient, K_D (e.g., see Eq. 8-82) and guide selection of a suitable solvent for liquid–liquid extraction. The charge on bioproducts affects rejection and passage through ultrafiltration membranes (see §14.8.3) and determines adsorptive partitioning in ion-exchange chromatography (see §15.3.3). Interactions between pH and bioproduct isoelectric points are the basis for bioproduct separation using different modes for electrophoresis, distinguished in §15.8.2.

§2.9.2 Biocolloid Interactions

Biological polymers, macromolecular species, and cells exhibit many features of colloids—0.001 to ~1.0 μm particles that interact via long-range *hydrophobic*, *electrostatic*, and *van der Waals* forces, which arise from colloid size and accessible surface features [72, 73]. Such forces contrast with short-range *hydrogen bonding* and *dipole-dipole* interactions, which originate from electron orbitals of chemical functional groups on biocolloid surfaces and occur at separations approximately the length of a chemical bond. Separation distances and bond energies of interactions between biocolloids are summarized in Table 2.14. Colloid forces impact

Table 2.14 Bond Energies and Separation Distances of Biomolecular Interactions

Interaction	Equilibrium Separation (nm)	Bond Energy (kJ/mol)
Ionic bond	0.23	580–1050
Covalent bond		60–960
Metallic bond		105–355
Ion–dipole interaction	0.24	84
Dipole–dipole (hydrogen bond) interaction	0.28 (0.18–0.30)	5–30
Dipole-induced dipole interaction		<21
Hydrophobic	0.30	4.0
Dispersion forces	0.33	<42 (~0.25)

dissolution, aggregation, and other interactions between biological species such as cells, micelles, vesicles, and virus particles [74]. For example, Allison and Valentine [75, 76] reported binding of fowl plague and *vaccinia* virus to suspended HeLa cells at one-third the rate predicted by Fick's first and second laws of diffusion, due to electrostatic repulsion. The impact of colloid forces on biomolecular interaction affects properties in many bioseparations, including salting out effects in precipitation (see §17.11), particle aggregation in flocculation, solute mobility in electrophoresis (see §15.8.3), and charge dependence in phase partitioning (e.g., liquid–liquid extraction in §8.6 and liquid–solid adsorption in §15.3), and filtration in Chapter 19.

Consider the forces that contribute to the double-helix structure of DNA. *Covalent bonds* link adjacent nucleotides in each individual DNA strand. *Hydrogen bonds* between nucleotide bases (Watson–Crick base pairing) and *van der Waals' interactions* between stacked purine and pyrimidine bases hold the two complementary DNA strands in a helix together. Relatively *hydrophobic* nucleotide bases are buried in the helical interior, while charged phosphate groups and polar ribose sugars *solvate* dsDNA in aqueous solutions. *Electrostatic* interactions between adjacent negatively charged backbone phosphates are minimized by the extended backbone.

Cyclic manipulation of noncovalent force interactions by precise, consecutive, temperature adjustments—a technique called *polymerase chain reaction* (PCR)—allows a specific gene fragment (template) to be amplified for purposes such as gene sequencing or analysis of genetic mutations. In PCR, complementary DNA strands are thermally denatured (separated) at 94°C and then annealed to 21 base-pair complementary *primer* strands at ~55°C. Primers are subsequently elongated by polymerase at ~72°C using dissolved nucleotide base pairs. Repeating this cycle n times allows 2^n amplification of the original DNA template. The forces that bind DNA and influence other biomolecular interactions originate in colloidal interactions between suspended particles, small solutes, and solvent molecules.

DLVO theory

The theory of Derajaguin and Landau (of Russia) and Vervey and Overbeek (DLVO) describes attractive forces such as *van der Waals* (vdW) interactions and repulsive *double-layer* (*electrostatic*) forces between suspended colloids at approach distances >2 nm in the limit of low surface potentials [77], which occur when an elementary charge on the colloid surface has a potential energy $\ll k_B T$ (the thermal energy scale), where k_B is the Boltzmann constant. *Potential energy*, $\psi(r)$, between two like-charged colloids separated by distance r is the sum of attractive vdW and repulsive electrostatic forces. Coulomb's law holds that the force of electrical interaction between two charged particles varies directly with the product of their charges and inversely to the square of the distance between them, r^2. Adjacent colloids are repelled—thereby stabilizing colloid suspensions—by net respective surface charges (same sign) of 30–40 mV. These charges

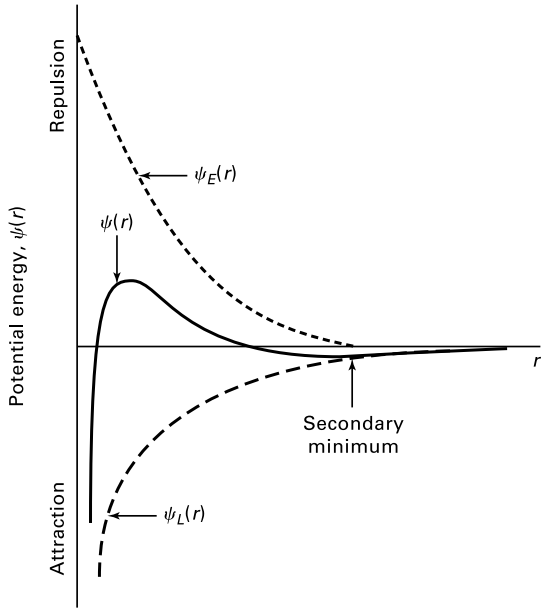

Figure 2.18 Potential energy between two like-charged particles.

arise from intrinsically high-area colloid surfaces that encourage (1) adsorption of ions; (2) molecular ionization on the surface, which leaves behind a surface charge; and/or (3) dissolution of ions from the solid into the suspending liquid [78].

The Gouy–Chapman theory postulates that an *electrostatic potential*, $\psi_E(r)$, forms at a surface with uniformly distributed charge and decays exponentially away with distance, r, due to thermal motion of oppositely charged ions in the adjacent solution

$$\Psi_E\{r\} = \Psi_{E,o}\exp(-\kappa r) \tag{2-131}$$

where $\psi_{E,o}(r)$ is the potential at the surface and κ is the *Debye–Hückel constant*. An *attractive potential* $\psi_L(r)$ arises due to long-range induction, orientation, and dispersion forces (simple systems consider only attractive vdW forces). Evaluated together, as in Figure 2.18, these potentials yield an overall interaction energy curve—$\psi(r)$—that exhibits two minima: a shallow *secondary minimum* at $r \sim 4/\kappa$ in which colloids remain stably suspended (>5 nm apart at low I values); and a deep *primary minimum* associated with rapid coagulation. Coagulation results from increasing I such that free energy due to electrostatic interactions between particles decreases to $\leq k_B T$, corresponding to particle separations $\leq \kappa^{-1}$, the *Debye length*.

Electrostatic double-layer interactions

Colloid surface charges form an electrical *double layer* that surrounds ionic charged particles and exerts electrostatic forces on adjacent colloids when their double layers overlap [80]. To maintain electrical neutrality, a charged surface dissolved in a medium attracts hydrated ions of opposite charge (counterions), which become strongly bound, forming an inner *Stern*

(or *Helmholtz*) *layer* of thickness, δ. A less-homogeneous, diffuse outer shell of moderately bound *Gouy* (or *Gouy–Chapman*) *second-layer* ions is comprised of hydrated ions of alternating charge. An external electric current will move the hydrated ions in the Gouy layer toward the electrode, forming a line of shear between fixed counterions and migrating ions. The measurable difference in electro-kinetic potential between the fixed boundary layer of charges on a surface and the shear line of mobile charges in the bulk of the solution is the *zeta potential* (or Stern potential), ζ. It indicates the fixed-charge density unsatisfied by counterions in the Stern layer and the corresponding distance into the solution required to satisfy it. That distance, the Debye length, κ^{-1}, or *double-layer thickness*, may be estimated with the Debye–Hückel approximation for modest surface potentials ($\Psi_o <$ 25 mV) as

$$\frac{1}{\kappa} = \left(\frac{2000e^2 N_A I}{\varepsilon k_B T}\right)^{-1/2} \tag{2-132}$$

in an electrolyte or colloid dispersion, where N_A is Avogadro's number. The ionic strength, I, is given by (2-120) for c_i (M_i) in mol/dm^3 (M)

$$I = \frac{1}{2}\sum_i z_i^2 M_i \tag{2-133}$$

The static permittivity for zero wavelength, ϵ, of the medium is given by

$$\varepsilon = \varepsilon_r \varepsilon_o = 78.54 \times 8.85 \times 10^{-12} \frac{C^2}{\text{J} \cdot \text{m}} \tag{2-134}$$

for water, using the relative static permittivity, ϵ_r, of H_2O at 25°C (commonly called the *dielectric constant*) and the electric constant, ϵ_o (i.e., vacuum permittivity, $\varepsilon_o = \mu_o^{-1} c_o^{-2}$, where μ_o is a magnetic constant and c_o is speed of light in a vacuum). The Boltzmann constant, k_B, is

$$k_B = 1.381 \times 10^{-23} \text{J/K} \cdot \text{molecule} \tag{2-135}$$

The charge on an electron, e, is

$$e = 1.60 \times 10^{-19} \text{coulomb} \tag{2-136}$$

The *dielectric constant* measures how much a material reduces the magnitude of an electric field. At 25°C for I in mol/dm^3, this gives [81]

$$\kappa^{-1} = 3.05 \times 10^{-10} I^{-1/2} \tag{2-137}$$

in meters.

In practice, it is easier to measure the streaming current potential by anchoring charged particles and moving the hydrated ions past them than it is to measure ζ. The Debye length decreases as ionic strength increases from ∼100 Å (10^{-3} M); 30 Å (10^{-2} M) to 10 Å (10^{-1} M) for a 1-1 (monovalent) electrolyte solution. These values are small relative to particle diameter and decrease as zeta potential is lowered. Repulsive forces are <1 mN/m for spheres with moderate surface potentials ($\Psi_o <$ 100 mV). Electrostatic repulsion can be felt at up to 60 nm in deionized water, but weakens to ∼1–3 nm at physiologic conditions normally found in biological fluids ($0.01 < c_i < 0.2$ M).

EXAMPLE 2.12 Colloidal Forces of Dissolved Biomolecules.

Colloidal forces on dissolved biomolecules affect their separability. Selection of appropriate molecular-weight cut-off values for an ultrafiltration bioseparation requires accurate estimation of bioproduct size (see §14.8.3). Determine the concentration of a 1:1 salt in moles/dm^3 below which the apparent radius of *bovine serum albumin* (BSA) is more than 10% larger than its actual radius of $a = 3.6$ nm.

Solution

For a 1:1 salt, ionic strength, I, in (2-133) reduces to c in mol/dm^3. The apparent radius ($a + \kappa^{-1}$) of a molecule is significantly different from its actual radius a if $\kappa^{-1}/a > 0.1$. Substituting this expression into (2-137) and solving for c in mol/dm^3 yields

$$c < \left(\frac{3.05 \times 10^{-9}}{a}\right)^2 \tag{2-138}$$

for a in meters. Therefore, the apparent radius of BSA is greater than its actual radius, $a = 3.6 \times 10^{-9}$ m, if salt concentration is less than 0.72 M.

Van der Waals forces

Instantaneous quantum fluctuations in charge distribution of one molecule distort the electron cloud in a neighboring atom or molecule to induce momentary polarization, and vice versa, resulting in short-range attraction between the transient dipole moments [82]. The cumulative effect is van der Waals (vdW), or *London dispersion* forces. Between atoms, these forces act over distances that are of the order of atomic dimensions, while between colloids, they are of the order of colloid dimensions. vdW forces are responsible for phase transitions (e.g., condensation of gas to liquid) and interfacial tension between adjacent phases, reaching up to 10 mN/m at ∼1 nm separations. The potential energy of interaction, W_D, via dispersion forces between two identical atoms separated by distance r is

$$W_D = -\frac{\lambda}{r^6} \tag{2-139}$$

where λ is a constant parameter of interaction given by

$$\lambda = \frac{3}{4}\alpha^2 h\nu_o \tag{2-140}$$

for atom polarizability α and ionization potential $h\nu_o$. The characteristic energy for the quantized energy at frequency ν_o constitutes the ionization potential. A single atom that closely approaches a macroscopic body of volume V produces an overall dispersion force felt by each atom that is estimated by integrating the energy of dispersion, W_D,

$$F_{12} = \int_V \frac{dW_D}{dr} dV \tag{2-141}$$

Table 2.15 Interaction Energies for Several Geometries

Geometry	Interaction Energy
Atom—flat body	$w = -\dfrac{\pi q \lambda}{6r^3}$
Two flat bodies	$w = -\dfrac{A}{12\pi r^2}$
Sphere—flat body	$w = -\dfrac{Aa}{6r}$
Two spheres	$w = -\dfrac{Aa_1a_2}{6r(a_1 + a_2)}$

Source: A.A. Garcia et al. [73].

Potential energies of interaction, w, for more complex geometries may be obtained by extending this approach. Table 2.15 shows values of w for spheres of radius a_i, as well as other superatomic scale geometries. Negative interaction energies are associated with spontaneous processes.

Comparing (2-139) with the interaction energies in Table 2.15 shows that dispersion forces decay more slowly as separation increases for colloidal bodies than for atoms. At separations exceeding ~10 nm, vdW interaction potential decays faster than r^{-6} due to retardation by phase difference between instantaneous dipoles on opposing bodies. The *Hamaker constant*, A, for vdW interactions between body (1) and body (2) defined by

$$A_{1-2} = \pi^2 \lambda \rho_1 \rho_2 \tag{2-142}$$

indicates the interaction parameter, λ, and respective number of atoms per unit volume, ρ_i, (i.e., atomic densities) in each body, which determine the attractive force between them. The moderating influence of a fluid (1) intervening between two same bodies (2) may be determined using a pseudo-chemical model to modify the Hamaker constant

$$A_{2-1-2} = \left(A_{1-1}^{1/2} - A_{2-2}^{1/2}\right)^2 \tag{2-143}$$

Values of the Hamaker constant vary only slightly from one medium to another: 4.3×10^{-20} J for water, 7.8 to 9.8×10^{-20} J for polystyrene, and 8.6×10^{-20} J for natural rubber [83].

Colloid flocculation by electrolytes

Like-charged electrostatic double layers and lubrication forces inhibit close approach of repellant surfaces and association due to London dispersion or vdW forces. On the other hand, surfaces with oppositely charged ζ values are adherent. Addition of ions (electrolyte salts or hydronium ions) to a colloid suspension structures the waters, attenuates the zeta potential, reduces the Debye length, and allows closer approach of like-charged surfaces, while reducing adherence of oppositely charged double layers. Coulombic repulsive forces dominate until the distance separating two surfaces is reduced sufficiently (i.e., to $r \sim 4/\kappa$) for attractive forces to be asserted. DLVO theory predicts that the critical *flocculating electrolyte concentration*, c_i, for *symmetric* (e.g., 1:1, 2:2, 3:3, but not 1:2, etc.), indifferent (not chemically adsorbed into the Stern layer) electrolytes is [84]

$$c_i^{floc} = \frac{9.85 \times 10^4 \varepsilon^3 k_B^5 T^5 \gamma^4}{N_A e^6 A^2 z_i^6} \tag{2-144}$$

where γ is a constant that approaches 1.0 at high potentials (>240 mV) and $ze\psi_{E\delta}/4k_BT$ at low potentials ($\psi_{E\delta} \sim 75$ mV), and c_i^{floc} is the lower molar concentration of the electrolyte that induces particle coagulation. In water at 25°C, this relation becomes

$$c_i^{floc} = \frac{\left(3.38 \times 10^{-36} \text{J}^2\text{-mol-m}^{-3}\right)\gamma^4}{A^2 z_i^6} \tag{2-145}$$

with c_i^{floc} in mol/m^3 and the Hamaker constant A in J. Equation (2-145) predicts that the relative values for critical flocculating concentration of electrolytes such as K^+, Ca^{2+}, and Al^{3+} containing counterions with charge numbers $z = 1$, 2, and 3 will be $1{:}2^{-6}{:}3^{-6}$ or 1000:15.6:1.37 at wall potentials > 240 mV, where $\gamma \sim 1$. This is the *Schulze–Hardy rule*. It is illustrated by the common practice of settling colloids during water treatment by adding alum, a double salt of aluminum and ammonium sulfates, to increase ionic strength.

EXAMPLE 2.13 Temperature, Charge, and Colloid Effects on Flocculation by an Electrolyte.

The first step in recovering bioproducts expressed in bacterial fermentation is often removal of aqueous culture broth to reduce process volume. Flocculation of bacteria by adding electrolyte enhances settling and broth removal. The ease of flocculation is a function of the electrolyte concentration. Determine the critical flocculation concentration, c_i^{floc} (in mol/dm^3), of an indifferent 1-1 electrolyte at 25°C and low potential. Calculate the effect on c_i^{floc} of (a) lowering temperature to 4°C; (b) changing to an indifferent 2-2 electrolyte at 4°C (maintaining low potential); (c) using electrolyte in part (b) to flocculate a viral colloid at 1/10 the concentration; and (d) flocculating at high potential.

Solution

At 75 mV,

$$\gamma = \frac{ze\Psi_{E\delta}}{4k_BT} = \frac{(1)(1.6 \times 10^{-19}\text{C})(0.075\text{V})}{4(1.38 \times 10^{-23}\text{J/K})(298\text{K})} = 0.7295$$

$$c_i^{floc} = \frac{\left(3.38 \times 10^{-36}\text{J}^2 \cdot \text{mol} \cdot \text{m}^{-3}\right)(0.7295)^4}{\left(8 \times 10^{-20}\text{J}\right)(1)^6}\left(\frac{\text{m}^3}{1000\,\text{dm}^3}\right) = 0.15\,\text{M}$$

(a) $c_i^{floc}(277°\text{C}) = c_i^{floc}(298°\text{C})\dfrac{277}{298} = 0.14\,\text{M}$

(b) $c_i^{floc}(277°\text{C}; 2-2) = c_i^{floc}(298°\text{C}; 1-1)\dfrac{277}{298}\dfrac{1}{(2)^2} = 0.035\,\text{M}$

(c) DLVO theory and (2-145) indicate that while critical electrolyte flocculation concentration is sensitive to temperature and electrolyte valence, it is independent of colloid particle size or concentration.

(d) Equation (2-145) indicates that at high potential, c_i^{floc} is proportional to T^6 and z^{-6} rather than to T and z^{-2}, respectively, at low potential.

Protein aggregation, crystallization, and adsorption have been shown to be controlled by long-range DLVO forces. However, nonclassical DLVO forces due to solvation, and hydrodynamic and steric interactions also influence protein interactions—generally at short range and with magnitudes up to the order of several k_BT—by altering biomolecular association rates or enhancing stability of protein complexes.

Solvation or hydration forces

At separation distances closer than 3 to 4 nm, continuum DLVO forces based on bulk properties of intervening solvent (e.g., density, dielectric constant, refractive index) give way to non-DLVO forces that account for structures formed by individual solvent molecules at solid interfaces based on their discrete size, shape, and chemistry. Normal to a surface and within several molecular diameters, solvent molecules form ordered layers. Attractive interactions between the surface and liquid molecules and the constraining effect of an approaching surface, which squeezes one layer after another out of the closing gap, cause *desolvation* (''lubrication'') forces between the surfaces, F_{SOL} (known as *hydration*, *hydrodynamic*, or *drainage* forces when the solvent is water). These are decaying oscillatory functions of separation distance, D, for spherical molecules between two hard, smooth surfaces

$$F_{SOL}\{D\} = K\exp\left(-\frac{D}{l}\right) \tag{2-146}$$

where $K > 0$ and $K < 0$ relate to hydrophilic repulsion and hydrophobic attraction forces, respectively, and l is the correlation length of orientational ordering of water molecules. Equation (2-146) explains short-range forces measured between neutral lipid bilayer membranes, DNA polyelectrolytes, and charged polysaccharides that are relatively insensitive to ionic strength. Polar solvent molecules like water that intervene between adjacent colloids form head-to-tail (positive-to-negative) conduit chains of partial charge interactions that can either attenuate forces between charged colloids or increase the effective distance of typically short-range ion–ion or acid–base interactions.

Molecular dipoles align in an orientation that opposes (and thereby diminishes) the originating electric field. Water dipoles also surround charged ions (e.g., electrolytic salt molecules) and displace ionic bonds, solvating the individual ions. Long-range (>10 nm) *hydrophobic* effects are also produced by water molecules.

Hydrophobic interactions

The free energy of attraction of water for itself due to hydrogen bonding is significant. *Hydrophobic* (''water-fearing'') groups restrict the maximum number of energetically favorable hydrogen bonds (i.e., degrees of freedom) available to adjacent water molecules. Water thus forms ordered and interconnected tetrahedral hydrogen-bonded structures that exclude hydrophobic entities like hydrocarbons or surfaces to minimize the number of affected water molecules. These structures reduce *interfacial area* and *surface free energy* of hydrocarbon–water systems as they assemble, minimizing entropy (maximizing degrees of freedom) and maximizing enthalpy (from hydrogen bonding). This process drives attraction of nonpolar groups in aqueous solution via forces up to 100 mN/m at separations <3 nm, culminating in *phase separation*. Hydrophobic interactions allow formation of reverse micelles (§8.6.1) into which bioproducts partition for subsequent extraction. Other biological examples of hydrophobic interactions include aggregation of mycobacteria to form cords and clustering of hydrophobic protein patches due to side chains of phenylalanine (Phe), tyrosine (Tyr), tryptophan (Trp), leucine (Leu), isoleucine (Ile), methionine (Met), and valine (Val). Hydrophobic forces between macroscopic surfaces are one to two orders of magnitude greater than vdW attraction, decaying exponentially with a characteristic length of 1–2 nm in the range 0–10 nm and remaining significant at distances up to 80 nm. Hydrophobicity scales developed for amino acids are useful to explain protein partitioning in liquid–liquid extraction (see ''Reverse Micelles'' in §8.6.1 and ''Salt Effect'' in §8.6.2), retention order, and retention time in reversed-phase and hydrophobic-interaction chromatography.

Structuring water, kosmotropes and chaotropes

Hydrophobic forces are influenced by biomolecule structures and the nature of dissolved ionic and nonionic species. Hydrophobic interactions are increased by dispersion forces between planar surfaces (i.e., stacking) of aromatic groups in aromatic amino acids, purines or pyrimidines, chlorophyll, and haem, for example. Small or multiple-charged ionic *kosmotropes* (''order-maker,'' e.g., citrate, sulfate, phosphate, hydroxide, magnesium, and calcium) interact more strongly with water than water itself. This enhances formation of water structure, stabilizes biomolecule structures in solution, and promotes hydrophobic interactions like aggregation. Large, singly charged ions with low charge density, called *chaotropes* (e.g., guanidinium, tetramethylammonium, and thiocyanate), interact weakly with water and disrupt water structure formation, which solvates hydrophobic structures and unfolds amphipathic proteins, which have interior regions rich in nonpolar characteristics as well as polar functional groups on the exterior. Chaotropic ions like octylmethylammonium chloride enhance aqueous/organic extraction (§8.6.1) of polar zwitterions like amino acids.

Nonionic kosmotropes including zwitterions (e.g., proline, ectoine, glycine, betaine) and polyhydroxy compounds (e.g., trehalose) hydrogen-bond strongly to water (e.g., sugar hydration). This reduces availability of water freely diffusing around proteins, exchange rates of backbone amide protons, and hydration of larger surfaces exposed by denaturation. Dehydration reduces biomolecule flexibility, which promotes stability in solution and prevents thermal denaturation, but reduces enzymatic activity. Kosmotropic ions and nonionic polymers are used to form partially miscible aqueous phases that allow stable, two-phase aqueous extraction of biomolecules (§8.6.2). Nonionic chaotropes (e.g., urea) weaken

hydrogen bonding, decrease the order of water, and increase its surface tension, which weakens macromolecular structure.

The Hofmeister series

The *Hofmeister series* classifies ions in order of their ability to change water structure. It was initially developed to rank cations and anions in terms of their ability to increase solvent surface tension and lower solubility of (''salt out'') proteins [85]:

Anions: $F^- \approx SO_4^{2-} > HPO_4^{2-} >$ acetate $> Cl^- > NO_3^- > Br^- > ClO_3^- > I^- > ClO_4^- > SCN^-$

Cations: $NH_4^+ > K^+ > Na^+ > Li^+ > Mg^{2+} > Ca^{2+} >$ guanidinium

Early ions in the series strengthen hydrophobic interactions (e.g., ammonium sulfate is commonly used to precipitate proteins). Later ions in the series increase solubility of nonpolar molecules, ''salting in'' proteins at low concentrations: iodide and thiocyanate, which weaken hydrophobic interactions and unfold proteins, are strong *denaturants*. Effects of pH, temperature, T, and ionic strength, I, of an ionic salt on solubility, S, of a given solute may also be correlated using

$$\log S = \alpha - K_s I \tag{2-147}$$

where K_s is a constant specific to a salt–solute pair and α is a function of pH and T for the solute. The relative positions of ions in the Hofmeister series change depending on variations in protein, pH, temperature, and counterion. Anions typically have a larger influence. The series explains ionic effects on 38 observed phenomena, including biomolecule denaturation, pH variations, promotion of hydrophobic association, and ability to precipitate protein mixtures. The latter two phenomena occur in roughly reverse order. Hofmeister ranking of an ionic salt influences its effect on solvent extraction of biomolecules, including formation of and partitioning into reverse micelles, and lowers partition coefficients, K_D, of *anionic* proteins between upper PEG-rich and lower dextran-rich partially miscible aqueous phases (§8.6.2, ''Aqueous Two-Phase Extraction''). Table 2.16 orders ions in terms of their ability to stabilize protein structure and to accumulate or exclude proteins from chaotropically disordered (e.g. low-density) water.

Steric forces

Either repulsive stabilizing or attractive coagulating forces may be produced by dissolved biopolymers in solution. The close approach of two surfaces at which polymers are anchored confines the thermal mobility of dangling chain molecules, resulting in a repulsive entropic force. Adding polysaccharides or proteins can sterically stabilize coagulative colloids with a force that depends on surface coverage, reversibility of anchoring, and solvent. One example is gelatin, an irreversibly hydrolyzed form of collagen, which constitutes ~50% of proteins in mammals and is commonly used as a gelling agent in foods, pharmaceuticals, and cosmetics. On the other hand, colloid flocculation may be induced by polymeric *nonionic or ionic surfactants*. Nonionic [nondissociating, e.g., polyethylene oxide (PEO), polyethylene glycol (PEG)] or ionic [e.g., polyacrylamide and sodium dodecylsulfate (SDS)] polymer surfactants may adsorb to and envelope adjacent repellant surfaces via hydrophobic interactions. This results in steric (or entropic) stabilization, which can match the potential energy barrier that prevents the approach of repellent colloids and induce flocculation. At the same time, attractive interactions like biomolecular interactions or affinity adsorption may be buffered or prevented by polymer surfactants. A surfactant may disrupt mutual hydrophobic interactions by masking a hydrophobic ligand, while the hydrophilic moiety of the surfactant interacts with water.

Surface force measurements of protein interactions

Particle detachment and peeling experiments, force-measuring spring or balance, and surface tension and contact angle measurements are used to gauge surface interaction; but these conventional methods do not provide forces as a function of distance. Scanning force probes [atomic force microscopy (AFM), scanning probe microscopy (SPM)] use improved piezoelectric crystals, transducers and stages, nanofabricated tips and microcantilevers, and photodiode-

Table 2.16 Ability of Cations and Anions to Stabilize Protein Structure

Effect of Ion on Proteins	Cations	Anions	Effect of Ion on Proteins
Protein stabilizing	$N(CH_3)_4^+$	Citrate $C_3H_4(OH)(COO)_3^{3-}$	Protein stabilizing
Weakly hydrated	NH_4^+	Sulfate SO_4^{2-}	Strongly hydrated
Accumulate in low-density water	Cs^+	Phosphate HPO_4^{2-}	Excluded from low-density water
	Rb^+	Acetate CH_3COO^-	
	K^+	F^-	
	Na^+	Cl^-	
	H^+	Br^-	
Protein destabilizing	Ca^{2+}	I^-	Protein destabilizing
Strongly hydrated	Mg^{2+}	NO_3^-	Weakly hydrated
Excluded from low-density water	Al^{3+}	ClO_4^-	Accumulate in low-density water

detectable laser light to measure the accuracy of calculated DLVO and non-DLVO potentials for biological systems.

Applications to bioseparations

In §8.6, it is shown how biocolloid interactions that influence solvation, hydrophobicity, water structure, and steric forces can enhance extraction of bioproducts via organic/aqueous and aqueous two-phase extraction. In §14.9.2, it is observed how biocolloid interactions affect membrane selectivity, sieving, and prediction of permeate flux. In §15.3.3, effects of biocolloid interactions on ion-exchange interactions are described. Bioproduct crystallization, §17.11, is also affected by biocolloid interactions.

§2.9.3 Biomolecule Reactions

Unique structural features of ligands or their functional groups allow specific, noncovalent interactions (e.g., ionic and hydrogen bonding, hydrophobic effects, vdW forces, and steric forces) with complementary structures of target biomolecules like receptor proteins that result in biochemical reactions, which sustain viability of cells. These interactions typically operate over short (<2 nm) intermolecular distances with binding energies associated with noncovalent bond formation, typically $>4k_BT$. Examples include: (1) immunologic recognition of a specific region (*epitope*) on a foreign substance (*antigen*) by protein immunoglobulins (*antibodies*); (2) regulation of gene expression by protein transcription factors that bind to control regions of DNA with high-affinity domains (*motifs*), such as zinc finger, leucine zipper, helix-turn-helix, or TATA box; (3) cell surface receptor (e.g., ion-channel, enzyme-linked, and g-protein linked receptor classes) binding to chemical substances (*ligands*) secreted by another cell in order to transduce cell-behavior-modifying signals; and (4) specific binding of a monosaccharide isomer by a carbohydrate-specific lectin—a protein with 2+ carbohydrate-binding sites.

Binding energies of noncovalent interactions require intermolecular proximities on the order of 0.1 nm and contact areas up to 10 nm^2 (usually ~1% of total solvent-accessible surface area) for these reactions to occur. Hydrogen bonds involving polar charged groups, for example, add 2.1 to 7.5 kJ/mol, or 12.6 to 25.1 kJ/mol when uncharged groups are involved. Hydrophobic bonds may generate 10 to 21 kJ/mol/cm^2 contact area.

Ligand–receptor binding cascade

Recognition and binding of the receptor by a ligand is initiated by electrostatic interactions. Solvent displacement and steric selection follow, after which charge and conformational rearrangement occur. Rehydration of the stabilized complex completes the process. From 20 to 1 nm, the approach and complementary pre-orientation of ligand and receptor maximize dominant coulombic attractive forces. Binding progresses from 10 to 1 nm as hydrogen-bonded solvent (water) molecules are displaced from hydrated polar groups on hydrophilic exteriors of water-soluble biomolecules. Release of bound water decreases its fugacity and increases the solvent entropic effect associated with surface reduction, which contributes to binding energy. Solvent displacement can make sterically hindered ligands more accessible for interaction through short-range, dipole–dipole, or charge-transfer forces. Next, conformational adjustments in ligand and receptor produce a steric fit (i.e., ''lock-and-key'' interaction). Steric effects and redistribution of valence electrons in the ligand perturbed by solvent displacement produce conformational rearrangements that yield a stable complex. Rehydration completes the binding process. Methods to compute forces that control protein interactions account for (1) absorbed solvent molecules and ions; (2) non-uniform charge distributions; (3) irregular molecular surfaces that amplify potential profiles at dielectric interfaces; (4) shifts in ionization pK's due to desolvation and interactions with other charged groups; and (5) spatially varying dielectric permittivity across the hydration shell between the protein surface and bulk solvent. Interaction with a PEG-coupled ligand may be used to increase selective partitioning of a target biomolecule into an upper PEG-rich phase during aqueous two-phase extraction (§8.6.2).

Ionic interactions

Ionic interactions between a net charge on a ligand and counterions in the receptor have high dissociation energies, up to 10^3 kJ/mol. As an example, amino groups RNH_3^+, protonated at physiologic pH on lysine [R = $(CH_2)_4$; pK = 10.5], or arginine [R = $(CH_2)_3NHCNH$; pK = 12.5] can interact with carboxyl groups, R'COO^-, on ionized aspartate (R' = CH_2; pK = 3.9) or glutamate [R' = $(CH_2)_2$; pK = 4.2] forms of aspartic acid and glutamic acid, respectively. Hard (soft) acids form faster and stronger ionic bonds with hard (soft) bases. Hard acids (e.g., H^+, Na^+, K^+, Ti^{4+}, Cr^{3+}) and bases (e.g., OH^-, Cl^-, NH_3, CH_3COO^-, CO_3^{2-}) are small, highly charged ions that lack sharable pairs of valence electrons (i.e., the nucleus strongly attracts valence electrons precluding their distortion or removal), resulting in high electronegativity and low polarizability. Soft acids (e.g., Pt^{4+}, Pd^{2+}, Ag^+, Au^+) and bases (e.g., RS^-, I^-, SCN^-, C_6H_6) are large, weakly charged ions that have sharable *p* or *d* valence electrons, producing low electronegativity and high polarizability. Examples of ionic stabilization of ligand–biomolecule or intrabiomolecule interactions are bonding between oppositely charged groups (i.e., salt bridges) and bonding between charged groups and transition-series metal cations. Example 8.15 in §8.6.1 demonstrates how desolvation via ion-pairing or acid–base pairing of organic extractants can enhance organic/aqueous extraction of bioproducts.

EXAMPLE 2.14 Selection of a Metal for Immobilized Metal Affinity Chromatography (IMAC).

Using the stability constant of metal-ion base complexes in Table 2.17, identify an appropriate metal to entrap in the solid phase via

Table 2.17 Stability Constants of Metal-Ion Base Complexes

		Thiourea (Log K)	Histidine (Log K)
Soft metal ions	Ag^{+}	$7.11 \pm 0.07^{*}$	–
	Cd^{2+}	$1.3 \pm 0.1^{*}$	5.74^{*}
Borderline metal ions	Cu^{2+}	$0.8^{\#}$	$10.16 \pm 0.06^{*}$
	Zn^{2+}	0.5^{*}	$6.51 \pm 0.06^{*}$

*in aqueous solution: $I = 0.1$, 25°C

$^{\#}$in aqueous solution: $I = 1.0$, 25°C

Source: A.A. Garcia et al. [73]

chelation to perform immobilized metal affinity chromatography (IMAC) of thiourea and histidine.

Solution

The R-group nitrogen in the amino acid histidine donates an electron pair to borderline soft-metal ions such as Cu^{2+}, Zn^{2+}, Ni^{2+}, or Co^{2+} to form a coordination covalent bond that can be displaced upon elution with imidazole. Data in the table suggest $Cu^{2+} > Zn^{2+}$ for histidine and $Ag^{+} > Cd^{2+}$ at the conditions shown. rDNA techniques can be used to genetically modify target proteins to include multiples of this amino acid as a tag (His_6-tag) on a *fusion* protein to facilitate purification.

Amino acid–metal bonds

Nearly all amino acids exhibit affinity for divalent metal ions. Log K-values for interacting amino acids range from 1.3 to 2.4 for Mg^{2+} and Ca^{2+}, and from 2.0 to 10.2 for Mn^{2+}, Fe^{2+}, Co^{2+}, Ni^{2+}, Cu^{2+}, and Zn^{2+}. Interactions between amino acids and copper generally exhibit the highest log K-values. Histidine and cysteine exhibit the strongest metal affinities. Double-stranded nucleic acids contain accessible nitrogen (i.e., N7 atom in guanidine and adenine) and oxygen (i.e., O4 atom in thymine and uracil) sites that donate electrons to metal ions in biospecific interactions. Soft- and borderline-metal ions generally have stronger affinity for N7 and O4, while hard-metal ions have greater affinity for oxygen atoms in the phosphate groups of nucleic acids.

Hydrogen bonds

Hydrogen bonds between biomolecules result from electrostatic dipole–dipole interactions between a hydrogen atom covalently bonded to a small, highly electronegative *donor* atom (e.g., amide nitrogen, N) and an electronegative *acceptor* (e.g., backbone O or N), which contributes a lone pair of unshared electrons. Regular spacing of hydrogen-bonded amino acid groups between positions i and $i + 4$ forms an α-helix protein 2° structure. Hydrogen bonding between alternate residues on each of two participating amino acid strands forms a β-pleated sheet. Tertiary protein structures form in part through hydrogen bonding between R-groups. Hydrogen bonding between G–C and A–T base pairs forms the *antiparallel* double-helical DNA structure.

Affinity thermodynamics and equilibrium

From a thermodynamics perspective, the overall Gibbs free-energy change in forming the receptor-ligand complex, ΔG, consists of free-energy contributions due to water displacement from receptor and ligand ($-\Delta G_{R,L\_hydration}$), receptor-ligand interactions ($\Delta G_{RL\_interactions}$), and rehydration of the stabilized complex ($\Delta G_{RL\_hydration}$), viz.,

$$\Delta G = -\Delta G_{R,L\text{-}hydration} + \Delta G_{RL\text{-}interaction} + \Delta G_{RL\text{-}hydration} \tag{2-148}$$

The free-energy change contributed by receptor-ligand interactions results from an increase in receptor potential energy from a low-energy, unbound state to a high-energy, complex state, ΔU_{conf}, a change in potential energy due to receptor-ligand interactions in the complex, ΔU_{RL}; and an entropy change due to receptor-ligand interactions, viz.,

$$\Delta G_2 = \Delta U_{conf} + \Delta U_{RL} - T\Delta S \tag{2-149}$$

This thermodynamic model is supplemented by computational chemistry calculations that quantify alterations in arrangements of chemical bonds using quantum mechanics and statistical physics. From an equilibrium perspective, bioaffinity interaction between a ligand, L, and a complementary receptor, R, may be expressed as

$$\mathrm{R} + \mathrm{L} \underset{k_D}{\overset{k_A}{\rightleftharpoons}} \mathrm{RL} \tag{2-150}$$

where k_A and k_D are forward (association) and reverse (dissociation) rate coefficients, respectively. Diffusion-controlled binding rates are typically less than 10^8/s, compared with diffusion-controlled collision rates of 10^{10}/s, because spatial localization reduces the probability of binding. Rate constants define the *equilibrium dissociation constant*, K_D,

$$K_D = \frac{k_D}{k_A} = \frac{[\mathrm{R}][\mathrm{L}]}{[\mathrm{RL}]} = \frac{\left(z_R - [\mathrm{RL}]/[\mathrm{R}]_o\right)[\mathrm{L}]}{[\mathrm{RL}]/[\mathrm{R}]_o} \tag{2-151}$$

where bracketed terms denote concentrations (unity activity coefficients have been applied), subscript o represents an initial value, and z_R is the receptor valency, the number of ligand binding sites per receptor molecule. Reaction thermodynamics is related to equilibrium by

$$\Delta G = -RT \ln K_D^{-1} \tag{2-152}$$

Table 2.18 shows values of K_D decrease from 10^{-3} M for enzyme-substrate interactions to 10^{-15} M for avidin-biotin complexation.

Scatchard plots

Equilibrium concentration values of L obtained from dialyzing a known initial mass of ligand against a number of solutions of known initial receptor concentration may be used to determine the dissociation constant and receptor valency by plotting $([\mathrm{RL}]/[\mathrm{R}]_o)/[\mathrm{L}]$ versus $[\mathrm{RL}]/[\mathrm{R}]_o$ in a *Scatchard plot*, viz.,

$$\frac{[\mathrm{RL}]/[\mathrm{R}]_o}{[\mathrm{L}]} = -\frac{[\mathrm{RL}]/[\mathrm{R}]_o}{K_D} + \frac{z_R}{K_D} \tag{2-153}$$

Table 2.18 Dissociation Constants of Some Bioaffinity Interactions

Ligand–Receptor Pair	K_D (M)
Enzyme-substrate	$10^{-3} - 10^{-5}$
Lectin-monosaccharide	$10^{-3} - 10^{-5}$
Lectin-oligosaccharide	$10^{-5} - 10^{-7}$
Antibody-antigen	$10^{-7} - 10^{-11}$
DNA-protein	$10^{-8} - 10^{-9}$
Cell receptor—ligand	$10^{-9} - 10^{-12}$
Avidin/Streptavidin—biotin	$\sim 10^{-15}$

Inhomogeneous receptor populations with varying affinity values (i.e., K_D) will produce nonlinearity in the plot.

EXAMPLE 2.15 Scatchard Analysis of Ligand-Receptor Binding.

From the Scatchard plot for two antibodies (Ab1 and Ab2) interacting with an antigen in Figure 2.19, determine: (a) the respective dissociation constants; (b) the valency for each antibody; and (c) the homogeneity of population for each antibody.

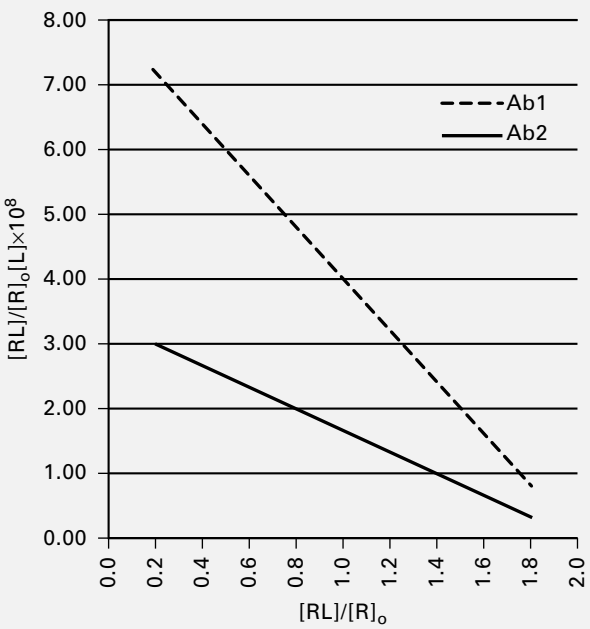

Figure 2.19 Scatchard plot for ligand–receptor interaction.

Solution

Equation (2-153) shows that the slope and intercept of each line correspond to K_D^{-1} and z_R/K_D, respectively. The dissociation constants are therefore $[(8\text{-}0)/(2\text{-}0)]^{-1} \times 10^{-8} = 0.25 \times 10^{-8}$ M and $[(3\text{-}0.33)/(1.8\text{-}0.2)]^{-1} \times 10^{-8} = 0.60 \times 10^{-8}$ M for antibody 1 and 2, respectively. These values lie within the range given in Table 2.18 for antibody–antigen interactions. From (2-153), the valency values are 2 for each antibody, meaning each antibody can bind 2 antigens. Homogeneity of the antibody and receptor preparations is indicated by the linear data in the Scatchard plot.

Bioaffinity interaction rate measurements

Quantifying interactions of macromolecules such as DNA, a protein or a virus is important to developing bioseparations, biocompatible materials, biosensors, medical devices, and pharmaceuticals. Intrinsic sorption (i.e., forward and reverse interaction) rates provide information about specificity, affinity, and kinetics [86, 87]. Intrinsic sorption rates of macromolecules including whole virus [88] can be measured by *surface plasmon resonance* (SPR) in label-free methods that are simpler, faster, and potentially more sensitive than *total internal reflectance fluorescence* (TIRF) or *nuclear magnetic resonance* (NMR) spectroscopy. Alternatives for quantitative sorption rate measurement include *quartz crystal microbalance/dissipation* (QCMD), calorimetry, ellipsometry, and voltammetry. SPR has the advantage of providing direct, unambiguous measurements to evaluate effects of binding site and concentration down to subnanomolar analyte levels without secondary reagents to enhance the signal. SPR measurements are $\geq$15 times faster and consume $\leq$100-fold less sample than curve-fitting chromatographic breakthrough profiles to determine protein sorption rates.

Applications to bioseparations

In ''Extractant/diluent Systems'' (§8.6.1), it is shown how desolvation via ion pairing or acid–base pairing can enhance organic/aqueous extraction of bioproducts. Ion pairing and acid–base pairing are also used to enhance selectivity of high-performance tangential flow filtration (see §14.9.2) and biochromatographic adsorption (§15.3.3).

SUMMARY

1. Separation processes are energy-intensive. Energy requirements are determined by applying the first law of thermodynamics. Estimates of irreversibility and minimum energy needs use the second law of thermodynamics with an entropy or availability balance.
2. Phase equilibrium is expressed in terms of vapor–liquid and liquid–liquid K-values, which are formulated in terms of fugacity and activity coefficients.
3. For separation systems involving an ideal-gas and an ideal-liquid solution, thermodynamic properties can be estimated from the ideal-gas law, a vapor heat-capacity equation, a vapor-pressure equation, and an equation for the liquid density.
4. Graphical representations of thermodynamic properties are widely available and useful for making manual calculations, and for visualizing effects of temperature and pressure.
5. For nonideal mixtures containing nonpolar components, P–υ–T equation-of-state models such as S–R–K, P–R, and L–K–P can be used to estimate density, enthalpy, entropy, fugacity, and K-values.

6. For nonideal liquid solutions of nonpolar and/or polar components, free-energy models such as Margules, van Laar, Wilson, NRTL, UNIQUAC, and UNIFAC are used to estimate activity coefficients, volume and enthalpy of mixing, excess entropy of mixing, and *K*-values.
7. Special models are available for polymer solutions, electrolyte solutions, mixtures of polar and supercritical components, and biochemical systems.
8. Effects of solution conditions on solubility and recovery of active biological products can be quantified by evaluating the ionization of water and organic acids and bases as a function of temperature, ionic strength, solvent, and electrostatic interactions.
9. Evaluating effects of electrolyte and solvent composition on electrostatic double layers and forces due to vdW, hydrophobic, solvation, and steric interactions allows engineering of separation systems that control solubility and maintain structural stability of biocolloid suspensions.
10. Characterizing noncovalent interaction forces and free-energy changes by interpreting measurements using applicable theory allows quantitative evaluation of biospecific interactions in order to enhance biorecovery operations.

REFERENCES

1. Mix, T.W., J.S. Dweck, M. Weinberg, and R.C. Armstrong, *AIChE Symp. Ser., No. 192*, Vol. **76**, 15–23 (1980).

2. Felder, R.M., and R.W. Rousseau, *Elementary Principles of Chemical Processes*, *3rd ed.*, John Wiley & Sons, New York (2000).

3. de Nevers, N., and J.D. Seader, *Latin Am. J. Heat and Mass Transfer*, **8**, 77–105 (1984).

4. Prausnitz, J.M., R.N. Lichtenthaler, and E.G. de Azevedo, *Molecular Thermodynamics of Fluid-Phase Equilibria*, *3rd ed.*, Prentice-Hall, Upper Saddle River, NJ (1999).

5. Starling, K.E., *Fluid Thermodynamic Properties for Light Petroleum Systems*, Gulf Publishing, Houston, TX (1973).

6. Soave, G., *Chem. Eng. Sci.*, **27**, 1197–1203 (1972).

7. Peng, D.Y., and D.B. Robinson, *Ind. Eng. Chem. Fundam.*, **15**, 59–64 (1976).

8. Plöcker, U., H. Knapp, and J.M. Prausnitz, *Ind. Eng. Chem. Process Des. Dev.*, **17**, 324–332 (1978).

9. Chao, K.C., and J.D. Seader, *AIChE J.*, **7**, 598–605 (1961).

10. Grayson, H.G., and C.W Streed, Paper 20-P07, Sixth World Petroleum Conference, Frankfurt, June 1963.

11. Poling, B.E., J.M. Prausnitz, and J.P. O'Connell, *The Properties of Gases and Liquids*, *5th ed.*, McGraw-Hill, New York (2001).

12. Rackett, H.G., *J. Chem. Eng. Data*, **15**, 514–517 (1970).

13. Yaws, C.L., H.-C. Yang, J.R. Hopper, and W.A. Cawley, *Hydrocarbon Processing*, **71**(1), 103–106 (1991).

14. Frank, J.C., G.R. Geyer, and H. Kehde, *Chem. Eng. Prog.*, **65**(2), 79–86 (1969).

15. Hadden, S.T., and H.G. Grayson, *Hydrocarbon Process., Petrol. Refiner*, **40**(9), 207–218 (1961).

16. Robbins, L.A., Section **15**, "Liquid–liquid Extraction Operations and Equipment," in R.H. Perry, D. Green, and J.O. Maloney Eds., *Perry's Chemical Engineers' Handbook*, *7th ed.*, McGraw-Hill, New York (1997).

17. Pitzer, K.S., D.Z. Lippman, R.F Curl, Jr., C.M. Huggins, and D.E. Petersen, *J. Am. Chem. Soc*, **77**, 3433–3440 (1955).

18. Redlich, O., and J.N.S. Kwong, *Chem. Rev.*, **44**, 233–244 (1949).

19. Shah, K.K., and G. Thodos, *Ind. Eng. Chem.*, **57**(3), 30–37 (1965).

20. Glanville, J.W., B.H. Sage, and W.N. Lacey, *Ind. Eng. Chem.* **42**, 508–513 (1950).

21. Wilson, G.M., *Adv. Cryogenic Eng.*, **11**, 392–400 (1966).

22. Knapp, H., R. Doring, L. Oellrich, U. Plöcker, and J.M. Prausnitz, *Vapor-liquid Equilibria for Mixtures of Low Boiling Substances*, Chem. Data. Ser., Vol. VI, DECHEMA (1982).

23. Thiesen, M., *Ann. Phys.*, **24**, 467–492 (1885).

24. Onnes, K., *Konink. Akad. Wetens*, p. 633 (1912).

25. Walas, S.M., *Phase Equilibria in Chemical Engineering*, Butterworth, Boston (1985).

26. Lee, B.I., and M.G. Kesler, *AIChE J.*, **21**, 510–527 (1975).

27. Edmister, W.C., *Hydrocarbon Processing*, **47**(9), 239–244 (1968).

28. Yarborough, L., *J. Chem. Eng. Data*, **17**, 129–133 (1972).

29. Prausnitz, J.M., W.C. Edmister, and K.C. Chao, *AIChE J.*, **6**, 214–219 (1960).

30. Hildebrand, J.H., J.M. Prausnitz, and R.L. Scott, *Regular and Related Solutions*, Van Nostrand Reinhold, New York (1970).

31. Yerazunis, S., J.D. Plowright, and F.M. Smola, *AIChE J.*, **10**, 660–665 (1964).

32. Hermsen, R.W., and J.M. Prausnitz, *Chem. Eng. Sci.*, **18**, 485–494 (1963).

33. Ewell, R.H., J.M. Harrison, and L. Berg, *Ind. Eng. Chem.*, **36**, 871–875 (1944).

34. Van Ness, H.C., C.A. Soczek, and N.K. Kochar, *J. Chem. Eng. Data*, **12**, 346–351 (1967).

35. Sinor, J.E., and J.H. Weber, *J. Chem. Eng. Data*, **5**, 243–247 (1960).

36. Orye, R.V., and J.M. Prausnitz, *Ind. Eng. Chem.*, **57**(5), 18–26 (1965).

37. Wilson, G.M., *J. Am. Chem. Soc* **86**, 127–130 (1964).

38. Cukor, P.M., and J.M. Prausnitz, *Inst. Chem. Eng. Symp. Ser. No. 32*, **3**, 88 (1969).

39. Gmehling, J., and U. Onken, *Vapor-liquid Equilibrium Data Collection*, DECHEMA Chem. Data Ser., 1–8 (1977–1984).

40. Hiranuma, M., *J. Chem. Eng. Japan*, **8**, 162–163 (1957).

41. Renon, H., and J.M. Prausnitz, *AIChE J.*, **14**, 135–144 (1968).

42. Renon, H., and J.M. Prausnitz, *Ind. Eng. Chem. Process Des. Dev.*, **8**, 413–419 (1969).

43. Abrams, D.S., and J.M. Prausnitz, *AIChE J.*, **21**, 116–128 (1975).

44. Abrams, D.S.,Ph.D. thesis in chemical engineering, University of California, Berkeley, 1974.

45. Prausnitz, J.M., T.F. Anderson, E.A. Grens, C.A. Eckert, R. Hsieh, and J.P. O'Connell, *Computer Calculations for Multicomponent Vapor-*

Liquid and Liquid-liquid Equilibria, Prentice-Hall, Englewood Cliffs, NJ (1980).

46. Fredenslund, A., J. Gmehling, M.L. Michelsen, P. Rasmussen, and J.M. Prausnitz, *Ind. Eng. Chem. Process Des. Dev.*, **16**, 450–462 (1977).

47. Wilson, G.M., and C.H. Deal, *Ind. Eng. Chem. Fundam.*, **1**, 20–23 (1962).

48. Derr, E.L., and C.H. Deal, *Inst. Chem. Eng. Symp. Ser. No. 32*, **3**, 40–51 (1969).

49. Fredenslund, A., R.L. Jones, and J.M. Prausnitz, *AIChE J.*, **21**, 1086–1099 (1975).

50. Fredenslund, A., J. Gmehling, and P. Rasmussen, *Vapor-liquid Equilibria Using UNIFAC, A. Group Contribution Method*, Elsevier, Amsterdam (1977).

51. Gmehling, J., P. Rasmussen, and A. Fredenslund, *Ind. Eng. Chem. Process Des. Dev.*, **21**, 118–127 (1982).

52. Larsen, B.L., P. Rasmussen, and A. Fredenslund, *Ind. Eng. Chem. Res.* **26**, 2274–2286 (1987).

53. Gmehling, J., J. Li, and M. Schiller, *Ind. Eng. Chem. Res.*, **32**, 178–193 (1993).

54. Wittig, R., J. Lohmann, and J. Gmehling, *Ind. Eng. Chem. Res.*, **42**, 183–188 (2003).

55. Takeuchi, S., T. Nitta, and T. Katayama, *J. Chem. Eng. Japan*, **8**, 248–250 (1975).

56. Strubl, K., V. Svoboda, R. Holub, and J. Pick, *Collect. Czech. Chem. Commun.*, **35**, 3004–3019 (1970).

57. Kiser, R.W., G.D. Johnson, and M.D. Shetlar, *J. Chem. Eng. Data*, **6**, 338–341 (1961).

58. Holderbaum, T., and J. Gmehling, *Fluid Phase Equilibria*, **70**, 251–265 (1991).

59. Fischer, K., and J. Gmehling, *Fluid Phase Equilibria*, **121**, 185–206 (1996).

60. Pitzer, K.S., *J. Phys. Chem.*, **77**, No. 2, 268–277 (1973).

61. Chen, C.-C., H.I. Britt, J.F. Boston, and L.B. Evans, *AIChE Journal*, **28**, 588–596 (1982).

62. Chen, C.-C., and L.B. Evans, *AIChE Journal*, **32**, 444–459 (1986).

63. Mock, B., L.B. Evans, and C.-C. Chen, *AIChE Journal*, **28**, 1655–1664 (1986).

64. Chen, C.-C., *Fluid Phase Equilibria*, **83**, 301–312 (1993).

65. Lee, B.I., and M.G. Kesler, *AIChE Journal*, **21**, 510–527 (1975).

66. Benedict, M., G.B. Webb, and L.C. Rubin, *Chem. Eng. Progress*, **47**(8), 419 (1951).

67. Benedict, M., G.B. Webb, and L.C. Rubin, *Chem. Eng. Progress*, **47**(9), 449 (1951).

68. Russell, W.C., *Journal of General Virology*, **81**, 2573–2604 (2000).

69. Stryer, L., *Biochemistry*, *3rd ed.*, W.H. Freeman & Co., New York (1988).

70. Sandler, S.I., *Chemical, Biochemical and Engineering Thermodynamics*, John Wiley & Sons, Hoboken, NY (2006).

71. Scopes, R.K., *Protein Purification. Principles and Practice,* Springer-Verlag, New York (1987).

72. Meltzer, T.H., *Modus of filtration,* in *Adv. Biochem. Engin./Biotechnol.* Springer-Verlag, Heidelberg Vol. 98, pp. 27–71 (2006).

73. Garcia, A.A., M.R. Bonen, J. Ramirez-Vick, M. Sadaka, and A. Vuppu, *Bioseparation Process Science*, Blackwell Science, Malden, MA (1999).

74. Leckband, D., and S. Sivasankar, *Coll. Surf. B: Biointerfaces*, **14**, 83–97 (1999).

75. Valentine, R.C., and A.C. Allison, *Biochimica et Biophysica Acta*, **34**, 10–23 (1959).

76. Allison, A.C., and R.C. Valentine, *Biochem Biophys Acta*, **40**, 393–399 (1960).

77. Liang, Y., N. Hilal, P. Langston, and V. Sterov, *Adv. Coll. Int. Science*, 134–145, 151–166 (2007).

78. Pall, D.B., E.A. Kimbauer, and B.T. Allen, *Colloids Surf.*, **1**, 235–256 (1980).

79. Harrison, R.G., P. Todd, S.R. Rudge, and D.P. Petrides, *Bioseparations Science and Engineering*, Oxford University Press, New York (2003).

80. Hunter, R.J., *Foundations of Colloid Science*, Vol. I, Clarendon Press, Oxford (1986).

81. Hiemenz, P.C., *Principles of Colloid and Surface Chemistry*, *2nd ed.*, Marcel Dekker, New York (1986).

82. Gabler, R., *Electrical Interactions in Molecular Biophysics*, Academic Press, New York (1978).

83. Hiemenz, P.C., and R. Rajagopalan, *Principles of Surface and Colloid Chemistry*, *3rd ed.*, Dekker, New York (1997).

84. Shaw, D.J., *Introduction to Colloid and Surface Chemistry*, *3rd ed.*, Butterworths, London (1980).

85. Hofmeister, F., *Arch. Exp. Pathol. Pharmacol*, **24**, 247–260 (1888).

86. Rich, R.L., and D.G. Myszka, *Journal of Molecular Recognition*, **16**(6), 351–382 (2003).

87. Rich, R.L., and D.G. Myszka, *Journal of Molecular Recognition*, **15**(6), 352–376 (2002).

88. Roper, D.K., and S. Nakra, *Anal. Biochem*, **348**, 75–83 (2006).

89. Madeira, P.P., J.A. Teixeira, E.A. Macedo, L.M. Mikheeva, and B.Y. Zaslavsky, *Fluid Phase Equilibria*, **267**, 150–157 (2008).

90. King, R.S., H.W. Blanch, and J.M. Prausnitz, *AIChE Journal*, **34**, 1585–1594 (1988).

91. Haynes, C.A., R.A. Beynon, R.S. King, H.W. Blanch, and J.M. Prausnitz, *J. Phys. Chem.*, **93**, 5612–5617 (1989).

92. Gmehling, J., R. Wittig, J. Lohmann, and R. Joh, *Ind. Eng. Chem. Res.*, **41**, 1678–1688 (2002).

93. Jakob, A., H. Grensemann, J. Lohmann, and J. Gmehling, *Ind. Eng. Chem. Res.*, **45**, 7924–7933 (2006).

STUDY QUESTIONS

2.1. In an energy balance, what are the two most common references (datums) used for enthalpy and entropy? Does one have an advantage over the other?

2.2. How does availability differ from Gibbs free energy?

2.3. Why is fugacity used in place of chemical potential to determine phase equilibria? Who invented fugacity?

2.4. How is the K-value for vapor–liquid equilibria defined?

2.5. How is the distribution coefficient for a liquid–liquid mixture defined?

2.6. What are the definitions of relative volatility and relative selectivity?

2.7. What are the two types of models used to estimate thermodynamic properties?

2.8. What is the limitation of the Redlich–Kwong equation of state? How did Wilson and Soave modify it to overcome the limitation?

2.9. What is unique about regular-solution theory compared to other activity-coefficient models for nonideal solutions? (This difference makes it much easier to use regular-solution theory when it is applicable.)

2.10. What are the six most widely used methods for estimating liquid-phase activity coefficients?

2.11. What very important concept did Wilson introduce in 1964?

2.12. What is a minimum-boiling azeotrope? What is a maximum-boiling azeotrope? Which type is by far the most common?

2.13. What is the critical solution temperature?

2.14. Why must electrolyte-solution activity-coefficient models consider both chemical and physical equilibrium?

2.15. Describe three effects of pH on ionization of a weak acid or base that impact biological stability of a protein.

2.16. Compare Tris and PBS as buffers in terms of temperature, ionic strength, and solvent effects.

2.17. What colloidal features do proteins and DNA exhibit?

2.18. What is the relation between the Debye length and the zeta potential?

2.19. Describe the role that the following colloidal forces play in biomolecular reactions: electrostatic, steric, solvent, hydrogen-bonding, ionic.

2.20. What is responsible for the large range in values of dissociation constants listed in Table 2.18?

EXERCISES

Section 2.1

2.1. Minimum work of separation.

A refinery stream is separated at 1,500 kPa into two products under the conditions shown below. Using the data given, compute the minimum work of separation, $W_{\min}$, in kJ/h for $T_0 = 298.15$ K.

	kmol/h	
Component	Feed	Product 1
Ethane	30	30
Propane	200	192
n-butane	370	4
n-pentane	350	0
n-hexane	50	0

	Feed	Product 1	Product 2
Phase condition	Liquid	Vapor	Liquid
Temperature, K	364	313	394
Enthalpy, kJ/kmol	19,480	25,040	25,640
Entropy, kJ/kmol-K	36.64	33.13	54.84

2.2. Minimum work of separation.

In refineries, a mixture of paraffins and cycloparaffins is reformed in a catalytic reactor to produce blending stocks for gasoline and aromatic precursors for petrochemicals. A typical product from catalytic reforming is ethylbenzene with three xylene isomers. If this mixture is separated, these four chemicals can be processed to make styrene, phthalic anhydride, isophthalic acid, and terephthalic acid. Compute the minimum work of separation in Btu/h for $T_0 = 560$°R if the mixture below is separated at 20 psia into three products.

		Split Fraction (SF)		
Component	Feed, lbmol/h	Product 1	Product 2	Product 3
Ethylbenzene	150	0.96	0.04	0.000
p-xylene	190	0.005	0.99	0.005
m-xylene	430	0.004	0.99	0.006
o-xylene	230	0.00	0.015	0.985

	Product Feed	Product 1	Product 2	Product 3
Phase condition	Liquid	Liquid	Liquid	Liquid
Temperature, °F	305	299	304	314
Enthalpy, Btu/lbmol	29,290	29,750	29,550	28,320
Entropy, Btu/lbmol-°R	15.32	12.47	13.60	14.68

2.3. Second-law analysis of a distillation.

Column C3 in Figure 1.8 separates stream 5 into streams 6 and 7, according to the material balance in Table 1.5. The separation is carried out at 700 kPa in a distillation column with 70 plates and a condenser duty of 27,300,000 kJ/h. Using the following data and an infinite surroundings temperature T_0, of 298.15 K, compute: (a) the duty of the reboiler in kJ/h; (b) the irreversible production of entropy in kJ/h-K, assuming condenser cooling water at 25°C and reboiler steam at 100°C; (c) the lost work in kJ/h; (d) the minimum work of separation in kJ/h; and (e) the second-law efficiency.

Assume the shaft work of the reflux pump is negligible.

	Feed (Stream 5)	Distillate (Stream 6)	Bottoms (Stream 7)
Phase condition	Liquid	Liquid	Liquid
Temperature, K	348	323	343
Pressure, kPa	1,950	700	730
Enthalpy, kJ/mol	17,000	13,420	15,840
Entropy, kJ/kmol-K	25.05	5.87	21.22

2.4. Second-law analysis of membrane separation.

A spiral-wound, nonporous cellulose acetate membrane separator is used to separate a gas containing H_2, CH_4, and C_2H_6. The permeate is 95 mol% pure H_2 and contains no ethane. The relative split ratio (separation factor, SP) for H_2 relative to methane is 47. Using the following data and an infinite surroundings temperature of 80°F, compute the: (a) irreversible production of entropy in Btu/h-R; (b) lost work in Btu/h; and (c) minimum work of separation in Btu/h. Why is it negative? What other method(s) might be used to make the separation?

Stream flow rates and properties:

Feed flow rates, lbmol/h	
H_2	3,000
CH_4	884
C_2H_6	120

	Feed	Permeate	Retentate
Phase condition	Vapor	Vapor	Vapor
Temperature, °F	80	80	80
Pressure, psia	365	50	365
Enthalpy, Btu/lbmol	8,550	8,380	8,890
Entropy, Btu/lbmol-K	1.520	4.222	2.742

Section 2.2

2.5. Expressions for computing *K*-values.

Which of the following *K*-value expressions are rigorous? For the nonrigorous expressions, cite the assumptions.

(a) $K_i = \bar{\phi}_{iL}/\bar{\phi}_{iV}$
(b) $K_i = \phi_{iL}/\phi_{iV}$
(c) $K_i = \phi_{iL}$
(d) $K_i = \gamma_{iL}\phi_{iL}/\bar{\phi}_{iV}$
(e) $K_i = P_i^s/P$
(f) $K_i = \gamma_{iL}\phi_{iL}/\gamma_{iV}\phi_{iV}$
(g) $K_i = \gamma_{iL}P_i^s/P$

2.6. Comparison of experimental *K*-values to Raoult's law predictions.

Experimental measurements of Vaughan and Collins [*Ind. Eng. Chem.*, **34**, 885 (1942)] for the propane–isopentane system, at 167°F and 147 psia, show a propane liquid-phase mole fraction of 0.2900 in equilibrium with a vapor-phase mole fraction of 0.6650. Calculate:

(a) The *K*-values for C_3 and iC_5 from the experimental data.
(b) The *K*-values of C_3 and iC_5 from Raoult's law, assuming vapor pressures at 167°F of 409.6 and 58.6 psia, respectively.

Compare the results of (a) and (b). Assuming the experimental values are correct, how could better estimates of the *K*-values be achieved? To respond to this question, compare the rigorous $K_i = \gamma_{iL}\phi_{iL}/\bar{\phi}_{iV}$ to the Raoult's law expression $K_i = P_i^s/P$.

2.7. Distribution coefficients from L/L data.

Mutual solubility data for the isooctane (1) furfural (2) system at 25°C [*Chem. Eng. Sci.*, **6**, 116 (1957)] are:

	Liquid Phase I	Liquid Phase II
x_1	0.0431	0.9461

Compute:

(a) The distribution (partition) coefficients for isooctane and furfural
(b) The selectivity for isooctane relative to that of furfural
(c) The activity coefficient of isooctane in phase 1 and an activity coefficient of furfural in phase 2, assuming $\gamma_2^{(1)}$ and $\gamma_1^{(2)} = 1.0$

2.8. Activity coefficients of solids dissolved in solvents.

In refineries, alkylbenzene and alkylnaphthalene streams result from catalytic cracking operations. They can be hydrodealkylated to yield valuable products such as benzene and naphthalene. At 25°C, solid naphthalene (normal melting point = 80.3°C) has the following solubilities in liquid solvents including benzene [*Naphthalene*, API Publication 707, Washington, DC (Oct. 1978)]:

Solvent	Mole Fraction Naphthalene
Benzene	0.2946
Cyclohexane	0.1487
Carbon tetrachloride	0.2591
n-hexane	0.1168
Water	0.18×10^{-5}

For each solvent, compute the activity coefficient of naphthalene in the solvent phase using the following equations (with T in K) for the vapor pressure in torr of solid and liquid naphthalene:

$$\ln P^s_{\text{solid}} = 26.708 - 8{,}712/T$$
$$\ln P^s_{\text{liquid}} = 16.1426 - 3992.01/(T - 71.29)$$

Section 2.3

2.9. Minimum isothermal work of separation.

An ideal-gas mixture of A and B undergoes an isothermal, isobaric separation at T_0, the infinite surroundings temperature. Starting with Eq. (4), Table 2.1, derive an equation for the minimum work of separation, $W_{\min}$, in terms of mole fractions of the feed and the two products. Use your equation to plot the dimensionless group, $W_{\min}/RT_0n_F$, as a function of mole fraction of A in the feed for:

(a) A perfect separation
(b) A separation with $SF_A = 0.98$, $SF_B = 0.02$
(c) A separation with $SR_A = 9.0$ and $SR_B = 1/9$
(d) A separation with $SF = 0.95$ for A and $SP_{A,B} = 361$

How sensitive is $W_{\min}$ to product purities? Does $W_{\min}$ depend on the separation operation used? Prove, by calculus, that the largest value of $W_{\min}$ occurs for a feed with equimolar quantities of A and B.

2.10. Relative volatility from Raoult's law.

The separation of isopentane from *n*-pentane by distillation is difficult (approximately 100 trays are required), but is commonly

practiced in industry. Using the extended Antoine vapor pressure equation, (2-39), with the constants below and in conjunction with Raoult's law, calculate relative volatilities for the isopentane/*n*-pentane system and compare the values on a plot with the following experimental values [*J. Chem. Eng. Data*, **8**, 504 (1963)]:

Temperature, °F	$\alpha_{iC5,nC5}$
125	1.26
150	1.23
175	1.21
200	1.18
225	1.16
250	1.14

What do you conclude about the applicability of Raoult's law in this temperature range for this binary system? Vapor pressure constants for (2-39) with vapor pressure in kPa and T in K are

	iC$_5$	nC$_5$
k_1	13.6106	13.9778
k_2	−2,345.09	−2,554.60
k_3	−40.2128	−36.2529
k_4, k_5, k_6	0	0

2.11. Calculation of condenser duty.

Conditions at the top of a vacuum distillation column for the separation of ethylbenzene from styrene are given below, where the overhead vapor is condensed in an air-cooled condenser to give subcooled reflux and distillate. Using the property constants in Example 2.3, estimate the heat-transfer rate (duty) for the condenser in kJ/h, assuming an ideal gas and ideal-gas and liquid solutions. Are these valid assumptions?

	Overhead Vapor	Reflux	Distillate
Phase condition	Vapor	Liquid	Liquid
Temperature, K	331	325	325
Pressure, kPa	6.69	6.40	6.40
Component flow rates, kg/h:			
Ethylbenzene	77,500	66,960	10,540
Styrene	2,500	2,160	340

2.12. Calculation of mixture properties

Toluene is hydrodealkylated to benzene, with a conversion per pass through the reactor of 70%. The toluene must be recovered and recycled. Typical conditions for the feed to a commercial distillation unit are 100°F, 20 psia, 415 lbmol/h of benzene, and 131 lbmol/h of toluene. Using the property constants below, and assuming the ideal-gas, ideal-liquid-solution model of Table 2.4, prove that the mixture is a liquid and estimate υ_L and ρ_L in American Engineering units.

Property constants for (2-39) and (2-38), with T in K, are:

	Benzene	Toluene
M, kg/kmol	78.114	92.141
P^s, torr:		
k_1	15.900	16.013
k_2	−2,788.51	−3,096.52
k_3	−52.36	−53.67
k_4, k_5, k_6	0	0
ρ_L, kg/m^3:		
A	304.1	290.6
B	0.269	0.265
T_c	562.0	593.1

Section 2.4

2.13. Liquid density of a mixture.

Conditions for the bottoms at 229°F and 282 psia from a depropanizer distillation unit in a refinery are given below, including the pure-component liquid densities. Assuming an ideal-liquid solution (volume of mixing = 0), compute the liquid density in lb/ft^3, lb/gal, lb/bbl (42 gal), and kg/m^3.

Component	Flow rate, lbmol/h	Liquid density, g/cm^3
Propane	2.2	0.20
Isobutane	171.1	0.40
n-butane	226.6	0.43
Isopentane	28.1	0.515
n-pentane	17.5	0.525

2.14. Condenser duty for two-liquid-phase distillate.

Isopropanol, with 13 wt% water, can be dehydrated to obtain almost pure isopropanol at a 90% recovery by azeotropic distillation with benzene. When condensed, the overhead vapor from the column forms two immiscible liquid phases. Use Table 2.4 with data in *Perry's Handbook* and the data below to compute the heat-transfer rate in Btu/h and kJ/h for the condenser.

	Overhead	Water-Rich Phase	Organic-Rich Phase
Phase	Vapor	Liquid	Liquid
Temperature, °C	76	40	40
Pressure, bar	1.4	1.4	1.4
Flow rate, kg/h:			
Isopropanol	6,800	5,870	930
Water	2,350	1,790	560
Benzene	24,600	30	24,570

2.15. Vapor tendency from *K*-values.

A vapor–liquid mixture at 250°F and 500 psia contains N_2, H_2S, CO_2, and all the normal paraffins from methane to heptane. Use Figure 2.4 to estimate the *K*-value of each component. Which components will be present to a greater extent in the equilibrium vapor?

2.16. Recovery of acetone from air by absorption.

Acetone can be recovered from air by absorption in water. The conditions for the streams entering and leaving are listed below. If the absorber operates adiabatically, obtain the temperature of the exiting liquid phase using a simulation program.

	Feed Gas	Absorbent	Gas Out	Liquid Out
Flow rate, lbmol/h:				
Air	687	0	687	0
Acetone	15	0	0.1	14.9
Water	0	1,733	22	1,711
Temperature, °F	78	90	80	—
Pressure, psia	15	15	14	15
Phase	Vapor	Liquid	Vapor	Liquid

Concern has been expressed about a possible feed-gas explosion hazard. The lower and upper flammability limits for acetone in air are 2.5 and 13 mol%, respectively. Is the mixture within the explosive range? If so, what can be done to remedy the situation?

Section 2.5

2.17. Volumetric flow rates for an adsorber.

Subquality natural gas contains an intolerable amount of N_2 impurity. Separation processes that can be used to remove N_2 include cryogenic distillation, membrane separation, and pressure-swing adsorption. For the last-named process, a set of typical feed and product conditions is given below. Assume a 90% removal of N_2 and a 97% methane natural-gas product. Using the R–K equation of state with the constants listed below, compute the flow rate in thousands of actual ft^3/h for each of the three streams.

	N_2	CH_4
Feed flow rate, lbmol/h:	176	704
T_c, K	126.2	190.4
P_c, bar	33.9	46.0

Stream conditions are:

	Feed (Subquality Natural Gas)	Product (Natural Gas)	Waste Gas
Temperature, °F	70	100	70
Pressure, psia	800	790	280

2.18. Partial fugacity coefficients from R–K equation.

Use the R–K equation of state to estimate the partial fugacity coefficients of propane and benzene in the vapor mixture of Example 2.5.

2.19. *K*-values from the P–R and S–R–K equations.

Use a process simulation program to estimate the *K*-values, using the P–R and S–R–K equations of state, of an equimolar mixture of the two butane isomers and the four butene isomers at 220°F and 276.5 psia. Compare these values with the following experimental results [*J. Chem. Eng. Data*, **7**, 331 (1962)]:

Component	*K*-value
Isobutane	1.067
Isobutene	1.024
n-butane	0.922
1-butene	1.024
trans-2-butene	0.952
cis-2-butene	0.876

2.20. Cooling and partial condensation of a reactor effluent.

The disproportionation of toluene to benzene and xylenes is carried out in a catalytic reactor at 500 psia and 950°F. The reactor effluent is cooled in a series of heat exchangers for heat recovery until a temperature of 235°F is reached at a pressure of 490 psia. The effluent is then further cooled and partially condensed by the transfer of heat to cooling water in a final exchanger. The resulting two-phase equilibrium mixture at 100°F and 485 psia is then separated in a flash drum. For the reactor-effluent composition given below, use a process simulation program with the S–R–K and P–R equations of state to compute the component flow rates in lbmol/h in both the resulting vapor and liquid streams, the component *K*-values for the equilibrium mixture, and the rate of heat transfer to the cooling water. Compare the results.

Component	Reactor Effluent, lbmol/h
H_2	1,900
CH_4	215
C_2H_6	17
Benzene	577
Toluene	1,349
p-xylene	508

Section 2.6

2.21. Minimum work for separation of a nonideal liquid mixture.

For a process in which the feed and products are all nonideal solutions at the infinite surroundings temperature, T_0, Equation (4) of Table 2.1 for the minimum work of separation reduces to

$$\frac{W_{min}}{RT_0} = \sum_{\text{out}} n\left[\sum_i x_i \ln(\gamma_i x_i)\right] - \sum_{\text{in}} n\left[\sum_i x_i \ln(\gamma_i x_i)\right]$$

For the separation at ambient conditions (298 K, 101.3 kPa) of a 35 mol% mixture of acetone (1) in water (2) into 99 mol% acetone and 98 mol% water, calculate the minimum work in kJ/kmol of feed. Activity coefficients at ambient conditions are correlated by the van Laar equations with $A_{12} = 2.0$ and $A_{21} = 1.7$. What is the minimum work if acetone and water formed an ideal solution?

2.22. Relative volatility and activity coefficients of an azeotrope.

The sharp separation of benzene (B) and cyclohexane (CH) by distillation is impossible because of an azeotrope at 77.6°C, as shown by the data of K.C. Chao [PhD thesis, University of Wisconsin (1956)]. At 1 atm:

T, °C	x_B	y_B	γ_B	γ_{CH}
79.7	0.088	0.113	1.300	1.003
79.1	0.156	0.190	1.256	1.008
78.5	0.231	0.268	1.219	1.019
78.0	0.308	0.343	1.189	1.032
77.7	0.400	0.422	1.136	1.056
77.6	0.470	0.482	1.108	1.075
77.6	0.545	0.544	1.079	1.102
77.6	0.625	0.612	1.058	1.138
77.8	0.701	0.678	1.039	1.178
78.0	0.757	0.727	1.025	1.221
78.3	0.822	0.791	1.018	1.263
78.9	0.891	0.863	1.005	1.328
79.5	0.953	0.938	1.003	1.369

Vapor pressure is given by (2-39), where constants for benzene are in Exercise 2.12 and constants for cyclohexane are $k_1 = 15.7527$, $k_2 = -2766.63$, and $k_3 = -50.50$.

(a) Use the data to calculate and plot the relative volatility of benzene with respect to cyclohexane versus benzene composition in the liquid phase. What happens in the vicinity of the azeotrope?

(b) From the azeotropic composition for the benzene/cyclohexane system, calculate the van Laar constants, and then use the equation to compute the activity coefficients over the entire range of composition and compare them, in a plot like Figure 2.12, with the experimental data. How well does the van Laar equation fit the data?

2.23. Activity coefficients from the Wilson equation.

Benzene can break the ethanol/water azeotrope to produce nearly pure ethanol. Wilson constants for the ethanol (1)/benzene (2) system at 45°C are $\Lambda_{12} = 0.124$ and $\Lambda_{21} = 0.523$. Use these with the Wilson equation to predict liquid-phase activity coefficients over the composition range and compare them, in a plot like Figure 2.12, with the experimental results [*Austral. J. Chem.*, **7**, 264 (1954)]:

x_1	$\ln \gamma_1$	$\ln \gamma_2$
0.0374	2.0937	0.0220
0.0972	1.6153	0.0519
0.3141	0.7090	0.2599
0.5199	0.3136	0.5392
0.7087	0.1079	0.8645
0.9193	0.0002	1.3177
0.9591	−0.0077	1.3999

2.24. Activity coefficients over the composition range from infinite-dilution values.

For ethanol(1)-isooctane(2) mixtures at 50°C, the infinite-dilution, liquid-phase activity coefficients are $\gamma_1^\infty = 21.17$ and $\gamma_2^\infty = 9.84$.

(a) Calculate the constants A_{12} and A_{21} in the van Laar equations.

(b) Calculate the constants Λ_{12} and Λ_{21} in the Wilson equations.

(c) Using the constants from (a) and (b), calculate γ_1 and γ_2 over the composition range and plot the points as log γ versus x_1.

(d) How well do the van Laar and Wilson predictions agree with the azeotropic point $x_1 = 0.5941$, $\gamma_1 = 1.44$, and $\gamma_2 = 2.18$?

(e) Show that the van Laar equation erroneously predicts two liquid phases over a portion of the composition range by calculating and plotting a y–x diagram like Figure 2.16.

Section 2.9

2.25. Net charge and isoelectric point of an amino acid with an un-ionizable side group.

Consider the net charge and isoelectric point of an amino acid with an un-ionizable side group.

(a) Identify the amino acids that lack an ionizable R-group (Group I).

For an amino acid with a side (R-) chain that cannot ionize, derive a general expression in terms of measured pH and known pK_a values of α-carboxyl (pK_a^c) and α-amino (pK_a^a), respectively, for:

(b) the deprotonation ratio of the α-carboxyl group

(c) the fraction of un-ionized weak-acid α-carboxyl group in solution

(d) the positive charge of the amino acid group

(e) the fraction of ionized weak base α-amino group in solution

(f) the net charge of the amino acid

(g) the isoelectric point of the amino acid

(h) using the result in part (f), estimate the isoelectric point of glycine (p$K_a^c = 2.36$ and p$K_a^a = 9.56$). Compare this with the reported value of the pI.

2.26. Net charge and isoelectric point of an amino acid with an ionizable side group.

Consider the net charge and isoelectric point of an amino acid with ionizable side (R-) group.

(a) Identify the acidic amino acid(s) capable of having a negatively charged carboxyl side group.

(b) Identify the basic amino acid(s) capable of having a positively charged amino side group.

(c) For an amino acid with a side (R-) chain that can ionize to a negative charge, derive a general expression in terms of measured pH and known pK_a values of α-carboxyl (pK_a^c), α-amino (pK_a^a), and side group (pK_a^R), respectively, for the net charge of the amino acid.

(d) For an amino acid with a side (R-) chain that can ionize to a positive charge, derive a general expression in terms of measured pH and known pK_a values of α-carboxyl (pK_a^c), α-amino (pK_a^a), and side group (pK_a^R), respectively, for the net charge of the amino acid.

(e) Determine the isoelectric point of aspartic acid (the pH at which the net charge is zero) using the result in part (c) and pK values obtained from a reference book.

2.27. Effect of pH on solubility of caproic acid and tyrosine in water.

Prepare total solubility curves for the following species across a broad pH range (∼pH 1 to pH 11).

(a) Caproic acid ($C_8H_{16}O_2$) is a colorless, oily, naturally occurring fatty acid in animal fats and oils. Its water solubility is 9.67 g/kg 25°C with a value of p$K_a = 4.85$.

(b) The least-soluble amino acid is tyrosine (Tyr, Y, $C_9H_{11}NO_3$), which occurs in proteins and is involved in signal transduction as well as photosynthesis, where it donates an electron to reduce oxidized chlorophyll. Its water solubility is 0.46 g/kg at 25°C, at which its p$K_a^c = 2.24$ and its p$K_a^a = 9.04$ (neglect deprotonation of phenolic OH-group, p$K_a = 10.10$).

Calculate the solubility of each component in the following bodily fluids:

Arterial blood plasma	pH = 7.4
Stomach contents	pH = 1.0 to 3.0

2.28. Total solubility of a zwitterionic amino acid.

Derive a general expression for the total solubility of a zwitterionic amino acid in terms of pH, pK_a^c, and pK_a^a from definitions of the respective acid dissociation constants, the expression for total solubility,

$$S_T = S_o + M_{-NH_3} + M_{-COO^-}$$

and the definition of solubility of the uncharged species, $S_o = M_{uncharged\ species}$.

2.29. Thermodynamics of Warfarin binding to human plasma albumin.

Warfarin (coumadin) binds to human plasma albumin to prevent blood clotting in the reaction

$$\mathrm{W} + \mathrm{A} \rightleftarrows \mathrm{WA}$$

Measured thermodynamic values for this reaction at 25°C are $\Delta G = -30.8$ kJ/mol, $\Delta H = -13.1$ kJ/mol, and $\Delta C_p \sim 0$.

(a) Determine the entropy change for this reaction at 25°C.

(b) Determine the fraction of unbound albumin over a temperature range of 0 to 50°C for a solution initially containing warfarin and albumin at 0.1 mM.

Source: Sandler [70].

2.30. Affinity of drugs to a given receptor.

Different drug candidates are analyzed to determine their affinity to a given receptor. Measured equilibrium dissociation constants are listed in the following table. Rank-order the drug candidates from highest affinity to weakest affinity for the receptor.

Drug	K_D (M)
A	0.02×10^{-6}
B	7.01×10^{-6}
C	0.20×10^{-6}

2.31. Binding of hormone to two different receptors.

Examination of the binding of a particular hormone to two different receptors yields the data in the following table. What is the reverse (dissociation) rate coefficient, k_D, for the release of the hormone from the receptor?

Receptor	K_D(M)	k_A($\mathrm{M^{-1}s^{-1}}$)
A	1.3×10^{-9}	2.0×10^{7}
B	2.6×10^{-6}	2.0×10^{7}